Relationship between the Magnitude and Location of Thigh-Calf Contact Force in High Flexion and Anthropometric Measures

by

Taya Lynn McGillivary

A thesis

presented to the University of Waterloo

in fulfillment of the

thesis requirement for the degree of

Master of Science

in

Kinesiology

Waterloo, Ontario, Canada, 2015

Author's Declaration

This thesis consists of material all of which I authored or co-authored: see Statement of Contributions included in the thesis. This is a true copy of the thesis, including any required final revisions, as accepted by my examiners.

I understand that my thesis may be made electronically available to the public.

Statement of Contributions

The following people have made significant contributions to this work:

Taya McGillivary: First author of all content in this thesis, making substantial contributions to protocol design, data acquisition, analysis and interpretation of data, and thesis writing.

Stacey Acker: Senior author and thesis supervisor, making substantial contributions to study conception and design, interpretation of data, critical revisions for intellectual content, and final approval of the submitted thesis.

Liana Tennant: Significant contributions to protocol and data collection.

Helen Chong: Significant contributions to protocol and data collection.

Abstract

The soft-tissue contact between the thigh and calf during deep knee flexion results in tibiofemoral joint contact force reductions at angles beyond 134º of flexion (Caruntu et al., 2003; Zelle et al., 2009; Hirokawa et al., 2013). Many knee models that predict tibiofemoral joint contact forces in high flexion neglect to account for this force. Very few investigations have attempted to characterize thigh-calf contact force, and even fewer have directly measured thigh-calf contact or attempted to model thigh-calf contact force and contact force location on the tibia (Zelle et al. 2007; Zelle et al. 2009). This study focused on the following four thigh-calf contact parameters: (1) maximum total thigh-calf contact force, (2) the corresponding flexion angle, (3) the corresponding centre of pressure, and (4) the starting angle of thigh-calf contact (the flexion angle at the initiation of thigh-calf contact when transitioning into a kneeling or squatting posture). This study addresses limitations of previous work by investigating how the thigh-calf contact parameters are correlated to anthropometric measures after accounting for correlations between body mass and contact force (by normalizing thigh-calf contact force to body mass), comparing parameters between sexes and activities, and presenting an equation for the average thigh-calf contact force and location from 30 participants as a function of percent thigh-calf contact flexion range (this has only been done previously for a single participant as a function of flexion angle).

Anthropometric measurements from 30 healthy participants (16 male and 14 female) were recorded. Instrumentation included opto-electronic markers to track dominant leg motion and an interface pressure mapping system to determine the thigh-calf contact force during three

deep flexion movements: dorsi-flexed kneeling, plantar-flexed kneeling, and plantar-flexed squatting. Four two-way (3 activities x 2 sexes) ANOVAs were used to compare the mean values for maximum total thigh-calf contact force (in N/kg), centre of pressure at maximum total force (in cm), flexion angle at maximum total force (in degrees) and the starting angle of thigh-calf contact (in degrees) between sexes and between the three activities. Pearson product-moment correlation coefficients (R) were calculated in order to investigate the relationship between the anthropometric measures and the four outcome parameters. In cases where the R value exceeded 0.5 for one or more of the anthropometric measures for a given outcome parameter, predictive modeling of the outcome parameter based on anthropometric measures was pursued using multivariate linear regression with forward stepwise selection. A mean curve for thigh-calf contact force and a mean curve for centre of pressure were created for all participants for each activity. Equations were fit to the mean curves to express each of the measures as a function of percent range of flexion after contact.

Based on the average thigh-calf contact force curve for 30 participants, the maximum thigh-calf contact force occurred at maximum flexion and was 1.1 N/kg (S.D. 0.6 N/kg) during squatting, 2.0 N/kg (S.D. 0.7 N/kg) during dorsi-flexed kneeling and 2.2 N/kg (S.D. 0.9 N/kg) during plantar-flexed kneeling. The average centre of pressure, corresponding to those maximum total thigh-calf contact force values, was found to be closer to the epicondylar axis during squatting (13.7 cm, S.D. 1.6cm) than for dorsi-flexed kneeling (14.9 cm, S.D. 1.7 cm) and plantar-flexed kneeling (14.6 cm, S.D. 1.9 cm).

There was a significant difference in the maximum total thigh-calf contact force, centre of pressure at maximum total force, and starting angle of thigh-calf contact between squatting and each of the two kneeling activities, however, for all outcome parameters, dorsi-flexed and

plantar-flexed kneeling were not significantly different. There was a significant main effect of sex on the starting angle of thigh-calf contact ($p = 0.004$), whereas, with all other outcome parameters, there was no sex main effect. Unlike the previous investigation that measured thigh-calf contact (Zelle et al., 2007), there was little correlation between anthropometric measures and maximum total thigh-calf contact force or location of centre of pressure at maximum total thigh-calf contact force. This discrepancy likely occurred because thigh-calf contact force was normalized to body mass in this study, whereas non-normalized contact force was used in the previous study.

The joint reaction forces, net joint moment, and joint contact forces at the knee joint in the sagittal plane during static full flexion squatting were calculated for a single participant both with and without the addition of thigh-calf contact force. The addition of thigh-calf contact force into the model reduced the knee joint reaction forces by 101.09 N in the anterior-posterior direction and the net sagittal plane knee joint moment by 13.14 Nm at maximal flexion. Based on a single muscle equivalent estimate, the compressive tibiofemoral joint contact force decreased by 221.78 N in the longitudinal direction and 84.96 N in the anterior-posterior direction.

Acknowledgements

First I must thank my supervisor Dr. Stacey Acker for opening the door to so many opportunities and experiences over the past few years. Thank you for your compassion and support throughout this degree, I have learned so much from you and I do not have the words to describe how much I appreciate everything that you have done for me. Your energy, drive and enthusiasm for everything you do will forever leave a strong impression on me and I hope to bring some of it with me as I move forward into dentistry.

The success of this work is due, to a large degree, to the unwavering support, friendship and guidance from my friends and family. To Dan Mines and Meg Warnica, thank you for being my support network and getting me through the tough times and celebrating with me during the awesome times. To Eric, my best friend and love of my life. Thank you for being my rock when I needed someone to keep me grounded while at the same time being my cheerleader and helping me to follow my dreams and aspirations no matter where they take me.

I would also like to thank all the members of the Biomechanics of Human Mobility (BOHM) Lab, especially, Helen Chong and Lia Tennant. Thank you for the countless hours you generously dedicated to helping me with data collection. I could have not done it without you

Finally, I must thank my biggest supporters, my parents. While I was working through this degree you both had the hardest few years of your lives. Regardless of everything you went through you were there for me from the start to finish, all hours of the day and night. You performed well above the norm, even for the world's greatest parents. Thank you.

Table of Contents

List of Figures

List of Tables

1. Introduction

1.1. Rationale

There have been many detailed studies conducted on the biomechanics of the knee joint during gait and at low knee joint flexion. However, limited attention has focused on the knee during deep flexion, such as that observed during squatting or kneeling, despite the fact that these deep flexion postures are common in daily living (Hefzy et al., 1998; Smith et al., 2008; Argenson et al., 2004). Current models that estimate tibiofemoral joint contact forces have only been applied to flexion angles up to 140° and have neglected to account for the contact between the thigh and calf which occurs during high-flexion. This results in maximum tibiofemoral joint contact force estimates occurring near full flexion (Hefzy et al., 1998; Nagura et al., 2002; Argenson et al., 2004). Excluding thigh-calf contact could mean that musculoskeletal models overestimate tibiofemoral joint contact forces in high flexion. This overestimation could be problematic in high flexion total knee replacement (TKR) testing since force requirements for the design and testing of TKRs are based on tibiofemoral joint contact force estimates from models, rather than on direct measurements (Hefzy et al., 2009).

Very few investigations have attempted to characterize thigh-calf contact force, and even fewer knee joint contact force models have incorporated thigh-calf contact force. Caruntu et al. (2003) calculated knee joint forces during deep knee flexion using a simplified, two-dimensional mathematical model which took into account thigh-calf contact force. With this model, they showed that thigh-calf contact force produces a moment around the joint in high-flexion that is in the same direction as the moment created by the quadriceps' tendon, thereby reducing the quadriceps muscle forces required to maintain equilibrium in comparison to when thigh-calf

contact was neglected. Zelle et al. (2009) used thigh-calf contact measurements from one participant from a previous experiment to develop a predictive equation for thigh-calf contact force and location during squatting. The resultant thigh-calf contact force and the contact force location on the tibia were expressed as functions of the knee flexion angle using a polynomial data-fitting technique. These equations were applicable to a flexion range of 125-155° for a single participant. The omission of anthropometric characteristics in these predictive equations was surprising, given correlations found during a previous investigation (Zelle et al., 2007). This previous investigation showed strong, significant correlations between anthropometric characteristics, such as thigh and calf circumference, and the maximum resultant thigh-calf contact force measurements and starting angle of thigh-calf contact during squatting and kneeling. Given the strong correlation between anthropometric characteristics and the maximum resultant thigh-calf contact force, it would be expected that a predictive equation for the magnitude of thigh-calf contact force during high-flexion, that incorporates the effects of anthropometric measures, would improve upon the existing model put forth by Zelle et al. (2009) and could be incorporated in the estimate of tibiofemoral joint contact forces.

1.2 Purpose

The main objectives of this Master's thesis project were:

- To compare thigh-calf contact forces between activities and sexes.
- To determine the correlation between anthropometric measures and thigh-calf contact parameters
- To develop predictive equations for thigh-calf contact force and centre of pressure based on anthropometric measures and flexion angle.

- To develop a predictive equation for starting angle of thigh-calf contact based on anthropometric measures.

Covariates that were candidates for inclusion in the predictive models were: height, body weight, sex, distal and maximal thigh circumferences, and proximal and maximal calf circumferences.

1.3 Hypotheses

The following hypotheses guided the direction of this work

1. The **maximal thigh-calf contact force** will not be statistically different between three high flexion activities: squatting, dorsi-flexed kneeling, and plantar-flexed kneeling. (Zelle et al., 2007: Pollard, J. 2009)
2. *Anthropometric properties will affect thigh-calf contact force.* **Body weight, and all thigh and calf circumference** measures will be significantly, positively correlated to maximum total thigh-calf contact force (Zelle et al., 2007). The greater the participant's body weight, thigh and calf circumference, the greater the maximum total thigh-calf contact force.
3. *The starting angle of thigh-calf contact will differ depending on anthropometric characteristics and sex.*
    a. All **thigh and calf circumference** measures will be significantly, negatively correlated to the **starting angle of thigh-calf contact** (Zelle et al., 2007). The larger the thigh and calf segment, the earlier the starting angle of thigh-calf contact.

b. **Women** will have an **earlier starting angle of thigh-calf contact** than men, meaning contact will be initiated at a lower flexion angle. Women are characterized by having more of a peripheral and lower body fat distribution, with generally larger thigh circumferences than men (Shimokata et al., 1989; Schwartz et al 1990; Canoy et al 2007). Furthermore, thigh circumference has been shown to have a strong correlation to the starting flexion angle of thigh-calf contact (Zelle et al., 2007).

4. *Thigh and calf circumference will be a significant predictor of the location of the centre of pressure on the tibia.*

    a. A participant's maximal **thigh and calf circumference** will be significantly correlated to the **location of the centre of pressure on the tibia at maximum total thigh-calf contact force (**Zelle et al., 2007). Larger thigh and calf circumferences will result in a more distally located COP at maximum flexion.

    b. **Women** will have a more **distal location of centre of pressure** at maximum total thigh-calf contact force than men. Women generally have larger thigh circumferences than men (Shimokata et al., 1989), which are anticipated to result in larger maximal thigh-calf contact areas and a more distal centre of pressure of thigh-calf contact force along the y-axis of the tibia.

Chapter 2: Literature Review

Knowledge of healthy knee kinematics and kinetics for the full range of motion is important for identifying possible causes of joint disease, and the development or improvement of treatment options, including partial and total knee arthroplasty (TKA). The knee is distinct from other major load-bearing joints in that the surrounding soft tissues are major contributors to the stability of the joint (Gray, H. 2008). Some research has been published describing the kinetics and kinematics of the intact knee over the flexion range from 0˚ to 120˚ of flexion (Hirokawa et al., 1993; Karrholm et al., 2000; Iwaki et al., 2000; Hill et al., 2000; Jevsevar et al., 1993; Kutzner et al., 2010). However, limited quantitative data concerning the behaviour of the intact knee beyond 120˚ has been reported in literature (Dahklvist et al., 1981; Hefzy et al., 1998; Nagura et al., 2002; Nagura et al., 2006; Hemmerich et al., 2006; Smith et al., 2008).

Modeling approaches for the computation of knee joint forces, have been extensively investigated with methods varying from two-dimensional (2D) to three-dimensional (3D); with only some models simulating articular surface contact; incorporating the surrounding soft-tissues; accounting for muscle cocontraction; or incorporating the thigh-calf contact that occurs during high-flexion activities. The diversity of approaches and modeling assumptions has led to vast differences in predictions of tibiofemoral joint contact force, even for the same activities. For instance, predicted knee joint forces during walking range from 1.7 to 3 times body weight (Komistek et al., 2005; Morrison, JB., 1970) depending on the modeling approach used in the literature.

The primary aim of the research was to investigate the possibility of predicting thigh-calf contact force and location of centre of pressure by computing correlations between thigh-calf

contact parameters and anthropometric measures and comparing parameters between sexes and activities.

2.1 Predicted tibiofemoral joint contact forces in deep flexion – neglecting thigh-calf contact

There is limited information surrounding knee mechanics during deep knee flexion activities such as squatting or kneeling. Hefzy et al. (1998) used bi-planar radiographs to describe the kinematics of normal knees in-vivo during three sequential positions with progressively higher tibiofemoral joint flexion during kneeling and bowing positions of Muslims during prayer. It was observed that during high knee flexion tibiofemoral contact occurs on the most proximal aspect of the posterior femoral condyles. The first study to investigate the dynamic stress on the tibiofemoral joint during deep knee flexion was carried out by Dahlkvist et al. (1982). Knee joint and muscle forces were calculated during squatting and rising from a deep squat using EMG, a force plate and a cine film system. The estimated tibiofemoral joint contact forces were found to be between 3.7 and 5.6 times body weight along the long axis of the tibia.

Most of studies that have modeled tibiofemoral joint contact forces are limited in that they do not consider that, during performance of high tibiofemoral joint flexion activities, a point is reached where the posterior thigh and calf come into contact and start to deform. Nagura et al. (2002) modeled dynamic loads on normal knees during deep flexion activities such as squatting and kneeling. Limb position was obtained using an opto-electronic tracking system and ground reaction forces using a force plate. The peak tibiofemoral joint contact forces, calculated to be as high as 7.3 (S.D. 1.9) times body weight when rising from a full squat, occurred at approximately 146.3° of flexion. In addition, there was mention of contact between the thigh and

calf occurring when the knees were flexed beyond 140°, although this was not taken into account in the estimation of tibiofemoral joint contact forces during deep knee flexion.

Smith et al. (2008) predicted axial tibiofemoral joint contact forces during two high flexion squatting activities using an electromagnetic motion tracking system and a non-conductive force platform. The model was based on measured kinematics, anthropometrics, ground reaction forces and calculated kinetics. Using this reduction (single muscle equivalent) approach, the resultant tibiofemoral joint contact forces during high-flexion squatting were then compared to those present during stair climbing. The maximum average joint contact force during the squatting activities occurred at significantly higher flexion angles compared to those during stair climbing. The largest mean peak joint contact force was found during heels-up (dorsi-flexed) squatting, which was predicted to be approximately 3.73 times body weight.

2.2 Predicted tibiofemoral joint contact forces in deep flexion – accounting for thigh-calf contact

A study by Caruntu et al. (2003) was one of the first to postulate the effects of thigh-calf contact on the loads transmitted to the knee joint. A two-dimensional mathematical model of the knee was developed to determine the behavior of the knee joint and its structures when it was maximally flexed during a static, deep squat. The model included the tibiofemoral joint, patello-femoral joint, quadriceps and hamstring co-contractions and used a single force acting at the centre of pressure to represent the distributed contact force between the thigh and calf. It was found that the incorporation of thigh-calf contact into the model decreased the quadriceps force needed to maintain equilibrium in a maximal squatting position, estimated to be 165° of flexion,

from 3500N to 2800N and lowered both the predicted tibiofemoral and patello-femoral contact forces.

As of yet, the most instrumental work done with regards to thigh-calf contact during high-flexion activities was described in two papers by Zelle and colleagues. The first paper, Zelle et al. (2007), directly measured thigh-calf contact force and area during high flexion activities and the second paper, Zelle et al., (2009), incorporated those findings into a knee joint force model.

In the initial study (Zelle et al., 2007), thigh-calf contact characteristics were measured using a flexible pressure mapping sensor (Tekscan Conformat pressure mapping sensor, Tekscan, South Boston, MA, USA), in high-flexion activities such as squatting and kneeling. In this investigation, the centre of pressure of the resultant thigh-calf contact force was expressed as a distance along the long axis of the tibia from the midpoint on the epicondylar axis of the femur in the tibial coordinate system. During the kneeling exercise the pressure mapping sensor was placed on the participant's calf prior to the deep flexion movement. During the squatting exercise the sensor was manually put into place by the participant as they descended into a deep squat from an erect posture. During both deep flexion movements knee flexion angles were measured unilaterally using an infrared five-camera motion capture system. At maximal knee flexion, the average maximal contact forces between the thigh and calf for each leg were 0.34 times bodyweight during squatting and 0.30 times bodyweight during kneeling. Based on this finding, the authors hypothesized that during deep knee flexion, thigh-calf contact would substantially affect forces inside the knee. In addition, this investigation showed significant correlations between body weight and the maximal thigh-calf contact force (measured in Newtons) during both squatting ($R = 0.73$) and kneeling ($R = 0.72$) as well as a strong correlation between the

thigh and calf circumferences and the starting angle of thigh-calf contact (R = -0.54; -0.79 respectively) and the maximal contact force (R = 0.73; 0.77 respectively) (Zelle et al., 2007). These correlations indicate that inferences on the maximum thigh-calf contact force and starting angle of thigh-calf contact could be made based on the participant's anthropometrics.

In 2009, using the thigh-calf contact force magnitude and the location of the resultant thigh-calf contact force obtained from one person during the previous squatting investigation (Zelle et al., 2007), Zelle and colleagues used two methods to predict the effect of thigh-calf contact on knee forces and stresses that would be placed on the polyethylene component of a total knee replacement, at full knee flexion. Method 1 used a combination of a rigid link segment model and a single muscle equivalent (quadriceps only) model (FBD) whereas, method 2 used finite element (FE) modeling. The inclusion of thigh-calf contact force and location in the calculation of knee contact forces, calculated using method 1, considerably reduced knee contact forces and polyethylene stresses during deep knee flexion. Additionally, the joint forces calculated by the FE model were in good agreement with those computed by the FBD model (Zelle et al., 2009). At maximum flexion, the addition of thigh-calf contact to the model decreased the compressive knee force from 4.89 to 2.90 times bodyweight and decreased the polyethylene contact stress at the tibial post from 49.3 to 28.1 MPa. In addition to these findings, Zelle et al. (2009) also found a strong correlation between a participant's thigh and calf circumferences and the reduction in compressive tibiofemoral joint contact force at maximal flexion. Larger thigh and calf circumferences promoted the earlier initiation of soft-tissue contact during deep knee flexion which would result in a larger force reduction at maximal flexion. The authors concluded that, since most TKR patients have higher BMIs and larger leg circumferences (Gupta et al., 2006), the contact between the thigh and calf during high flexion would partly

compensate for the increase in knee joint contact force usually associated with obesity and increase in bodyweight (Zelle et al. 2009).

Recently, Hirokawa et al. (2013) created a two-dimensional mathematical model of the lower limb incorporating features such as a patello-femoral mechanism, thigh-calf contact in high flexion and a co-contracting muscle force ratio. This model, using data from a single participant, determined knee joint forces in four kneeling conditions: rising with legs in parallel; with one foot forward; and kneeling both with and without arm assistance. The ground reaction force data were collected using a force platform and the angles of each joint were collected using a Vicon motion capture system during the required squatting and kneeling activities. Similar to the findings of Zelle et al. (2009), the maximum tibiofemoral joint contact force calculated was not at the greatest flexion angle but rather around 125.5° (+/-10.70). The maximum tibiofemoral joint contact force when rising from a kneeling position was determined to be approximately 4.5 times the participant's bodyweight. Although thigh-calf contact during the high-flexion activities was not directly measured, the effect of thigh-calf contact, as described by Zelle et al. (2009) was incorporated into the 2D model. However, the activities which provided basis for the effect of thigh-calf contact used in the Hirokawa et al. (2013) model were different from those measured in the Zelle et al. (2007) investigation (rising from deep flexion kneeling versus squatting).

Although previous publications have included thigh-calf contact force when calculating tibiofemoral joint contact forces during high flexion activities (Caruntu et al., 2003; Zelle et al., 2009; Hirokawa et al., 2013), only one investigation directly measured thigh-calf contact force (Zelle et al., 2007) to be used in model development (Zelle et al., 2009). Notwithstanding, the model in the Zelle et al. (2009) investigation was developed using data from only one of the

participants from the Zelle et al. (2007) investigation, which measured thigh-calf contact directly using a pressure mapping sensor (Tekscan, South Boston, MA, USA).

The work in this defense has attempted to address several key limitations of previous studies. Thigh-calf contact parameters were compared between activities and sexes; correlations between anthropometric measures and thigh-calf contact parameters after accounting for correlations between body mass and thigh-calf contact force (by normalizing the contact force to body mass) were quantified; equations were fit to the mean (for 30 participants) of thigh-calf contact force and centre of pressure as a function of percent of flexion range after contact; and an equation was developed to predict starting angle of thigh-calf contact based on anthropometric measures.

2.3 Interface Pressure Mapping Systems: Use and Limitations

Interface pressure mapping systems (IPM) are used for a variety of pressure monitoring applications, such as: measuring the interface pressure between the body and a support such as a chair; joint contact pressure monitoring *in-vivo* to determine the magnitude and distribution of contact stress as a function of joint loading (Martinelle et al., 2006); and measuring the contact pressure between adjoining body segments when they make contact (Zelle et al., 2007). The knowledge of the patterns of contact stress and force is important in terms of assessing tissue viability (Stinson et al., 2002); contact stress in different injuries and treatments (Martinelle et al., 2006); as well as tissue modeling (Stinson et al., 2002). A resistive sensor, Tekscan Conformat pressure mapping sensor (model #5315, Tekscan, Boston, MA) was used in this investigation. Resistive sensors consist of two Mylar sheets that have electrically conductive electrodes that are separated by a semiconductive ink coating. When pressure is applied, the ink

provides a change of the electrical resistance. By measuring the changes in current flow and using calibration values, the applied force can be calculated (Martinelle et al., 2006). Artifacts such as temperature drift, creep, bending and hysteresis may affect overall sensor behavior with respect to accuracy and repeatability. These limitations must be considered when measuring a contact force using a pressure mapping system. Moreover, IPM systems only measure normal force and do not measure shear force (Fergenbaum et al., 2003).

Sensor creep, inherent in most IPM sensor technology, is the tendency for the sensors to increase their reading over time, given a constant load (Martinelle et al., 2006). Generally, corrections for creep are made during the calibration/equilibration process (Martinelle et al., 2006; Tekscan Inc., 1999; Stinson et al., 2002). However, this correction is most accurate if the time frame during the calibration and equilibrium process matches the time frame used during data acquisition (IScan User Manual, Tekscan Inc., Boston, MA., 1999). Stinson et al. (2002) studied the time required for the IPM pressure values to stabilize after an increase or change in pressure using participants in a seated position on an IPM. For prolonged pressure readings, defined as exceeding one minute in duration, there was a significant increase in both average and maximum pressures over time. It is important to note, however, that average and maximum pressure did not significantly change during the first several seconds after a change in the force applied, suggesting that, at least in short-duration data collections (a few seconds), creep was not a concern (Stinson et al., 2002).

Sensor hysteresis is the difference in the sensor output response during loading and unloading, at the same applied force (Martinelle et al., 2006). In terms of a resistive sensor, in particular the Tekscan Confortmat pressure mapping sensor (Model#5315, Tekscan, Boston, MA), the effects of hysteresis are claimed to be minimal where static force is applied and in

applications in which the force is only increased, not decreased (IScan User Manual, Tekscan Inc., Boston, MA). However, if a force application includes varying load increases and decreases, there may be error not accounted for by calibration and equilibrium measurements. Pavlovic et al. (1993) reported that a sensor is more accurate during loading than unloading, however, during prolonged step-and-hold loading it was concluded that the sensor can underestimate the actual load by an average of 22% with the greatest difference being close to the saturation point of the pressure mat, when pressureswere significantly greater than the calibration values used (Pavlovic et al., 1993).

Accuracy and repeatability testing were conducted on the Tekscan Confortmat pressure mapping sensor (Model#5315, Tekscan, Boston, MA) used for this Master's thesis project. The methodology for IPM validation can be found in Appendix C where the sensitivity, accuracy, drift and hysteresis of the Tekscan Confortmat pressure mapping sensor (Model#5315, Tekscan, Boston, MA) were quantified.

2.4 Application for Thigh-Calf Contact Models: High flexion Total Knee Arthroplasty Design Criteria.

Obtaining high degrees of flexion post-operatively is culturally important, especially for non-Western cultures where a range of motion greater than 120º of flexion is critical for activities of daily living (Hemmerich et al., 2006; Acker et al., 2011). In order to facilitate this demand, high-flexion knee implant designs have been developed (e.g. Sigma RP-F, DePuy, Warsaw, IN; Nexgen LPS Flex, Zimmer, Warsaw, IN; Scorpio Flex, Stryker, Kalamazoo, MI; Genesis II High Flex, Smith & Nephew, Memphis, TN) to provide a larger flexion range (ROM > 120º) after TKR than previous conventional implants (ROM < 120º) (Khaw et al., 2001).

High-flexion TKRs are designed based on the assumption that the highest forces are generated at maximal knee flexion angles (Nagura et al., 2002; Nagura et al., 2006).

However, with the addition of thigh-calf contact into models used to estimate knee joint contact forces during deep flexion activities, the highest forces are not occurring at maximal flexion, as previously thought (Nagura et al., 2002; Nagura et al., 2006), but rather at submaximal flexion angles (Zelle et al., 2009; Zelle et al., 2011; Hirokawa et al., 2013). Therefore, the need for reinforcement of high-flexion implants near end-range flexion, such as the metal pin in the tibial post of Sigma RP-F (Depuy, Warsaw, IN, USA), is debatable. Some may argue that this reinforcement and overestimation allows for a built-in safety factor into implant design. Contrarily, this excess reinforcement, such as reinforcing the polyethylene tibial post using metals in order to handle the predicted, but not truly representative, highest loads during very deep flexion, may in fact have a long-term detrimental effect on implant longevity (Bal & Greenberg, 2007).

2.5 Sex as a covariate in predicting thigh calf contact

Previous publications that have measured thigh and calf contact characteristics to calculate thigh-calf contact force (Zelle et al., 2007) or used thigh-calf contact force to calculate knee joint forces during high-flexion activities (Caruntu et al., 2003; Zelle et al., 2009; Hirokawa et al., 2013) were non-discriminate about the participant's sex during calculations. Previous publications have noted both anatomical differences (Chin et al., 2002; Hitt et al., 2003; MacDonald et al., 2008; Dargel et al., 2011) and differences in fat distribution patterns (Seidell et al., 1987; Shimokata et al., 1989; Schwartz et al 1990; Canoy et al 2007) between men and women. Men were shown to have a more truncal and upper body fat distribution, whereas

women were characterized by more of a peripheral and lower body fat distribution. Generally, when adjusted for age, women had larger thigh circumferences than men (Shimokata et a., 1989).

Given that thigh and calf circumference has previously been shown to be significantly correlated to the starting flexion angle of thigh-calf contact and maximal thigh-calf contact force during high-flexion activities, differences in thigh and calf circumferences between the sexes could mean differences in thigh-calf contact area and force distribution.

Chapter 3: Research Design and Methodology

This study had a cross-sectional design. Motion analysis and pressure data were collected during deep knee flexion squatting, dorsi-flexed and plantar-flexed kneeling. Motion data was used to determine segment positions and joint angles. Pressure data was used to determine the force between the thigh and the calf during these deep flexion positions. The mean thigh-calf contact force and centre of pressure from this study were used to estimate the effect of thigh-calf contact on knee joint reaction force forces, the sagittal net joint moment and the axial knee joint contact force in a single participant from another study.

3.1 Participants

This study was carried out at the University of Waterloo (Waterloo, Ontario), and ethics approval was obtained from the University Of Waterloo Office Of Research Ethics. Healthy volunteer participants were recruited from the university and local population. Participants provided informed consent to participate in the study.

Thirty people (16 male and 14 female) participated in this investigation. The mean age of the participants was 27.78 years (S.D.13 years), the mean height was 172.1 cm (S.D. 8.5 cm, Male: 178.3 cm, S.D. 5.0 cm; Female: 165.0 cm, S.D. 5.6 cm), and the mean body mass was 77.0 kg. (S.D.14.2 kg, Male: 82.9 kg, S.D. 13.1 kg; Female: 70.2 kg, S.D. 12.3 kg).

Participant masses ranged from 53 kg to 112 kg which approximately span the range from the 5^{th} to 95^{th} percentile of body mass for males and females, regardless of race and age in the United States from 2007-2010 (C.D.C, 2010). Participant body mass index (BMI) ranged

from the 5th to 80th percentile for women and 7th to 80th percentile for males regardless of race and age in the United States from 2007-2010 (C.D.C, 2010).

3.2 Equipment and data collection

Each participant's height, body mass, sex, and thigh and calf circumferences were measured prior to each data collection. The circumference of the thigh and calf was measured at two points along each segment. One circumference measure was measured around the largest point of each segment. The second thigh circumference was at approximately 90% of the segment length, measured distally from the greater trochanter, and was referred to as the distal thigh circumference. The second shank circumference at approximately 10% of the segment length, measured distally from the lateral condyle of the tibia, and was referred to the proximal shank circumference. These percentages were used in order to establish circumference measurements that were as close as possible to the popliteal crease, on the back of the knee, while avoiding boney landmarks surrounding the knee joint. Table 3-1 defines the anatomical landmarks and instrumentation used to measure participant anthropometrics.

Table 3-1: *Summary of anthropometric measures taken*

Anthropometric Measure	**Anatomical Landmarks**	**Instrumentation**
Height	Ground to top of head when standing upright	Standing weight scale with height rod
Weight		Standing weight scale with height rod
Maximal Thigh Circumference	Widest section of thigh	Measuring tape
Distal Thigh Circumference	90% of the distance from the greater trochanter to the lateral femoral condyle going distally	Measuring tape
Maximal Calf Circumference	Widest section of calf	Measuring tape
Proximal Calf Circumference	10% of the distance from the lateral tibial plateau to lateral malleolus	Measuring tape

The knee joint centre was assumed to be the midpoint between the medial and lateral epicondyles of the femur, measured by bony landmark digitization (Grood & Suntay, 1983). The midpoint of the participant's popliteal crease was approximated and digitized. The distance from the knee joint centre to the popliteal crease for each participant was calculated from a standing reference trial using Visual 3D V 4.85.0 (C-Motion Inc., Germantown), defined as the distance from the modeled knee joint centre to the digitized point on the popliteal crease in the tibial coordinate system. Knee flexion angles were measured unilaterally on the participant's dominant leg using an optoelectronic motion capture system with six 3-camera position sensors (Northern Digital Incorporated, Waterloo, ON). The dominant leg was determined by asking the participant to step forward (Velotta et al., 2011). Infrared marker clusters, consisting of 5 markers, were secured to the participant's foot, shank, and thigh on the dominant leg, and pelvis. Bony landmarks on each segment were digitized relative to the segment marker cluster and were used to define segment coordinate systems. The boney landmarks digitized relative to the pelvis were left and right ASIS, left and right PSIS and left and right iliac crest and the greater trochanter of the non-dominant femur. Landmarks digitized on the dominant femur were the greater trochanter and medial and lateral epicondyles of the femur. Landmarks digitized on the shank were lateral and medial tibial plateau and, lateral and medial malleolus. Landmarks digitized on the foot were lateral and medial malleolus, calcaneus and the 1st and 5th metatarsals. The motion data were collected at a frequency of 60Hz using First Principles Software (Northern Digital Inc., Waterloo, ON).

The distribution of contact pressure between the thigh and calf were measured using the Tekscan Conformat pressure mapping sensor (Model#5315, Tekscan, Boston, MA). The

measurable pressure range was 0.1-15 psi (0.7-103.4 kPa), which is larger than the range used in previous work (Zelle et al., 2007), which was 0.1-5 psi (0.7-34.5 kPa). The dimensions of the pressure mat were 0.62m x 0.53m, with the sensors covering an area 62.2 cmx 52.9 cm. The pressure mat was secured to the participant's popliteal crease on the back of the knee using adhesive in such a way that it reduced possible movement while minimizing the folding of the pressure mapping sensor (Figure 3-1).

Figure 3-1: Experimental set-up used in this investigation. The pelvis, thigh, shank and foot marker clusters are visible as well as the pressure mat attached just below the popliteal crease on the participant's calf.

The pressure mat sensor elements ("sensels") are arranged into 42 rows along the *x*-axis and 48 columns along the *y*-axis (sensel area: 103.23 mm^2). The *y*-axis of the pressure mat was aligned with the long axis of the tibia when the participant was in full flexion with the assumption that the mat stayed aligned in this way. This assumption was confirmed by tracing the active sensels, using the ISCAN software (ISCAN v3.820, Tekscan, Boston, MA), during the first trial of each activity for each participant while the participant was in full flexion. The full flexion pressure tracing was then compared to subsequent trials to determine if contact area a full

flexion was consistent across trials. Due to the location of the ribbon strip computer input cable, the pressure mat was secured to the participant's popliteal crease so that the mid-point of the back of the knee was around sensel (30, 48). A visual representation of the IPM as well as a reference location of anatomical landmarks can be found in Figure 3-2.

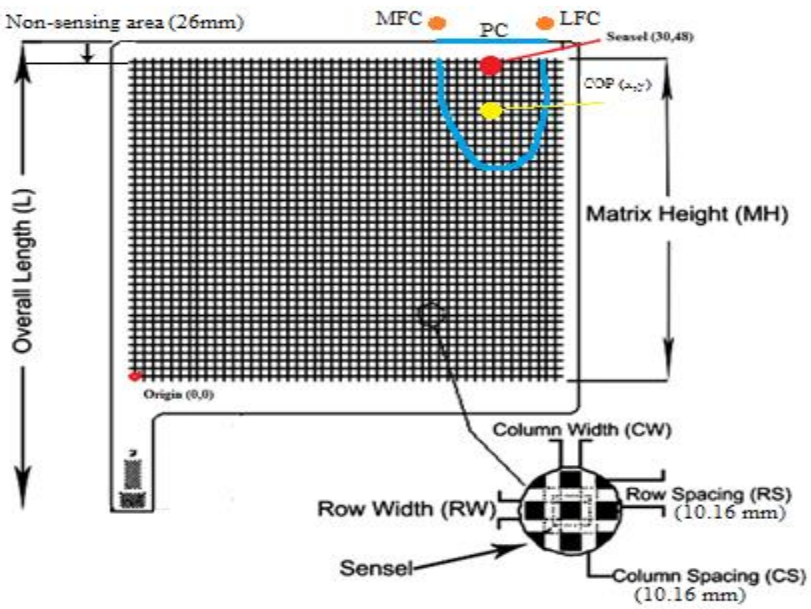

Figure 3-2: Depiction of Tekscan Conformat sensel array (Tekscan, Inc. Boston, MA) showing Sensel (0,0), the origin, and Sensel (30,48) which is the location of centre of the popliteal crease (PC). The light blue outline is a representation of thigh-calf contact area at full-flexion. MFC and LFC are the medial and lateral femoral condyles and the non-sensing area, represented by the white ring around the matrix, extends 2.6cm from the popliteal crease to the top column of sensels. COP is a general representation of the location of the centre of pressure at full-flexion.

Thigh-calf pressure distribution was collected at 60 Hz. The pressure mapping and motion tracking systems were synchronized via an external trigger device which signaled both systems to start recording. In pilot testing, a force was applied to the mat using a force transducer (Chatillion CDS 200, AMTEK Test & Calibration Instruments, Largo, Florida, U.S.A.) with an analog output, which was collected using the same software and same sampling frequency as would be used to collect the kinematic data (60 Hz, First Principles, Northern Digital Inc., Waterloo, ON). During pilot testing, it was noted that there was a variable difference in

magnitude and a delay between the Tekscan Conformat pressure mapping system output data and the start-pulse synchronized force transducer output from First Principles software. In order to determine the agreement between the force output from the force transducer and the force output from the pressure mapping sensor, a limits of agreement method was used on pilot data (Altman and Bland, 1983; Bland and Altman, 1986). Limits of Agreement (LoA) methods are used to determine agreement between different methods measuring the same quantity (Bland and Altman, 1992). For LoA methodology and results, refer to *Appendix B.* Since the difference between the force transducer and IPM data was variable, it could not be corrected for. However, the LoA provides an estimate of the range of differences that can be expected between the IPM-measured force and the actual force applied. The 95% limits of agreement for the difference in force output between the force transducer and the IPM system were estimated to be -39.4 to 40.3 N.

The delay between the force transducer and the IPM system was characterized during pilot testing through the analysis of multiple trials of force being applied to the Tekscan Conformat pressure mapping system (Tekscan Inc., Boston, MA) using a force transducer via a curved platen (Chatillion CDS 200 Dynamometer, AMTEK Test & Calibration Instruments, Florida, U.S.A.). These trials were all similar to what would have been expected in the actual experiment in terms of load profile. The applied force and the IPM output from each of the trials are shown in *Appendix C*. The time delay during the pilot trials was not uniform and varied between trials from 28 frames to 31 frames.

During actual thigh-calf contact force data collections, the force transducer was applied to the IPM system, attached to the participant's calf, during each trial before the deep flexion movement. The delay for each trial was calculated between the output from the force transducer

and the IPM. This was done by cross correlating the force transducer output and the IPM output. The calculated delay was then applied to the thigh-calf contact force measured by the IPM during squatting or kneeling by shifting the IPM output backwards by the calculated number of frames. In order to determine if the delay changed through a trial, the protocol with the force transducer was slightly altered for 13 participants from the study population and the force transducer was applied to the IPM system before and after the deep flexion movement. The delays calculated from the force transducer application before and after the deep flexion movement were compared and varied by no more than one frame.

Participants performed three randomized trials of three activities: squatting, dorsi-flexed kneeling and plantar-flexed kneeling (Figure 3-3). The squatting activity was performed with the participant descending from an erect standing posture (Figure 3-3a) to a squatting posture with the participant's heels up and mass balanced over the balls of the feet (Figure 3-3b). Two kneeling activities were performed by descending from an erect kneeling position (Figure 3-3c) to a deep kneeling posture with ankles plantar-flexed (Figure 3-3d) or with the ankles dorsi-flexed (Figure 3-3e).

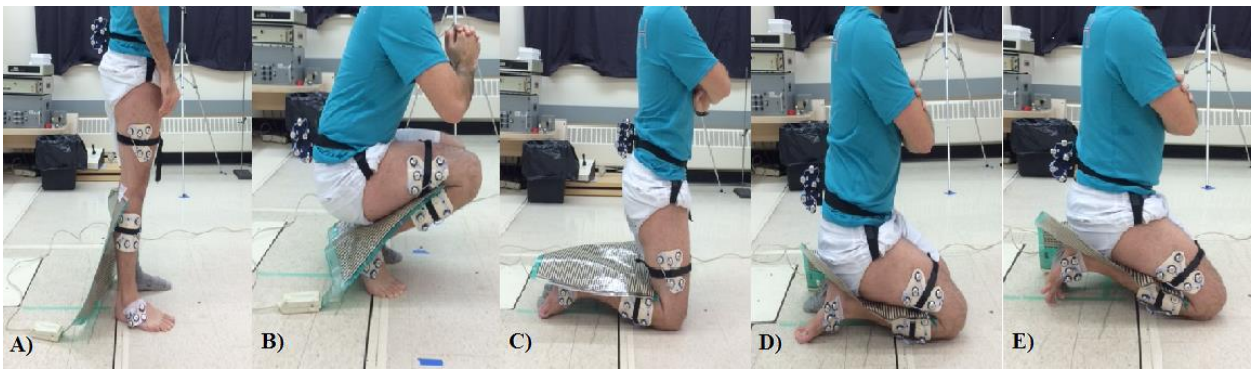

Figure 3-3: (A,B) Standing (A) to squatting (B) progression with pressure mapping sensor attached via adhesive just below the participant's popliteal crease. (C,D,E) Upright kneeling (C) to either full-flexion plantar-flexed kneeling (D) or full-flexion dorsi-flexed kneeling (E).

3.4 Data analysis

Visual 3D V 4.85.0 (C-Motion Inc., Germantown, Maryland, USA) was used for filtering and knee joint angle calculation. Raw kinematic data was filtered using a second-order, low-pass Butterworth filter (dual-passed to create a fourth-order filter with zero phase shift) with an upper cutoff frequency of 6 Hz (Winter et al., 1990). Missing data points were interpolated using a third-order cubic spline in order to fit the missing frames of data up to a maximum of 10 frames (Howarth & Callaghan, 2010).

A rigid link model was created with pelvis, thigh, shank and foot segments. The thigh and shank segments were used to calculate knee joint angles from the kinematic data. The proximal radius of the thigh was defined as a quarter of the distance between the femoral greater trochanters. The thigh coordinate system was defined proximally using the greater trochanter of the dominant leg and the proximal radius of the thigh which is defined using Visual 3D V 4.85.0 (C-Motion Inc., Germantown, Maryland, USA) as a quarter of the distance between the iliac crests of the pelvis. Distally the thigh was defined by the medial and lateral femoral condyles. The positive z-axis was defined as a vector pointing proximally from the midpoint between the medial and lateral femoral condyles to the hip joint center, also defined in Visual 3D V 4.85.0 (C-Motion Inc., Germantown, Maryland, USA) as a quarter of the distance between the iliac crests of the pelvis measured along the x-axis from the greater trochanter of the right thigh. The frontal plane was defined by the z-axis and the line formed between the lateral and medial femoral condyles. The positive y-axis was defined by a normal to the frontal plane, pointing anteriorly, and the positive x-axis was defined by the cross product of the y- and z-axes, pointing

laterally on the right leg. The shank coordinate system was defined proximally by the lateral and medial tibial condyles and distally by the lateral and medial malleoli. The z-axis was defined as a vector from the midpoint between the lateral and medial malleoli to the midpoint between the tibial condyles. The y-axis was defined by a normal to the z-axis, and the x-axis was defined by the cross product of the y- and z-axes. The x-axis was again defined as the cross product of the y- and z-axes. For the shank, positive *z* points proximally, positive *y* points anteriorly and positive *x* points laterally on the right leg. Knee joint angle rotations were described using a Cardan sequence of rotation (x,y,z) of the tibia with respect to the femur, where z is proximal/distal with positive pointing proximal, y axis is in the anterior/posterior direction, positive pointing anteriorly, and x axis is medial/lateral, positive pointing laterally on the right leg (Yeadon, 1990; Davis et al., 1991; Kadaba et al., 1990).

An IScan Pressure Measurement System (ISCAN v3.820, Tekscan, Boston, MA) was used to measure contact force, area, and centre of pressure on the pressure mat. The pressure mapping system used in this investigation has a 2.6 cm non-sensing ring surrounding the outside of the sensing area. The starting angle of thigh-calf contact was defined as the flexion angle at which contact appeared in the first row of sensels and was over 5 mmHg (0.7 kPa) (Stinson et al., 2002). The raw output from the pressure mapping system is expressed as the total force for each data collection frame. Thigh-calf contact force was calculated by the ISCAN software using Equation 3-1. For the purposes of this investigation only the data from participants descending from an erect into a fully flexed position were used:

Equation 3-1: $(F_{TC})_f = (\sum_{i=1}^{n}(S_a(P_i)_f))/BM$

P_i represents the pressure reading in each individual sensor from P_1 to P_n with n being the number of sensors in the contact area enclosed by the full flexion pressure tracing. S_a represents the surface area of an individual sensor, BM demotes participant body mass and f denotes frame number in Equation 3-1. Thigh-calf contact force was divided by (normalized to) each participant's body mass in order to reduce variability in thigh-calf contact force for the purposes of modeling and to be able to compare thigh-calf contact force values from this investigation to those calculated in other studies.

The centre of pressure of thigh-calf contact force along the y-axis of the tibia (COP) was determined in a two-step procedure. Centre of pressure coordinates on the pressure mat (X,Y) in sensels, were determined in the ISCAN software (ISCAN v3.820, Tekscan, Boston, MA) using Equation 3-2. While this equation does calculate centre of pressure, only force values are used because, in order to calculate pressure, the force values would each be multiplied by the area of a sensel. Since all sensels have the same area, every term in this equation would include the sensel area, and the common factor of sensel area in the numerator would be cancelled by the common factor of sensel area in the denominator. The origin (0,0) is the first row/column of sensor elements.

Equation 3-2: $X = \frac{\sum_{i=0}^{C-1}(i*\sum_{j=0}^{R-1}F_{ij})}{\sum_{i=0}^{C-1}(\sum_{j=0}^{R-1}F_{ij})} \qquad Y = \frac{\sum_{i=0}^{R-1}(i*\sum_{j=0}^{C-1}F_{ij})}{\sum_{i=0}^{R-1}(\sum_{j=0}^{C-1}F_{ij})}$

Where:

X = the (x) coordinate, in sensels, of the centre of pressure from the origin.

Y = the (y) coordinate, in sensels, of the centre of pressure from the origin.

i = the (x) coordinate, in sensels, of a sensel from the origin.

j = the (y) coordinate, in sensels, of a sensel from the origin.

F_{ij} = Force at each sensel (i,j) within the contact area enclosed by the full flexion pressure tracing

C= Total number of columns (on pressure mat)

R= Total number of rows (on pressure mat)

The Y-coordinate of the centre of pressure for each frame, calculated from Equation 3-2, was then subtracted from 48, in order to calculate the distance in sensels along the tibia from the edge of the sensels to the centre of pressure. This distance in sensels was then multiplied by 1.016cm, the width of a sensel, in order to get this distance in centimeters. The sum of this distance, the distance from the knee joint centre to the popliteal crease, and the length of the non-sensing area, 2.6cm surrounding the sensing matrix (Figure 3-2), was calculated.. This sum represented the distance from the joint centre to the centre of pressure in the direction of the y-axis of the pressure mat, which was approximately parallel to the z-axis of the tibia.

Thigh-calf contact force and COP were presented with respect to flexion angle. In order to reduce variability of the flexion angles corresponding to a given thigh-calf contact force or centre of pressure location, and to aid in fitting an equation to the data, flexion angles normalized to a percentage of the flexion range between the start of thigh-calf contact and maximal flexion ("percent flexion range after contact"). The trial mean curves were averaged to create one mean curve per participant for each activity. Participant mean curves were averaged in order to obtain one mean curve per activity. For thigh-calf contact force and COP, individual participant mean curves were used to obtain an overall mean curve and standard deviations for each activity. An exponential curve was then fit to the overall mean curves for thigh-calf contact force for each activity. For COP, a line of best fit was determined. The criterion that was used to determine the best fitting line was the line that minimized the sum of the squared errors of prediction.

The maximum total thigh-calf contact force, centre of pressure (COP) at maximum total force, flexion angle at maximum total force, and the starting angle of thigh-calf contact were identified for each individual trial. These outcome measures were then averaged across participant trials for each of the three activities to get four parameter means per activity per participant.

3.4.1 Knee joint reaction forces, net joint moments, and joint contact force

To determine the potential effect of thigh-calf contact forces measured in this study on tibiofemoral joint contact forces, force and motion data from a full-flexion, static, squatting trial from a single participant (from a previous study where thigh-calf contact was not measured) were used. A rigid link segment model was developed in Visual 3D V 4.85.0 (C-Motion Inc., Germantown, Maryland, USA). Ankle forces and moments were calculated using Visual 3D V 4.85.0 (C-Motion Inc., Germantown, Maryland, USA) in the shank coordinate system and were subsequently used to create free body diagrams (see Figure 3-4) that included thigh-calf contact. These free-body diagrams were used to calculate knee joint reaction forces and moments both with and without the addition of thigh-calf contact into the model. For the free body diagram calculations please refer to *Appendix E.* For Figure 3-4, *Rz* and *Ry* represent the *y* and *z* components of the ground reaction force, *Raz* and *Ray* represent the *y* and *z* components of the reaction force at the ankle, *Rkz* and *Rky* represent the *y* and *z* components of the reaction force at the knee, *Max* represents the net joint moment about the ankle, *Mkx* represents the net joint moment about the knee, F_{TC} and *COP* represent thigh-calf contact force and it's corresponding distance from the knee joint center along the z-axis of the tibia, and *Ms* represents the mass of the shank. Joint reaction force components are drawn in directions corresponding to the *y* and z

axes of the shank. In calculations based on these free body diagrams, a negative calculated force or moment indicated that the force or moment acted in a direction opposite of the direction drawn in the diagram.

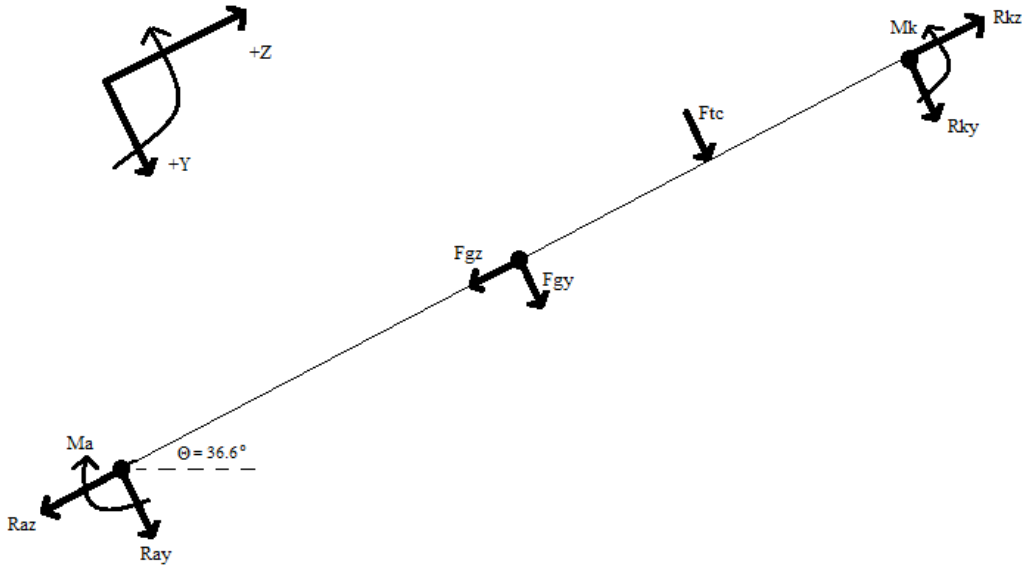

Figure 3-4: Free body diagram of the shank during squatting at full flexion. Ground reaction forces and ankle and knee joint reaction forces and net joint moments are drawn in the anatomical coordinate system of the shank.

The centre of mass location and mass of the shank and foot were determined in Visual 3D V 4.85.0 (C-Motion Inc., Germantown, Maryland, USA) using equations from Dempster and Gaughran (1967). The joint center of the knee was defined as the mid-point between the femoral condyles and joint center of the ankle was defined as the midpoint between the malleoli. Thigh-calf contact force was modeled as resultant force whose line of action was in the anterior (+Y) direction of the shank. The location of this force was determined from the calculated average centre of pressure at maximum total thigh-calf contact force. An estimate of the quadriceps muscle force both with and without the incorporation of thigh-calf contact into the model was calculated by dividing the calculated knee joint moment by the estimated moment arm of the

knee joint extensors, 5.91cm (Herzog, W. & Read, L.J., 1993). Knee joint contact force was calculated as reaction forces at the knee minus the quadriceps muscle force.

3.5 Statistical Analysis

Four two-way (3 activities x 2 sexes) ANOVAs were used to compare the mean values for maximum total thigh-calf contact force (in N/kg), centre of pressure at maximum total force (in cm), flexion angle at maximum total force (in degrees) and the starting angle of thigh-calf contact (in degrees) between sexes (2 levels: male, female) and between activities (3 levels: squatting; dorsi-flexed kneeling and plantar-flexed kneeling). A *post-hoc* Tukey test was run to determine which activities were significantly different from others. P-values were corrected for multiple tests using a Bonferroni correction. Statistical significance was defined by an adjusted p-value (the calculated p-value multiplied by 4 as that was the number of outcome parameters) less than 0.05.

Pearson product-moment correlation coefficients (R) were calculated in order to investigate the relationship between the anthropometric measures (maximal thigh circumference; distal thigh circumference; proximal calf circumference; maximal calf circumference; height) and the four outcome parameters (maximum total thigh-calf contact force, location of the centre of pressure at maximum total thigh-calf contact force, flexion angle at maximum total thigh-calf contact force and starting angle of thigh-calf contact). P-values were corrected for multiple tests using a Bonferroni correction and statistical significance was defined by an adjusted p-value (the calculated p-value multiplied by 4 as that was the number of outcome parameters) less than 0.05.

In cases where a linear relationship between an outcome parameter and an anthropometric measure did not exist, the relationship between the slope of the logarithm of the maximum total thigh-calf contact force and the anthropometric measures were also investigated; however R values between the slope of the logarithm of the maximum total thigh-calf contact force and anthropometric measures were very low in all investigated cases.

3.5.1 Predictive Modeling: Stepwise Linear Regression

In cases where the R value exceeded 0.5 for one or more of the anthropometric measures for a given outcome parameter, predictive modeling of the outcome parameter based on anthropometric measures was pursued. Data from 20 randomly selected participants (10 female and 10 male) for model development. Of those selected for model development the mean age of the participants was 27.4 years (S.D. 7.53 years), the mean height was 171.8 cm (S.D. 7.7 cm, Male: 175.8 cm, S.D. 7.8 cm; Female: 165.9 cm, S.D. 4.8 cm), the mean mass was 75.9 kg (S.D.14.7 kg, Male: 82.1 kg, S.D. 10.2; Female: 70.9 kg, S.D. 6.8 kg). External validation was performed on 10 additional participants (6 males and 4 females) not included in the creation of the prediction models. Measured outcome measures were compared to predicted values for these ten participants use root mean squared error (RMSE) and R^2 values.

Multivariate linear regression with forward stepwise selection was used to develop predictive equations. Covariates had to meet the 0.5 significant level for entry into the regression model. Covariates that were candidates for inclusion in the models were: maximal thigh circumference; distal thigh circumference; proximal calf circumference; maximal calf circumference; height; and sex. In multivariate regressions, maximum total thigh-calf contact force, COP at maximum total thigh-calf contact force, and the starting angle of thigh-calf contact

were the dependent variables. Anthropometric parameters and sex were the independent variables.

4. Results

The results of this study are organized as follows. First, curves for the thigh-calf contact force (section 4.1, Figure 4-1) and center of pressure (section 4.2, Figure 4-2) are presented for the full flexion range during thigh-calf contact. Mean values of the four thigh-calf contact parameters are then presented (section 4.3, Table 4-1). These are the values that were used in analyses of variance. The remainder of the results section is then divided by parameter, presenting the ANOVA results (sections 4.4.1, 4.5.1, 4.6.1, 4.7.1) and the correlations with anthropometric measures (sections 4.4.2, 4.5.2, 4.6.2, 4.7.2) for each of the four thigh-calf contact parameters separately. Section 4.8 shows the results from the stepwise linear regression models for the starting angle of thigh-calf contact during squatting and dorsi-flexion kneeling (Figure 4-19) and section 4.9 details the effect of thigh-calf contact force on tibiofemoral joint contact force.

4.1 Thigh-Calf Contact Force as a Function of Percent Flexion Range after Contact

Similar to the results found by Zelle et al. (2007), thigh-calf contact force increased exponentially with increasing knee flexion angles.

Figure 4-1 shows the average thigh-calf contact force curve for each participant for squatting, dorsi-flexed and plantar-flexed kneeling as a function of percent flexion range after contact. In order to reduce the variability in flexion angles that corresponded to a given level of force, the flexion angle was expressed as a percentage of the range of flexion angles between the starting angle of thigh-calf contact and the flexion angle at maximum total thigh-calf contact force ("percent flexion range after contact"). The equation presented on the graphs are the exponential equation fitted to the mean curve for each activity. For the average thigh-calf contact

force curve for each participant for squatting, dorsi-flexed and plantar-flexed kneeling as a function of flexion angle, please refer to *Appendix C*.

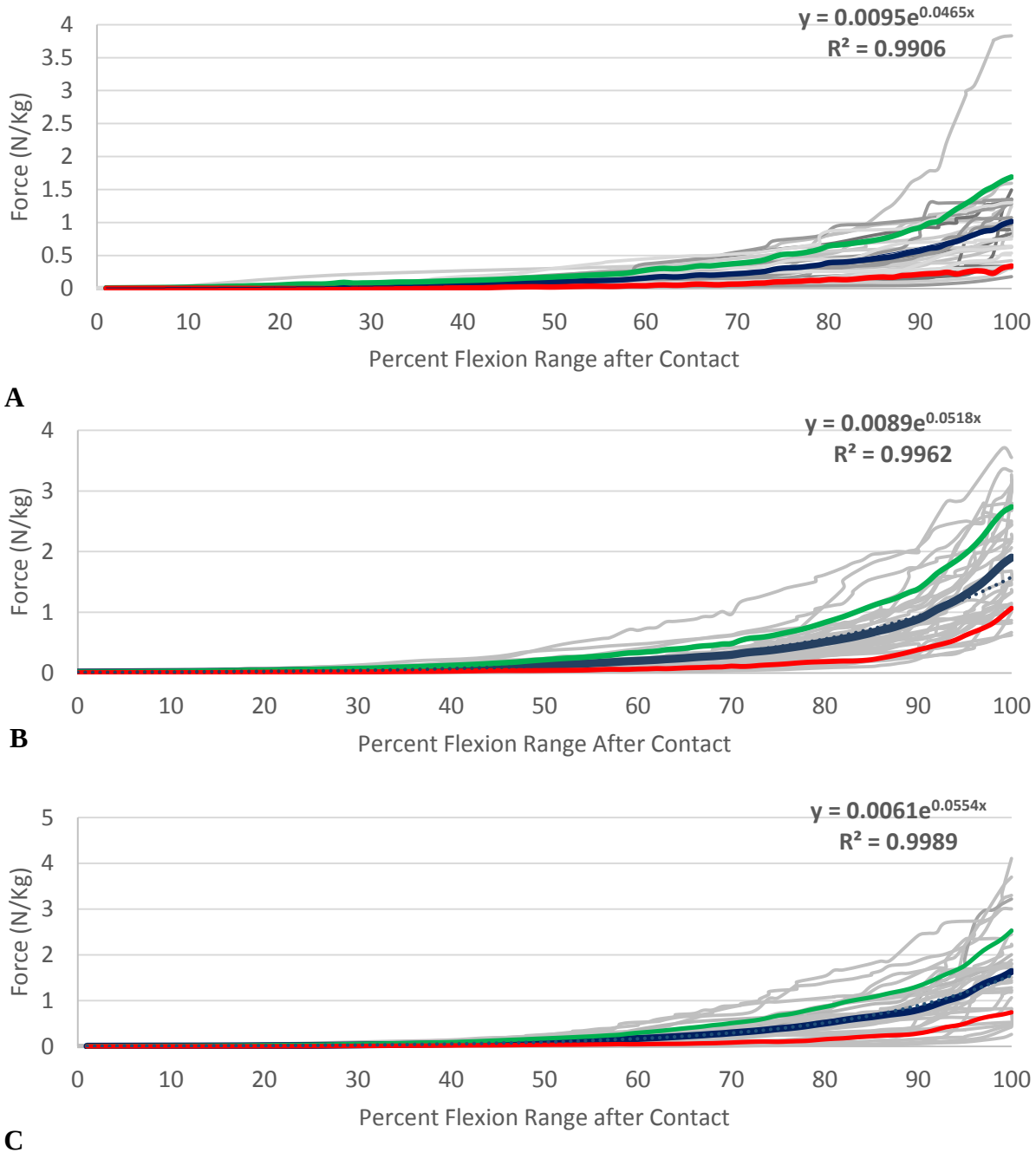

Figure 4-1: Thigh-calf contact force for squatting (A), dorsi-flexed kneeling (B), and plantar-flexed kneeling (C) for the full range of flexion expressed as a percent of the flexion range. Individual grey lines represent the average thigh-calf contact force curve for individual participants for each activity, whereas the thick blue line shows the average relationship between thigh-calf contact force and percent flexion range after contact. The green and red lines represent +/-1 standard deviation from the average. The equation and R^2 presented on the graphs are the exponential equation, represented by the dotted navy line, fitted to the mean curve for each activity.

4.2 Center of Pressure as a Function of Percent Flexion Range after Contact

The average location of the centre of pressure of the thigh-calf contact force, measured distally along the long-axis of the tibia from the epicondylar axis, for all participants during the squatting and kneeling activities are shown in Figure 4-2. In general, thigh-calf contact force, and as a result the centre of pressure, originated close to the epicondylar axis and then traveled distally along the long axis of the tibia with increasing flexion angle. For some participants, thigh-calf contact force originated closer to the muscle belly of the calf and then fluctuated along the long axis of the tibia.

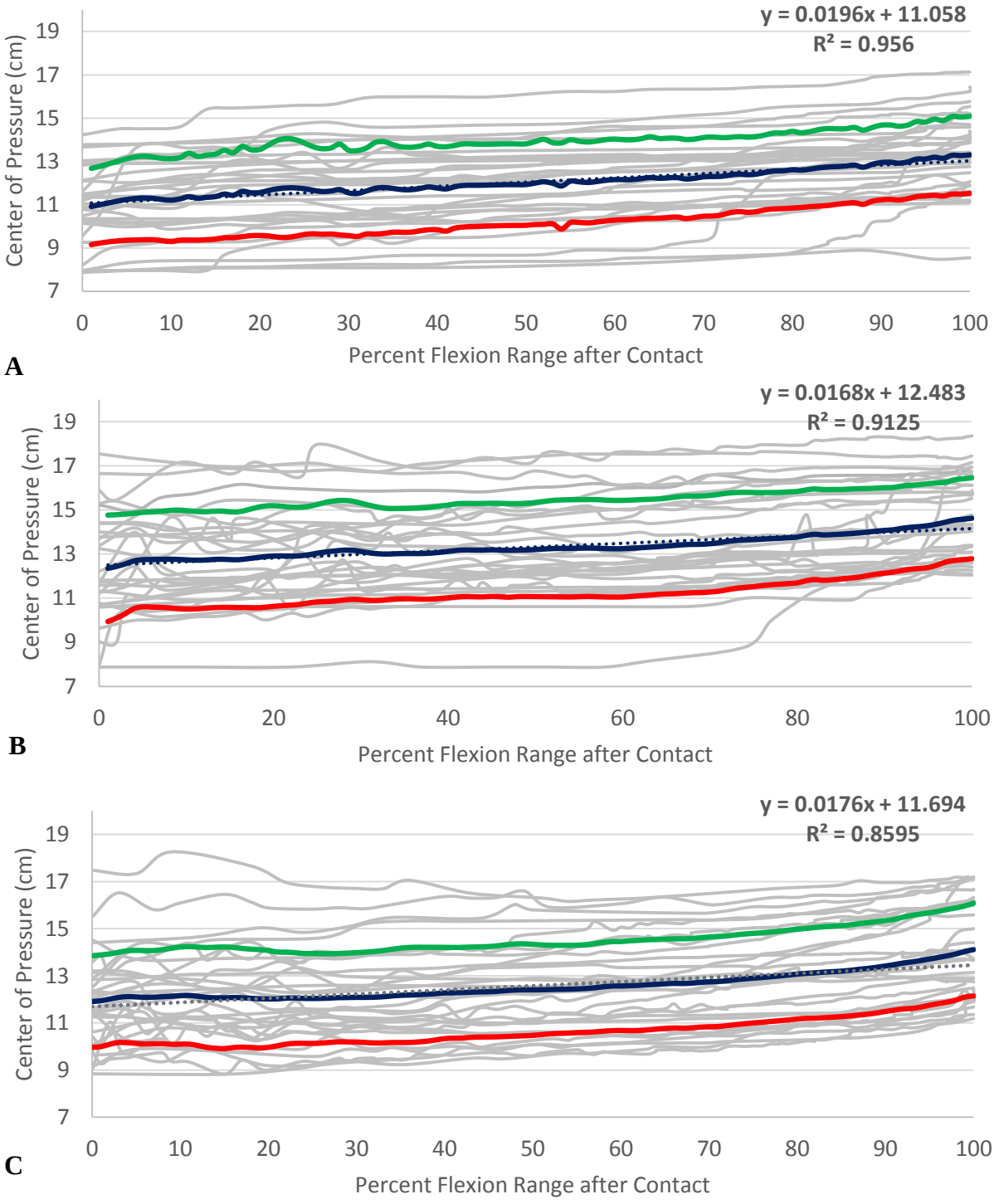

Figure 4-2 Average location of thigh-calf contact force (COP) for all participants after the start of thigh-calf contact during (A) squatting, (B) dorsi-flexed and (C) plantar-flexed kneeling represented in terms percent flexion range after contact. Individual grey lines represent the average center of pressure for individual participants for each activity, whereas the thick blue line shows the average relationship between centre of pressure and percent flexion range after contact. The green and red lines represent +/-1 standard deviation from the average. The equation and R^2 presented on the graphs are the exponential equation, represented by the dotted navy line, fitted to the mean curve for each activity.

Section 4.3 Average Thigh-Calf Contact Force Characteristics

Table 4-1 depicts the average thigh-calf contact characteristics for all participants with thigh-calf contact force being normalized to body mass.

***Table 4-1**: Average thigh-calf contact characteristics for all participants. Standard deviations are expressed in brackets.*

Event	**At Start of Thigh-Calf Contact**		**At Total Maximal Thigh-Calf Contact Force**					
Outcome Measure	**Flexion angle (º)**		**Flexion angle (°)**		**Normalized Thigh-Calf Contact Force (N/kg)**		**Location of Centre of Pressure* (cm)**	
	Male	**Female**	**Male**	**Female**	**Male**	**Female**	**Male**	**Female**
Squatting	135.5 (4.2)	138.5 (4.3)	146.1 (8.8)	146.8 (7.4)	1.0 (0.5)	1.1 (0.7)	13.9 (1.6)	13.4 (1.5)
Dorsi-flexed kneeling	138.6 (4.4)	140.7 (3.7)	149.2 (8.0)	149.7 (6.8)	1.8 (0.6)	2.1 (0.8)	15.4 (1.8)	14.5 (1.4)
Plantar-flexed kneeling	138.6 (3.4)	140.9 (3.7)	149.4 (7.1)	150.6 (6.8)	2.2 (0.8)	2.2 (0.9)	14.8 (1.9)	14.3 (2.0)
	*The location of the centre of pressure is expressed along the long axis of the tibia with respect to the knee joint centre which was assumed to be the midpoint between the medial and lateral epicondyles of the femur, measured by bony landmark digitization.							

4.4 Maximum Total Thigh-Calf Contact Force

4.4.1 Analysis of Variance for Maximum total Thigh-Calf Contact Force for Sex and Activity

For the maximum total thigh-calf contact force comparisons (Figure 4-3 and Table D-7), the ANOVA showed a main effect of activity ($p < 0.0001$), while there was no significant main effect of sex ($p = 0.41$) and no significant sex-by-activity interaction ($p = 0.76$). The Tukey post-hoc analysis showed that dorsi-flexed and plantar-flexed kneeling were not statistically different, however, there was a significant difference between the squatting activity and both kneeling activities (Table D-8).

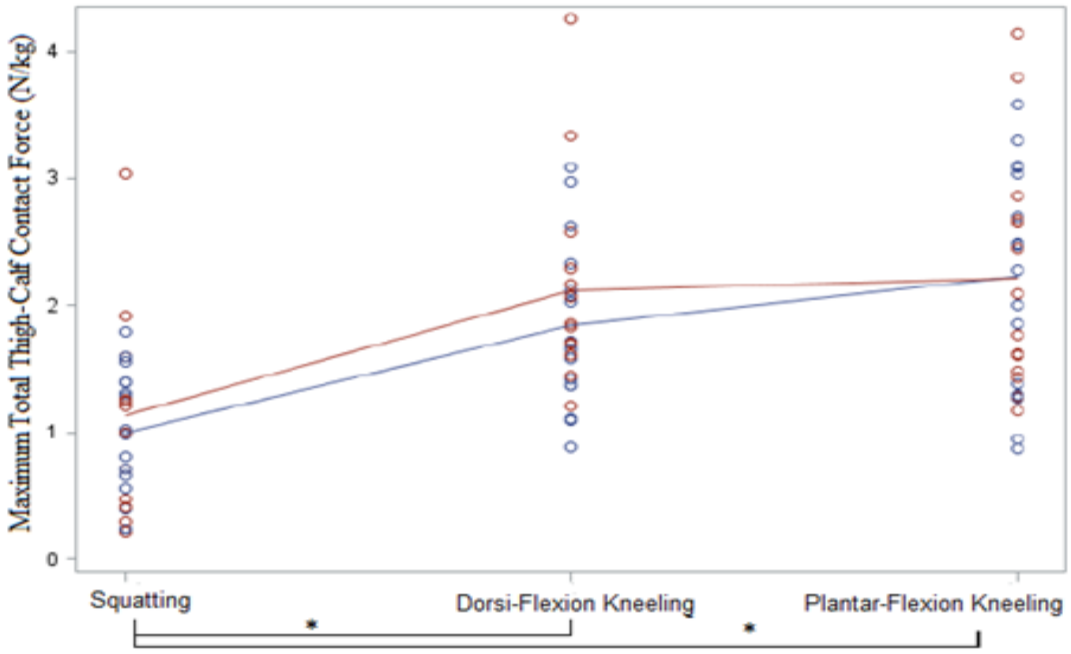

Figure 4-3: Interaction plot for the two-way ANOVA on maximum total thigh-calf contact force (sex x activity). Significant differences between activities are denoted with an asterisk (*).Blue indicates males and red indicates females.

4.4.2 Correlations between Anthropometric Measures and Maximum Total Thigh-Calf Contact Force

For squatting (Figure 4-4) and dorsi-flexed kneeling (Figure 4-5) only height was significantly correlated to maximum total thigh-calf contact force ($p = 0.03$ and $p = 0.04$, respectively). Maximal thigh circumference ($p = 0.03$) and maximal calf circumference ($p = 0.03$) were both significantly positively correlated to maximum total thigh-calf contact force during plantar-flexed kneeling (Figure 4-6).

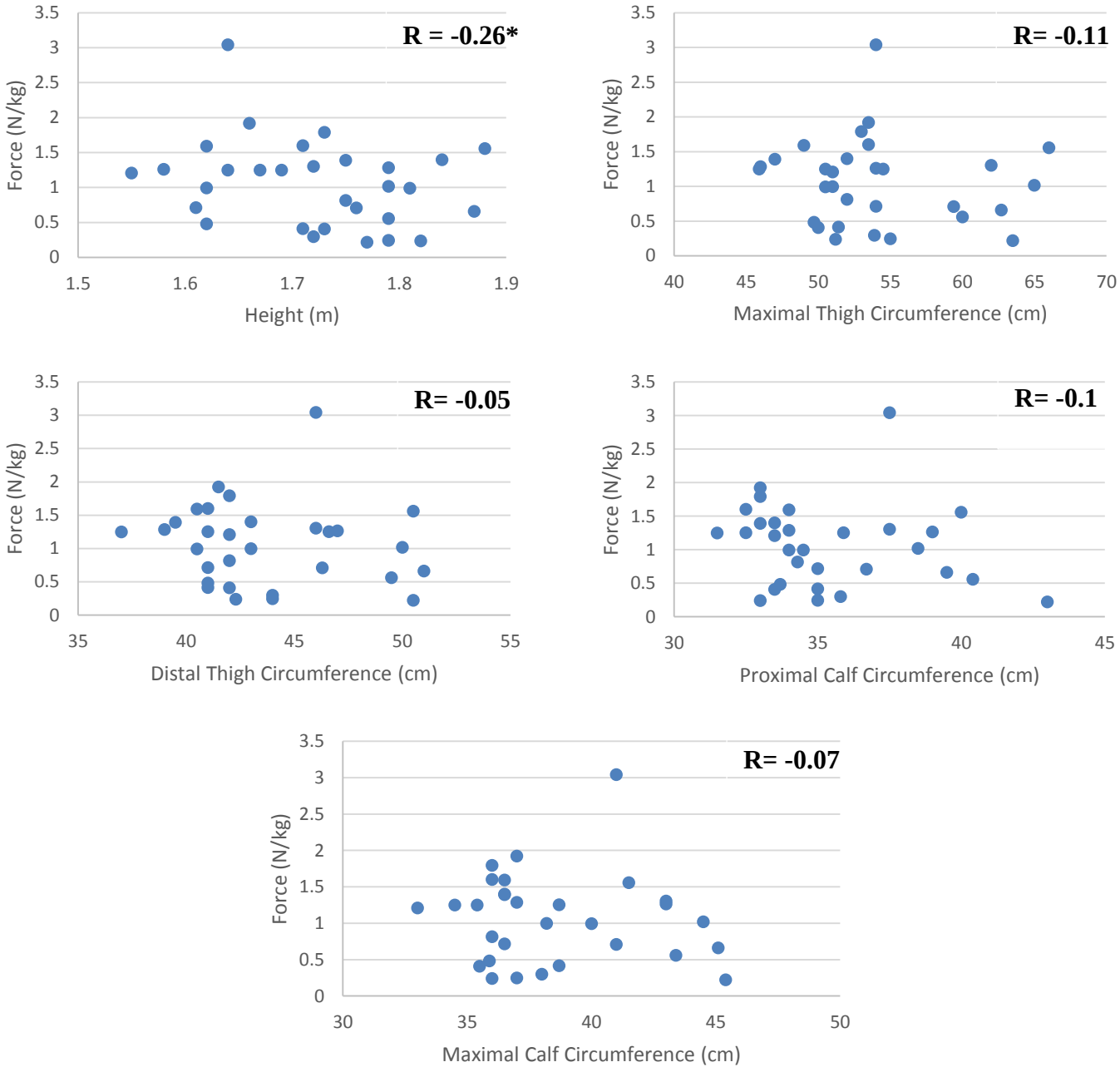

Figure 4-4: Graphs showing the relationship between the anthropometric covariates (maximal thigh circumference, distal thigh circumference, proximal calf circumference, maximal calf circumference and height) and maximum total thigh-calf contact force during squatting. R values are shown in the upper right hand corner of each graph. An asterisk(*) denotes a significant correlation.

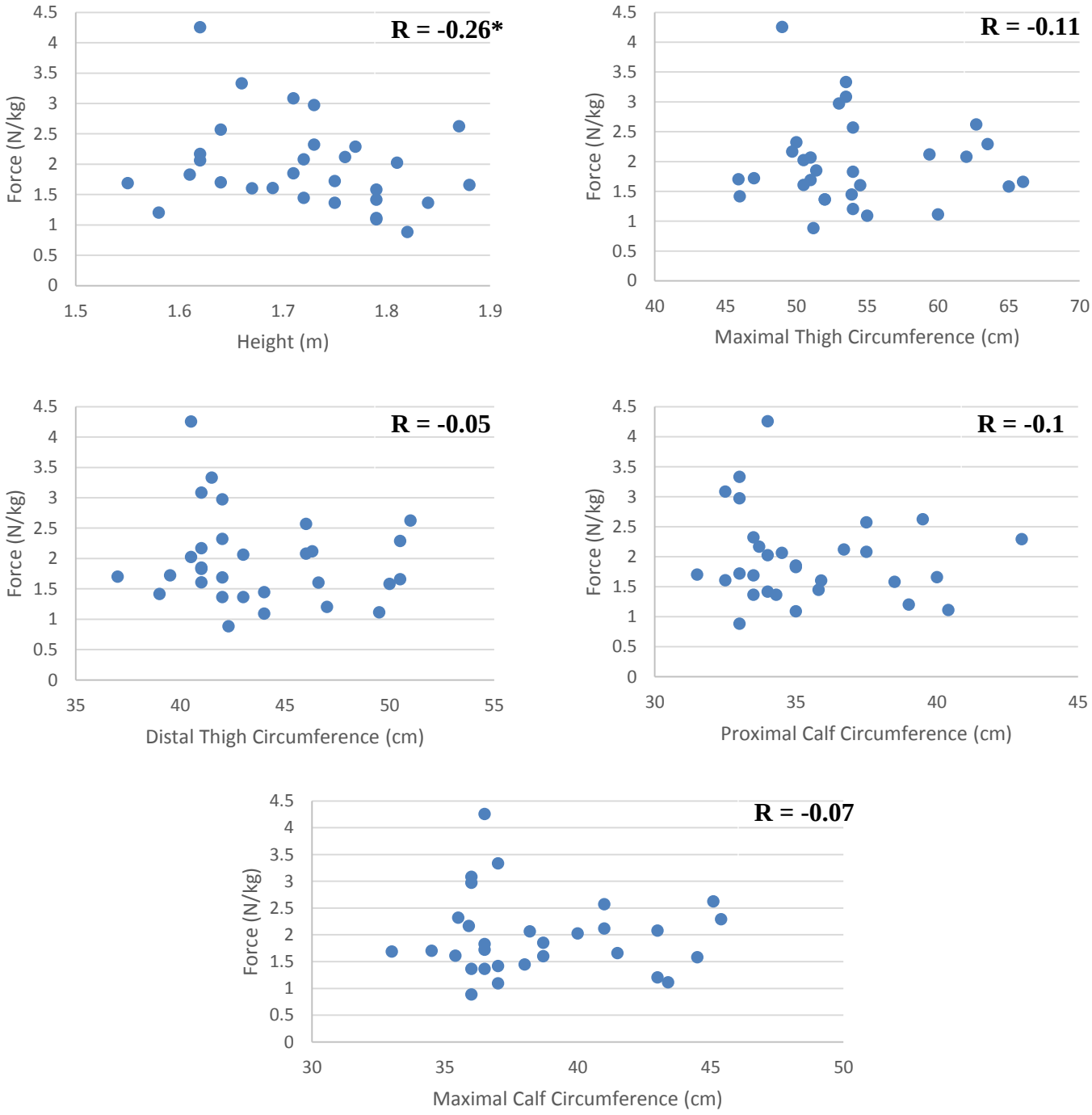

Figure 4-5: Graphs showing the relationship between the anthropometric covariates (maximal thigh circumference, distal thigh circumference, proximal calf circumference, maximal calf circumference and height) and maximum total thigh-calf contact force during dorsi-flexed kneeling. R values are shown in the upper right hand corner of each graph. An asterisk(*) denotes a significant correlation.

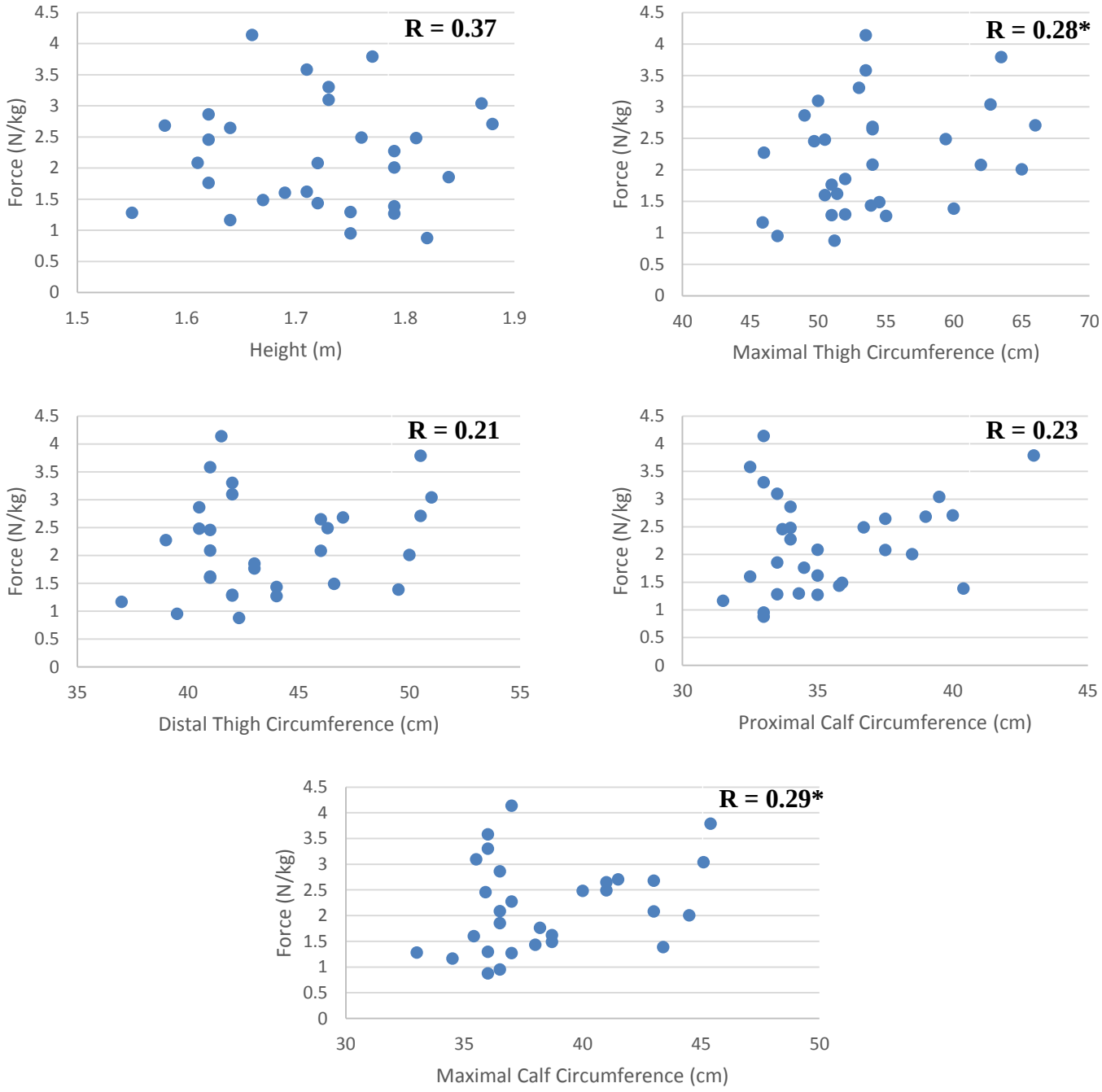

Figure 4-6: Graphs showing the relationship between the anthropometric covariates (maximal thigh circumference, distal thigh circumference, proximal calf circumference, maximal calf circumference and height) with maximum total thigh-calf contact force during plantar-flexed kneeling. R values are shown in the upper right hand corner of each graph. An asterisk(*) denotes a significant correlation.

4.5 Center of Pressure at Maximum Total Thigh-Calf Contact Force

4.5.1 Analysis of Variance for Center of Pressure at Maximum Total Thigh-Calf Contact Force for sex and activity

For the centre of pressure at maximum total thigh-calf contact force (Figure 4-7 and Table D-3) the ANOVA showed a main effect of activity ($p = 0.04$), while there was no significant main effect of sex ($p = 0.41$) and no significant sex-by-activity interaction ($p = 0.86$) (see Table D-3). The Tukey post-hoc analysis showed that dorsi-flexed and plantar-flexed kneeling were not statistically different. However, there was a significant difference between the squatting activity and both kneeling activities (Table D-4). Figure 4-7 shows the interaction plot for the ANOVA on the center of pressure at maximum total thigh-calf contact force. Significant differences found in the post-hoc analysis are denoted with an asterisk (*).

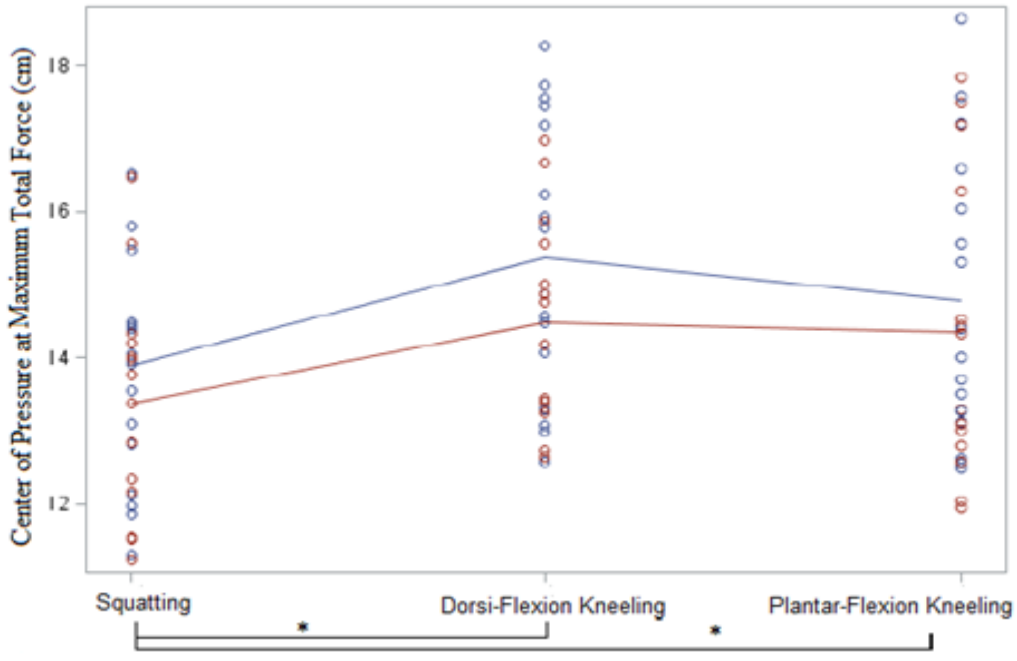

Figure 4-7: Interaction plot for the two-way ANOVA on center of pressure at maximum total thigh-calf contact force (sex x activity). Significant differences between activities are denoted with an asterisk (*).Blue indicates males and red indicates females.

4.5.2 Correlations with Anthropometric Measures and Center of Pressure at Maximum total Thigh-Calf Contact Force

The correlations and R values for the anthropometric covariates and center of pressure at maximum total thigh-calf contact force are displayed for squatting in Figure 4-8, dorsi-flexed kneeling in Figure 4-9 and plantar-flexed kneeling in Figure 4-10. For all activities, no anthropometric covariates measured were significantly correlated to COP except for height during plantar-flexed kneeling.

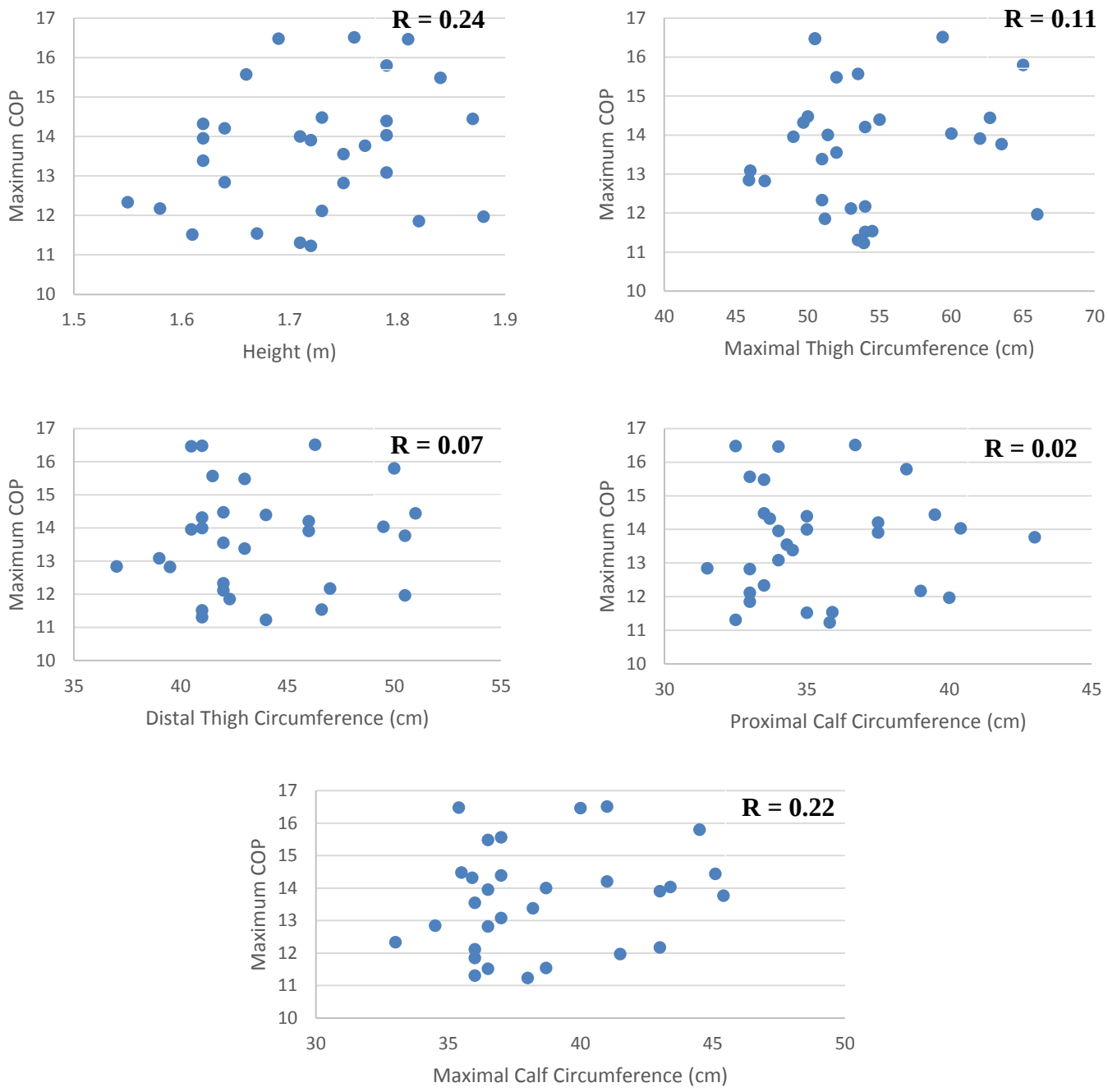

Figure 4-8: Graphs showing the relationship between the anthropometric covariates (maximal thigh circumference, distal thigh circumference, proximal calf circumference, maximal calf circumference and height) and center of pressure at maximum total thigh-calf contact force during squatting. R values are shown in the upper right hand corner of each graph. An asterisk(*) denotes a significant correlation.

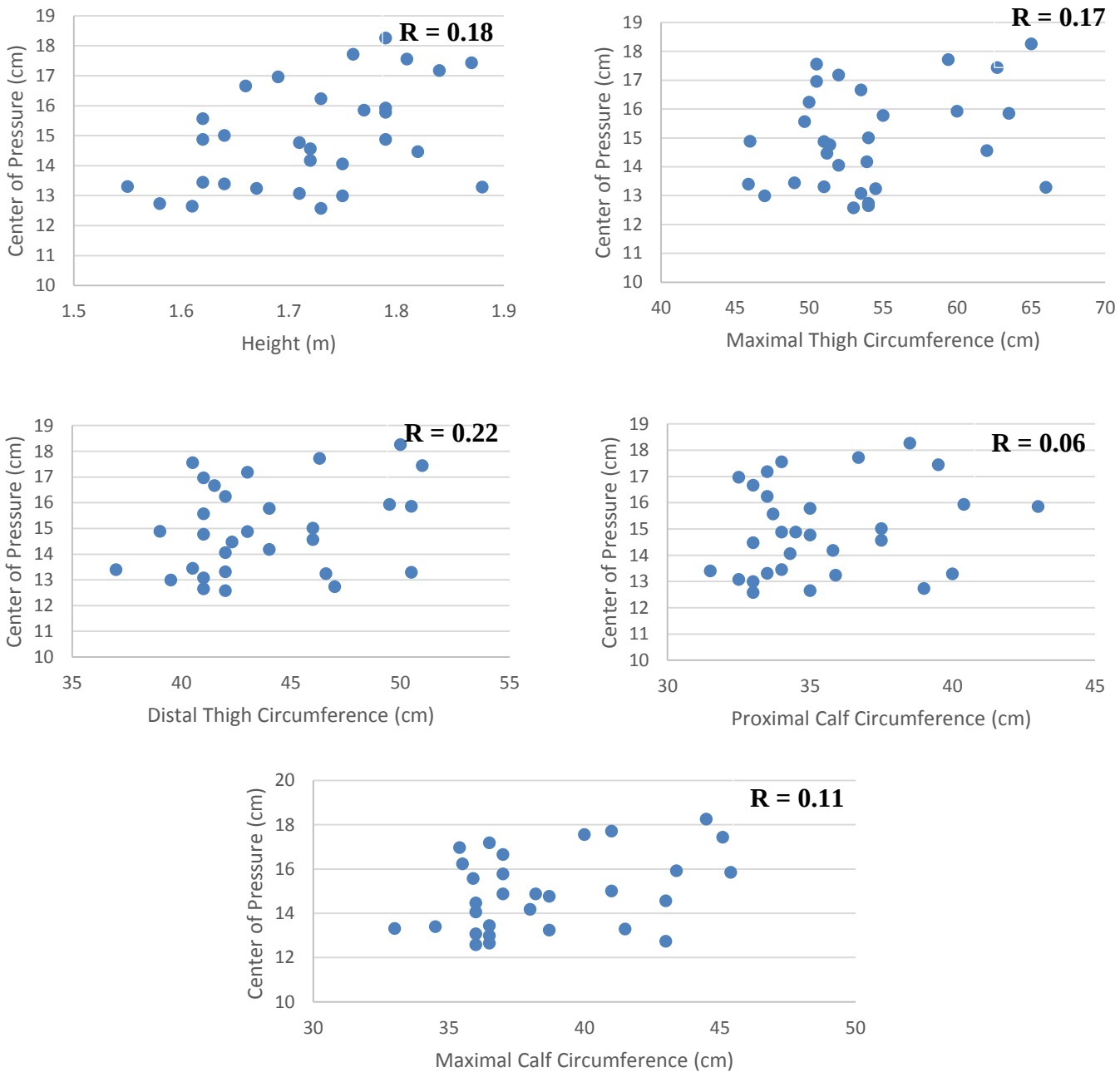

Figure 4-9: Graphs showing the relationship between the anthropometric covariates (maximal thigh circumference, distal thigh circumference, proximal calf circumference, maximal calf circumference and height) and center of pressure at maximum total thigh-calf contact force during dorsi-flexed kneeling. R values are shown in the upper right hand corner of each graph. An asterisk(*) denotes a significant correlation.

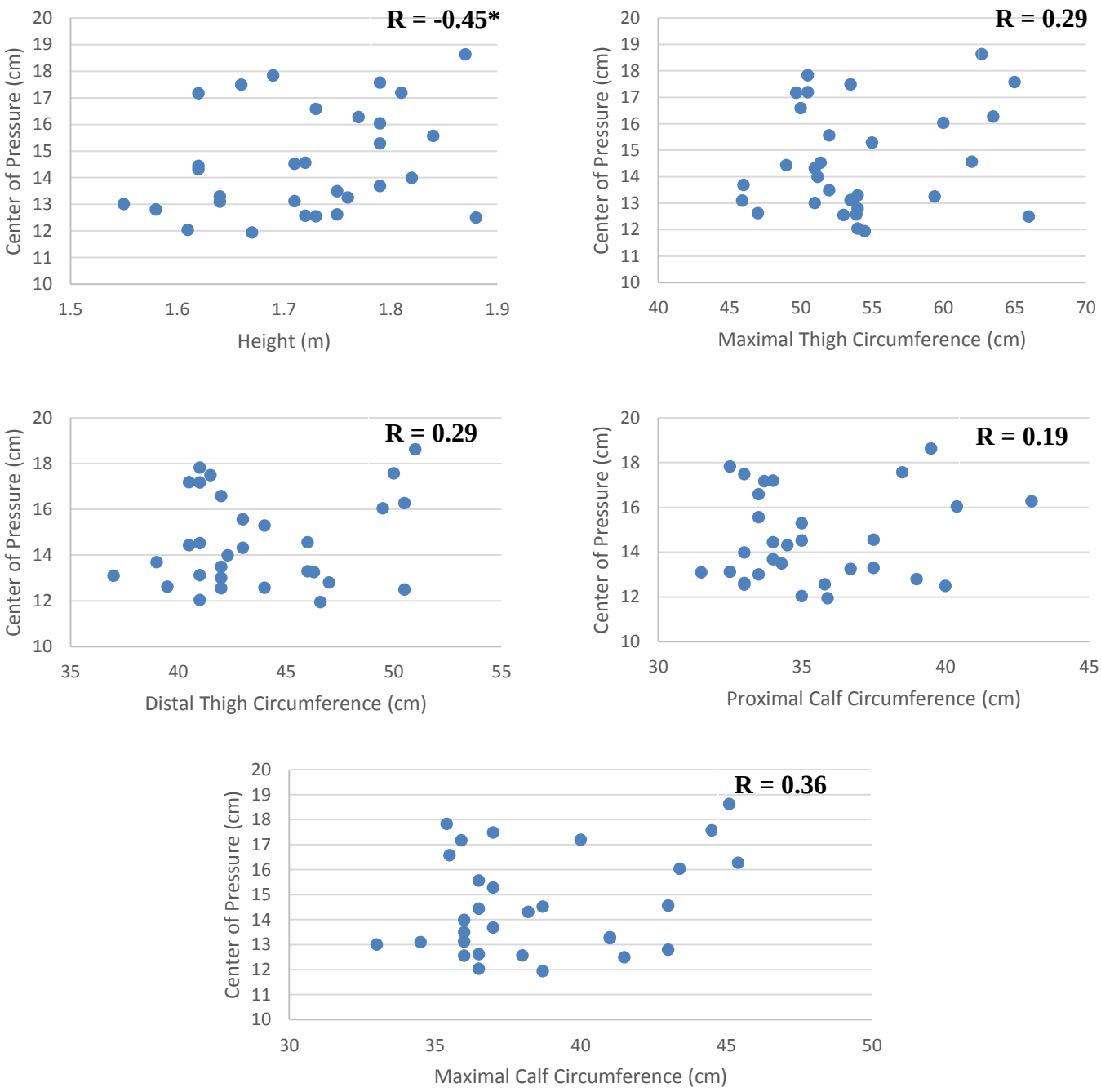

Figure 4-10: Graphs showing the relationship between the anthropometric covariates (maximal thigh circumference, distal thigh circumference, proximal calf circumference, maximal calf circumference and height) and center of pressure at maximum total thigh-calf contact force during plantar-flexed kneeling. R values are shown in the upper right hand corner of each graph. An asterisk(*) denotes a significant correlation.

4.6 Flexion Angle at Maximum Total Thigh-Calf Contact Force

4.6.1 Analysis of Variance for Flexion Angle at Maximum Total Thigh-Calf Contact Force for Sex and Activity

For the for flexion angle at maximum total thigh-calf contact force, there were no main effects of sex or activity (p= 0.17, p=0.68; Table D-5). Figure 4-11 shows the interaction plot for the ANOVA on flexion angle at maximum total thigh-calf contact force.

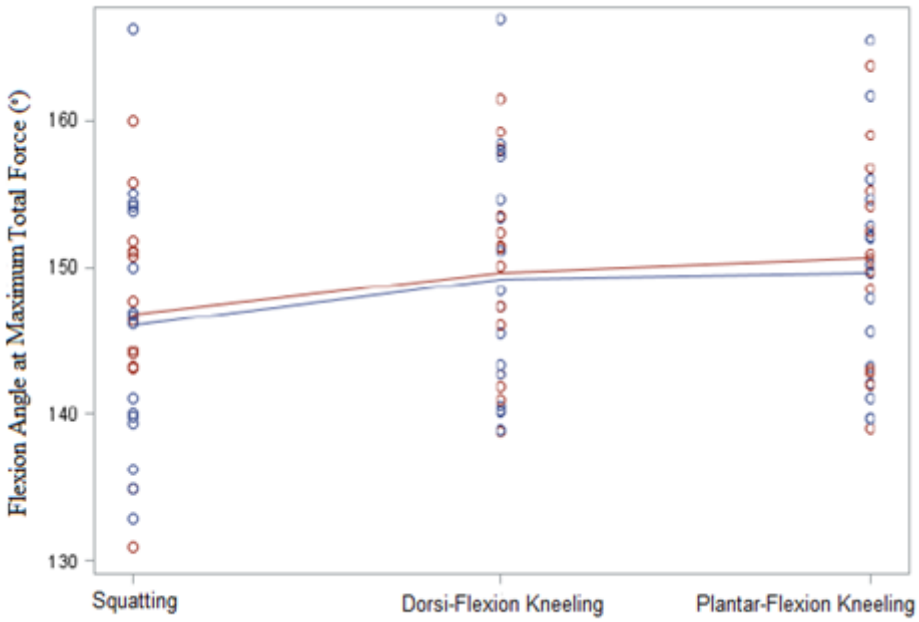

Figure 4-11: Interaction plot for the two-way ANOVA on flexion angle at maximum total thigh-calf contact force (sex x activity). Significant differences between activities are denoted with an asterisk (*).Blue indicates males and red indicates females.

4.6.2 Correlations with Anthropometric Measures and Flexion Angle at Maximum total Thigh-Calf Contact Force

The correlations and R values for the anthropometric covariates and flexion angle at maximum total thigh-calf contact force are displayed for squatting in Figure 4-12, dorsi-flexed kneeling in Figure 4-13 and plantar-flexed kneeling in Figure 4-14. For all activities, maximum thigh circumference (except during plantar-flexed kneeling), distal thigh-circumference and

proximal calf circumference were found to be significantly related to the flexion angle at maximum total thigh-calf contact force.

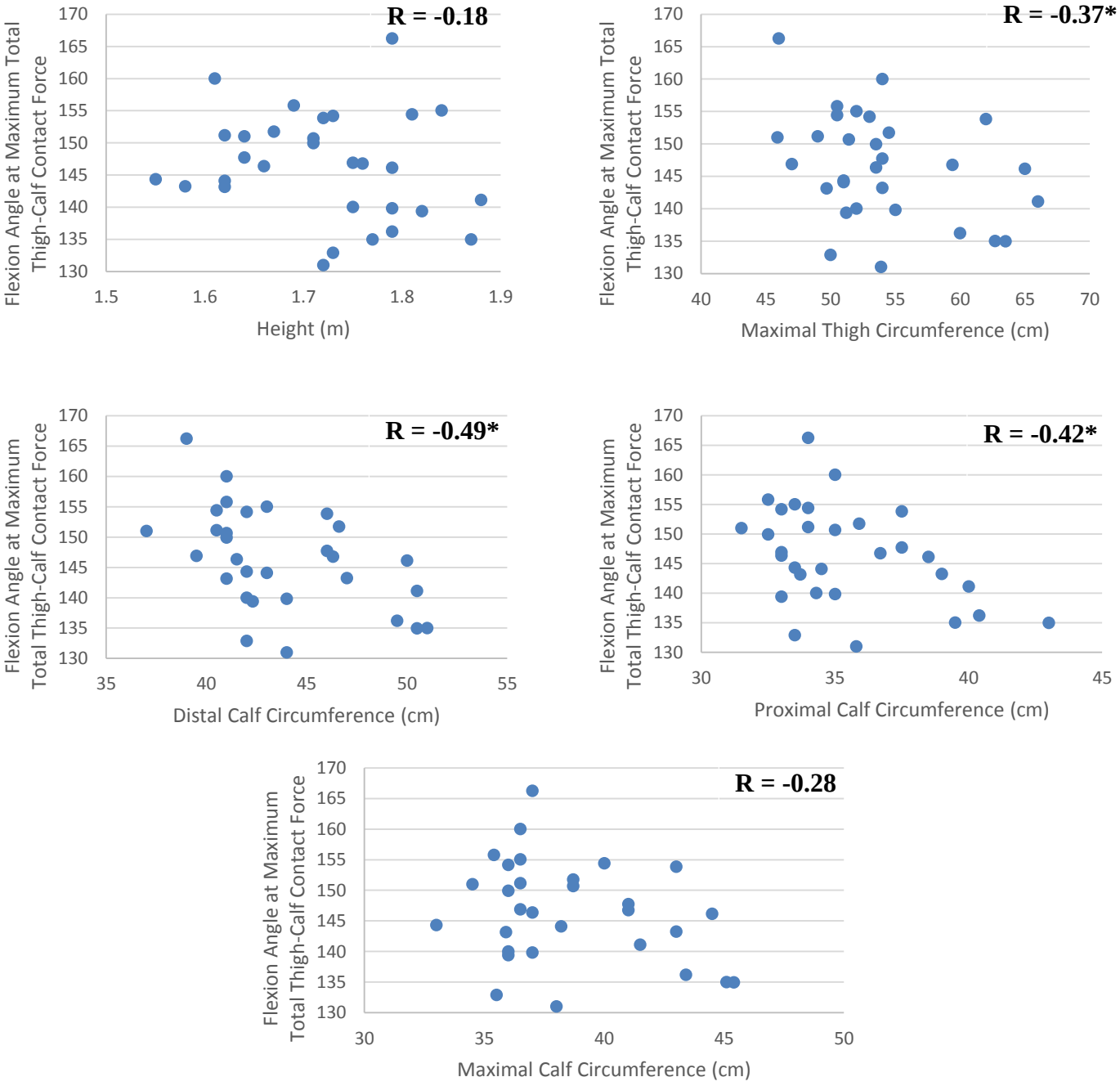

Figure 4-12: Graphs showing the relationship between the anthropometric covariates (maximal thigh circumference, distal thigh circumference, proximal calf circumference, maximal calf circumference and height) and flexion angle at maximum total thigh-calf contact force during squatting. R values are shown in the upper right hand corner of each graph. An asterisk(*) denotes a significant correlation.

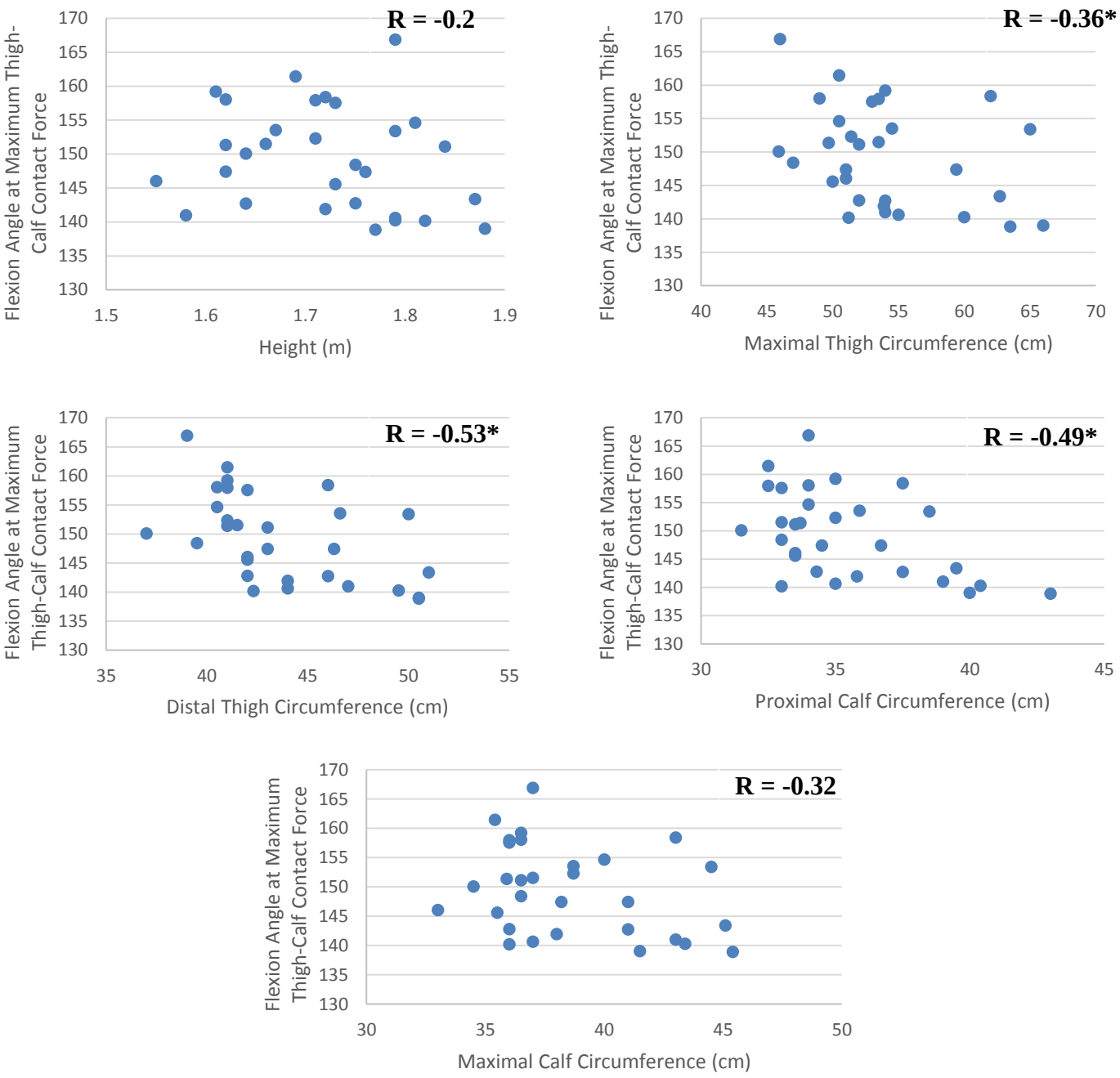

Figure 4-13: Graphs showing the relationship between the anthropometric covariates (maximal thigh circumference, distal thigh circumference, proximal calf circumference, maximal calf circumference and height) and flexion angle at maximum total thigh-calf contact force during dorsi-flexed kneeling. R values are shown in the upper right hand corner of each graph. An asterisk(*) denotes a significant correlation.

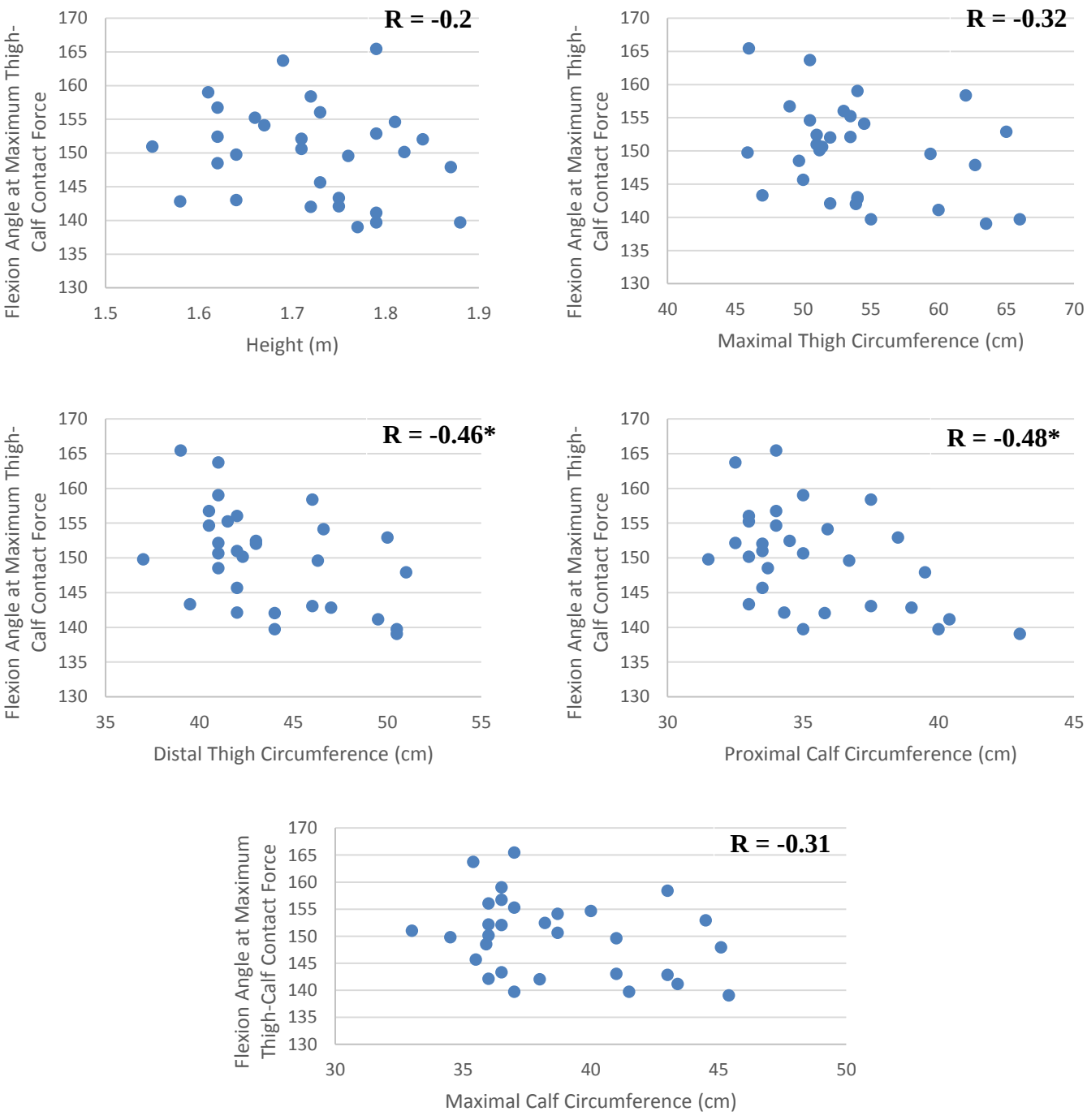

Figure 4-14: Graphs showing the relationship between the anthropometric covariates (maximal thigh circumference, distal thigh circumference, proximal calf circumference, maximal calf circumference and height) to flexion angle at maximum total thigh-calf contact force during plantar-flexed kneeling. R values are shown in the upper right hand corner of each graph. An asterisk(*) denotes a significant correlation.

4.7 Starting Angle of Thigh-Calf Contact

4.7.1 Analysis of Variance for the Starting Angle of thigh-calf contact for sex and activity

For any male during any activity, the lowest starting angle for thigh-calf contact was 126° of flexion, whereas the lowest starting angle was 128° for females. For all activities, thigh-calf contact was initiated at a lower flexion angle, on average, in men than in women. For the starting angle of thigh-calf contact (see Figure 4-15 and Table D-1), there was a main effect of activity ($p = 0.010$) and sex ($p = 0.016$), while the sex-by-activity interaction was not significant ($p = 0.93$). The Tukey post-hoc analysis showed that dorsi-flexed and plantar-flexed kneeling were not statistically different. However, there was a significant difference between the squatting activity and both kneeling activities (Table D-2). The output from the two-way ANOVA for the flexion angle at maximum total thigh-calf contact force for sex and activity is found in Appendix D. Figure 4-15 shows the interaction plots between center of pressure at maximum total thigh-calf contact force and each of the thigh-calf contact parameters, where significant differences are denoted with an asterisk(*).

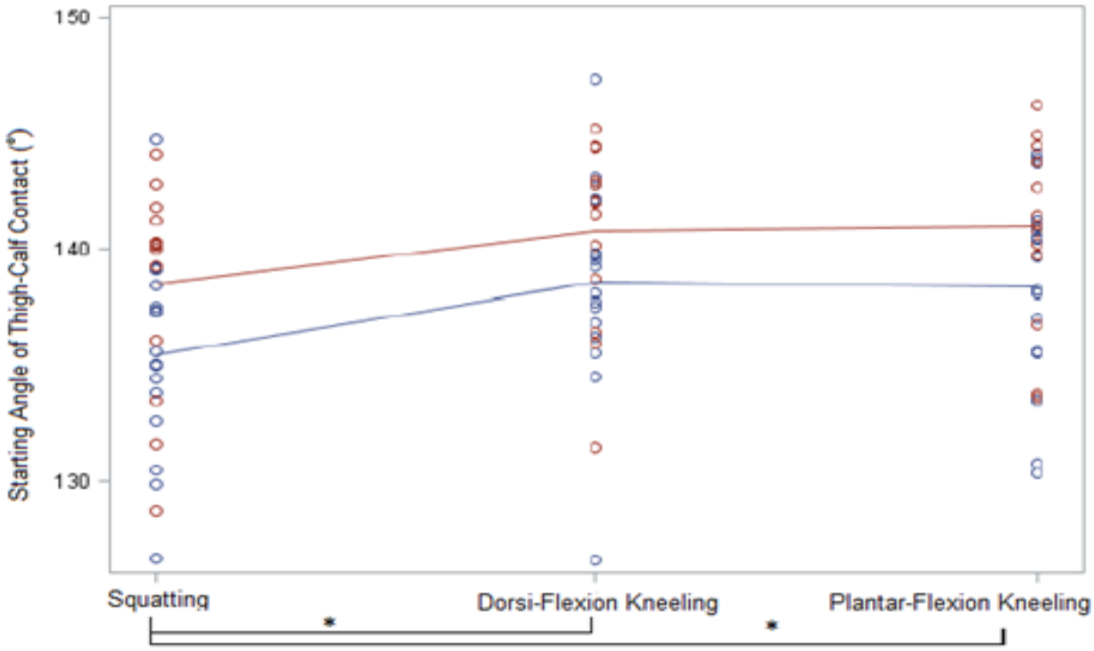

Figure 4-15: Interaction plot for the two-way ANOVA on starting angle of thigh-calf contact force (sex x activity). Significant differences between activities are denoted with an asterisk (*).Blue indicates males and red indicates females.

4.7.2 Correlations with Anthropometric Measures and the Starting Angle of Thigh-Calf Contact Force

The correlations and R values for the anthropometric covariates and the starting angle of thigh-calf contact force are displayed for squatting in Figure 4-16, dorsi-flexed in Figure 4-17 and plantar-flexed kneeling in Figure 4-18. The starting angles of thigh-calf contact force during all three activities were found to be significantly negatively related to all anthropometric parameters except for height during dorsi-flexed kneeling.

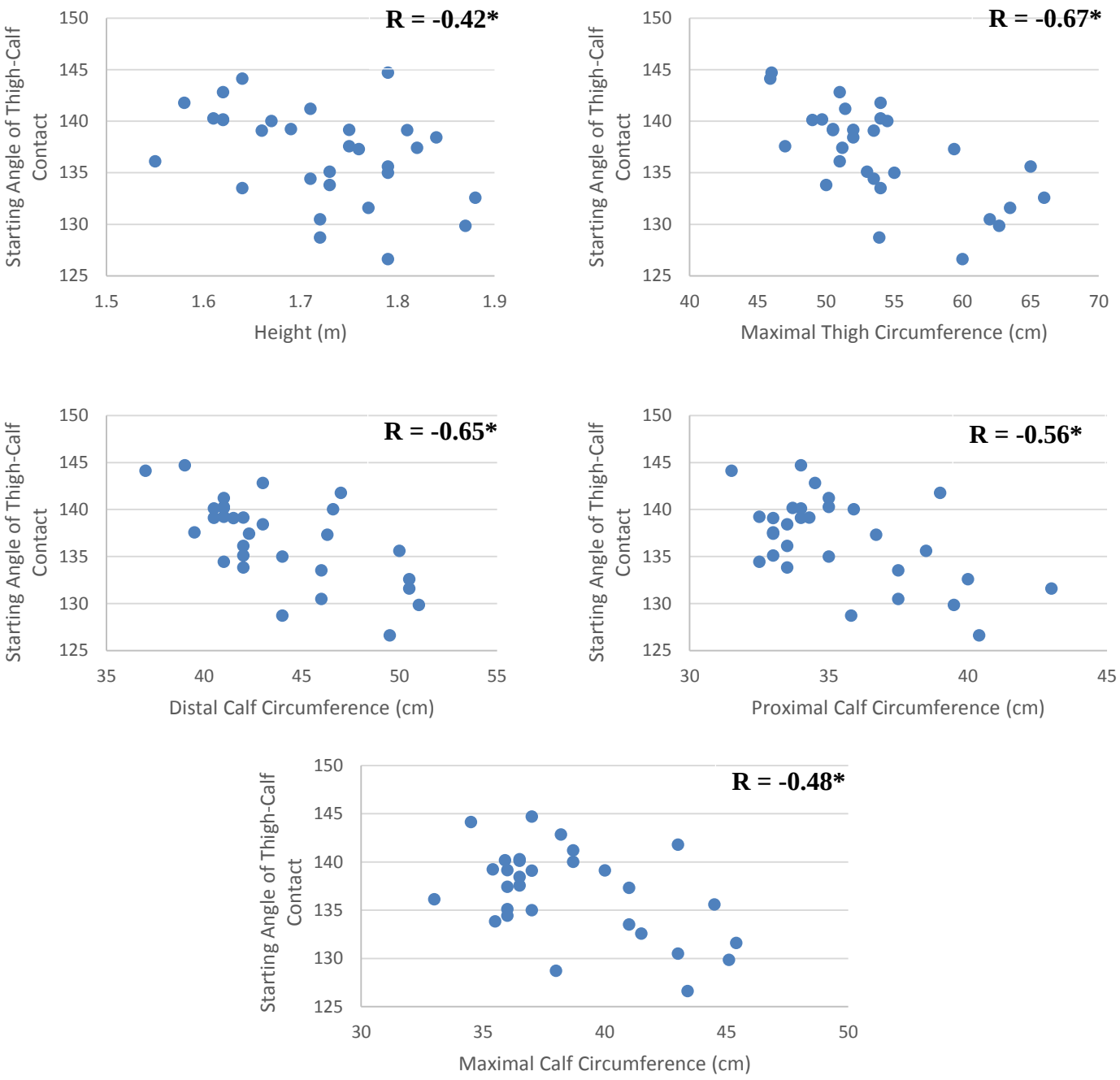

Figure 4-16: Graphs showing the relationship between the anthropometric covariates (maximal thigh circumference, distal thigh circumference, proximal calf circumference, maximal calf circumference and height) and the starting angle of maximum thigh-calf contact force during squatting. R values are shown in the upper right hand corner of each graph. An asterisk(*) denotes a significant correlation

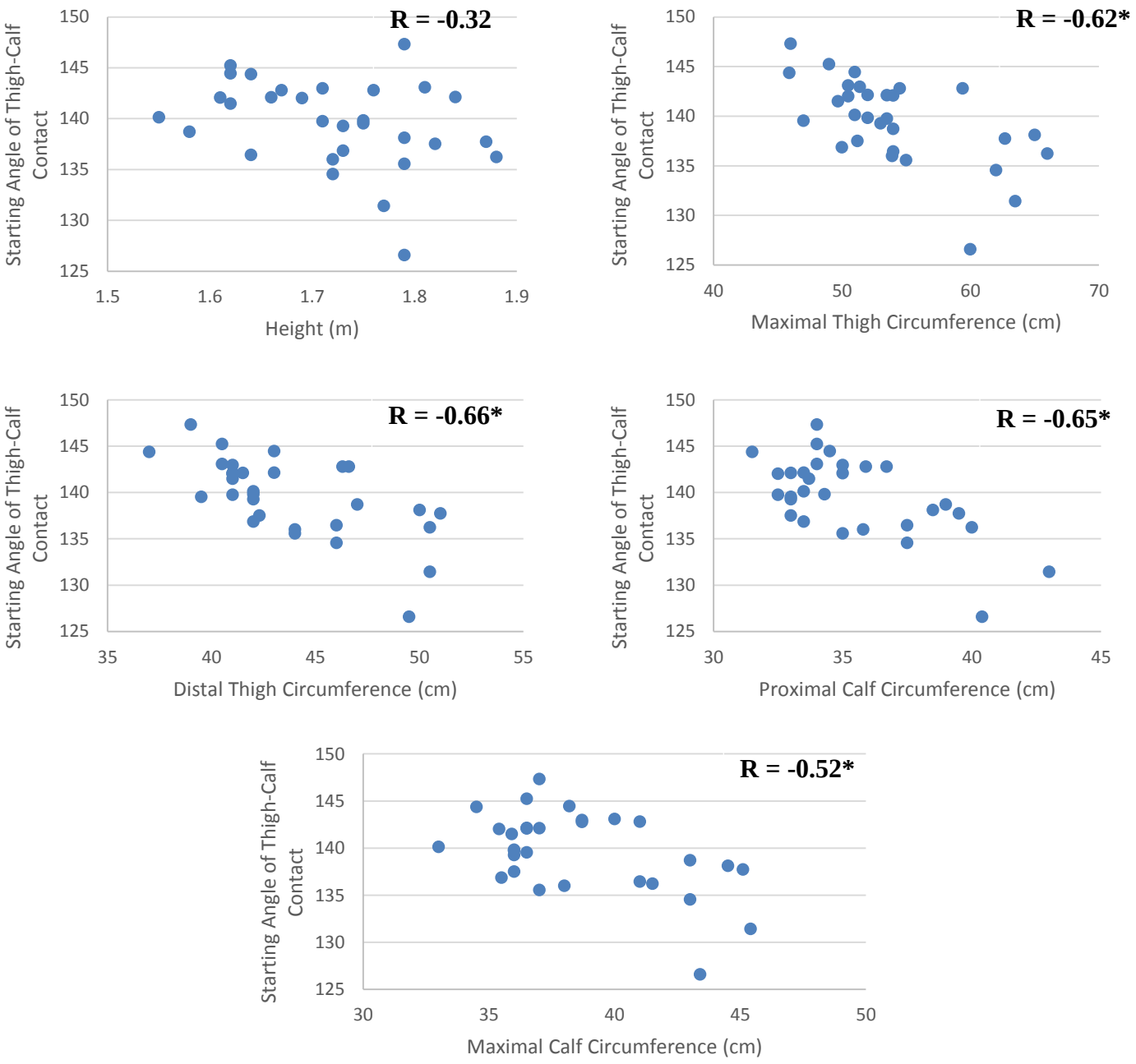

Figure 4-17: Graphs showing the relationship between the anthropometric covariates (maximal thigh circumference, distal thigh circumference, proximal calf circumference, maximal calf circumference and height) and the starting angle of maximum thigh-calf contact force during dorsi-flexed kneeling. R values are shown in the upper right hand corner of each graph. An asterisk(*) denotes a significant correlation.

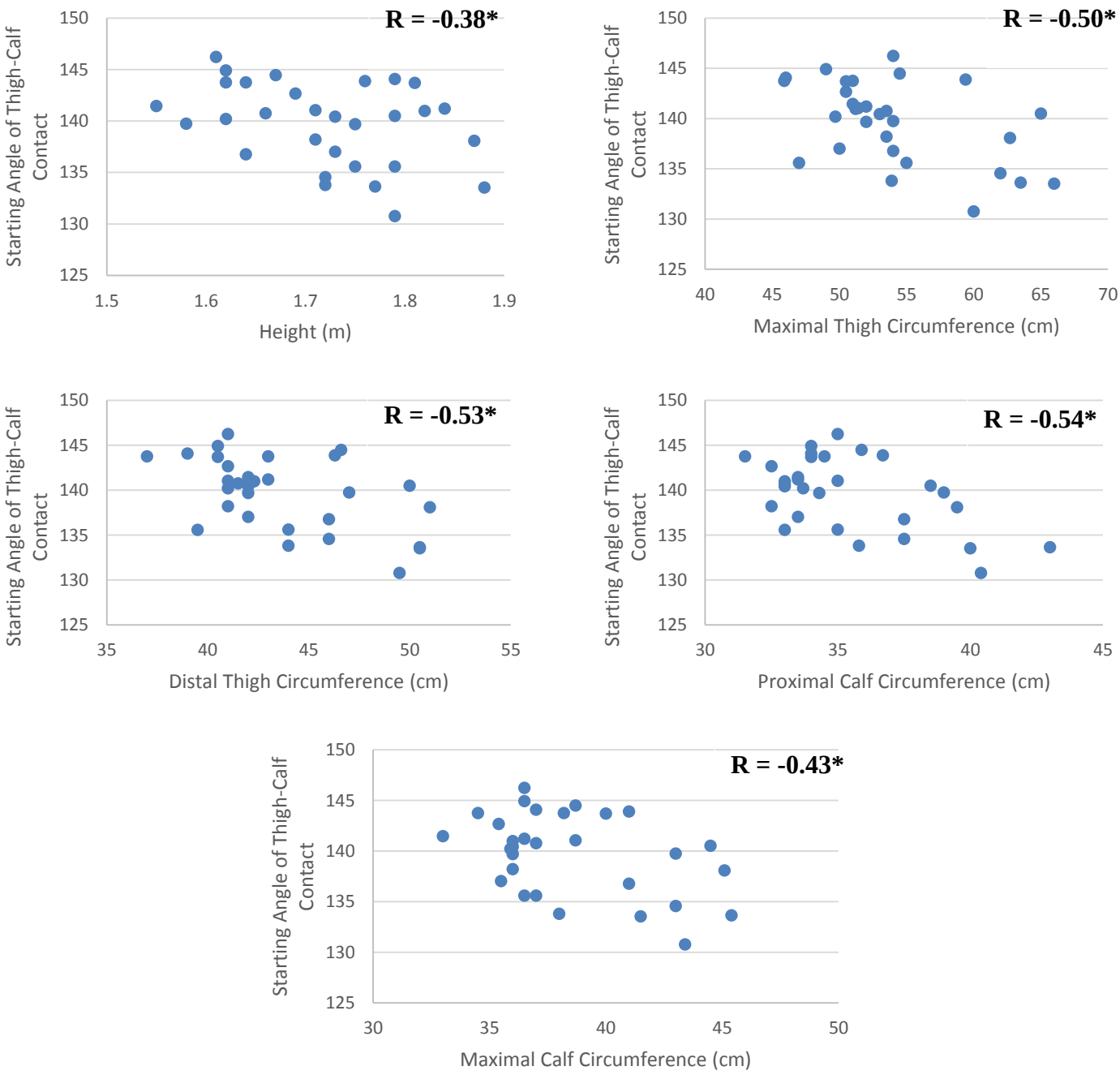

Figure 4-18: Graphs showing the relationship between the anthropometric covariates (maximal thigh circumference, distal thigh circumference, proximal calf circumference, maximal calf circumference and height) and the starting angle of maximum thigh-calf contact force during plantar-flexed kneeling. R values are shown in the upper right hand corner of each graph. An asterisk(*) denotes a significant correlation

4.8 Stepwise Linear Regression Models for the Starting Angle of Thigh-Calf Contact during Squatting and Kneeling

There was a lack of significant correlations between anthropometric covariates and all outcome parameters except starting angle of thigh-calf contact. Therefore, predictive models for only the starting angle of thigh-calf contact force during squatting (Equation 4-1) and dorsi-flexed kneeling (Equation 4-2) were created. Dorsi-flexed kneeling was chosen as the representative kneeling activity for modeling purposes as the results from the analyses of variance showed that there was no significant difference in the starting angle of thigh-calf contact between dorsi-flexed and plantar-flexed kneeling. In the equations presented below: SSA represents the starting angle of thigh-calf contact during squatting, SKA represents the starting angle of thigh-calf contact during kneeling, SX represents sex, MTC represents maximal thigh circumference, PCC represents proximal calf circumference and HT represents height. In Equation 4-1, the majority of the starting angle variance for squatting was explained was by MTC (partial R^2= 0.5, Table D-9. In Equation 4-2, the majority of the starting angle variance for kneeling was explained by PCC (partial R^2= 0.39, Table D-10).

Equation. 4-1: $SSA = 151.96376 + 5.38390SX + 0.04321MTC - 1.10174PCC + 11.18526HT$

Equation. 4-2: $SKA = 171.87+4.15SX+0.33MTC-1.47PCC$

The above equations were based on 20 randomly selected participants. Using data from the remaining 10 participants, the starting angle of thigh-calf contact, computed by the SSA and SKA models (Equation. 1 and 2), were compared to the mean values for each participant and each activities. Figure 4-19 shows the comparison between mean starting angle of thigh-calf contact and predicted values in comparison to perfect agreement for both squatting (R^2=0.71; RMSE=5.1°) and kneeling (R^2=0.6; RMSE= 4.6°).

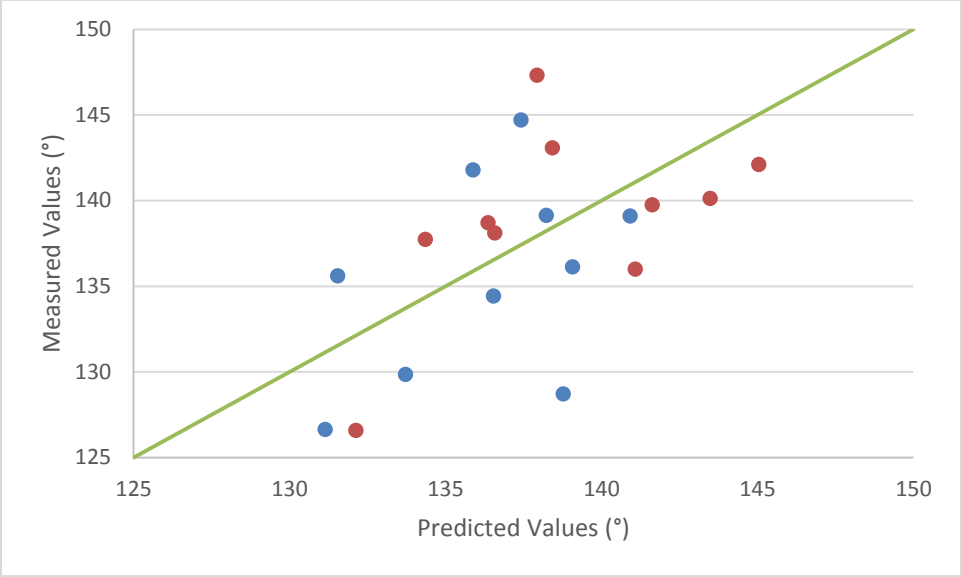

Figure 4-19: External validation performed on 10 additional participants not included in the creation of the prediction model showing the comparison between measured starting angle of thigh-calf contact force and predicted values. Each data point represents one participant for a given activity. Squatting values are shown in blue, kneeling values are shown in red and the green line represents perfect agreement.

4.9 The Effect of Thigh-Calf Contact Force on Tibiofemoral Joint Contact Force.

With the addition of thigh-calf contact force into the rigid link segment model inverse dynamics analysis, reduced the knee joint reaction force during static, full-flexion squatting decreased in the anterior-posterior direction from Rk_y= 3.21 N/kg to Rk_y= 2.19 N/kg. The net joint moment about the knee also decreased with the addition of thigh-calf contact force from 86.88 Nm to 73.75 Nm which in turn caused an approximate decrease in the compressive tibiofemoral joint contact force by 2.23 N/kg in the longitudinal direction and 0.85 N/kg in the anterior-posterior direction (Appendix E).

5. Discussion

This investigation involved the measurement and analysis of total thigh-calf contact force, flexion angle, and thigh-calf contact centre of pressure during transitions into high flexion postures (squatting and kneeling). Four thigh-calf contact parameters were identified: maximum total thigh-calf contact force, centre of pressure at maximum total thigh-calf contact force, the knee joint flexion angle at maximum total contact force, and the starting angle of thigh-calf contact. To the author's knowledge, this is the first investigation that has investigated the effect of kneeling type (dorsi-flexed versus plantar-flexed kneeling) and sex on thigh-calf contact based on data from several participants during squatting and two types of kneeling. The main objectives of this Master's thesis work were to compare thigh-calf contact forces between activities and sexes, to determine the correlation between anthropometric measures and thigh-calf contact parameters and to develop predictive equations for thigh-calf contact force and centre of pressure based on anthropometric measures and flexion angle and a predictive equation for starting angle of thigh-calf contact based on anthropometric measures. All objectives were met with the exception of developing predictive equations for thigh-calf contact force and center of pressure based on anthropometric measures and flexion angle. Instead, equations were fit to the thigh-calf contact force and centre of pressure data as a function of percent flexion range after contact because the anthropometric parameters had few or no significant correlations with the maximum total thigh-calf contact force or the corresponding center of pressure.

This investigation addressed four main hypotheses: that thigh-calf contact force characteristics would not differ between the squatting and kneeling activities; that anthropometric characteristics would affect maximum total thigh-calf contact force; the starting

angle of thigh-calf contact would differ depending on anthropometric characteristics and sex and that thigh and calf circumference would be a significant predictor of the location of centre of pressure on the tibia.

5.2 Comparison between Activities

For all outcome parameters, except the flexion angle at maximum total thigh-calf contact force, the squatting activity was found to be significantly different from the kneeling activities, whereas no significant differences were found between dorsi-flexed and plantar-flexed kneeling. In contrast, Zelle et al., (2007) reported that maximum total thigh-calf contact force between squatting and dorsi-flexed kneeling were comparable in both trend and magnitude. The average flexion angle at maximum total thigh-calf contact force obtained by the participants in this investigation for squatting and kneeling (146.5°, S.D.8.2°; 149.4°,S. D. 7.5°, for squatting and dorsiflexion kneeling respectively) were lower than values reported by Zelle et al., (2007) (151.8°+/-4.4; 156.4°+/-3.4, for squatting and dorsiflexion kneeling). The average maximum total thigh-calf contact force values measured in this current investigation were also found to be lower in both squatting and kneeling than those found by Zelle et al., (2007). Since the relationship between thigh-calf contact force and flexion angle appears to be exponential, a small difference in flexion angle near full flexion could mean a large change in thigh-calf contact force. Given that the average maximal flexion angle for this investigation was lower than those found by Zelle et al., (2007) it is uncertain if the differences in outcome parameters between squatting and kneeling activities observed in this investigation would remain if participants had reached greater flexion angles. It is important to note, however, that even at submaximal flexion

angles there were differences in thigh-calf contact force between squatting and kneeling at the same flexion angle for the same participant (Appendix C, Figure D-1).

5.3 Correlations between Anthropometric Measures and Maximum Total Thigh-Calf Contact Force

There were a few significant relationships between the anthropometric measures as well as between the outcome parameters. There was a high degree of multicollinearity between the all of the limb circumference measures ($P<0.0001$), although the results from the multicollinearity analysis showed that all anthropometric measures had a variance inflation factor (VIF) number of under 20. It can be assumed that weak dependencies might be starting to affect the regression estimates, however, these VIF numbers are not high enough to have a fair amount of numerical error (Belsey, Kuh, and Welsch., 1980).

Zelle et al., (2007) found significant positive correlations between body mass, maximum thigh and calf circumference and non-normalized maximum total thigh-calf contact force for both dorsi-flexed kneeling and squatting. Those findings agree with the significant positive correlations found between maximum thigh and calf circumference mass-normalized maximum total thigh-calf contact force during plantar-flexed kneeling in the current study. However, there were no significant correlations between anthropometric measures and mass-normalized maximum total thigh-calf contact force during squatting or dorsi-flexed kneeling. Given the differences in average maximal flexion angle at maximal thigh-calf contact force between investigations, the discrepancy in findings between this investigation and the previous investigation (Zelle et al., 2007) might indicate that anthropometric parameters have a greater influence on thigh-calf contact force at greater knee joint flexion angles. It is more likely,

however, that this discrepancy is due to differences in the normalization of total thigh-calf contact force between the two studies. The current investigation found strong significant relationships between participant mass and all lower limb circumference measures. As such, thigh-calf contact force was normalized to participant body mass (N/kg) in order to decrease the effect of multicollinearity between anthropometric measures. It is possible that all thigh and calf circumference measurements correlated with maximum total thigh-calf contact force in the previous investigation (Zelle et al., 2007) simply because the circumferences were significantly correlated to mass.

5.4 Correlations between Anthropometric Measures and Center of Pressure at Maximal Total Thigh-Calf Contact Force

The location of COP at maximal total thigh-calf contact force, was not determined by any measured anthropometric parameter, with the exception of a significant relationship between height and plantar-flexed kneeling. The location of COP at maximal total thigh-calf contact force may be determined by other parameters not included in this investigation, such as trunk position at maximum total thigh-calf contact force, or tissue compression. Correlations between centre of pressure and anthropometric parameters have not been calculated in previous literature.

5.5 Starting Angle of Thigh-Calf Contact, Maximum Flexion Angle Reached, and Range of Flexion after Start of Contact

Thigh-calf contact was initiated at a lower flexion angle, on average, in men than in women for all activities ($p= 0.02$). There was large variation in the average maximal flexion angle across all activities between participants (Appendix C, Figure C-1). Average maximum flexion angle obtained was significantly positively correlated to the starting angle of thigh-calf

contact for all activities (squatting R=0.60, p= 0.002; dorsi-flexed kneeling R=0.63, p=0.0008; plantar-flexed kneeling R=0.70, p<0.0001). As such, participants who had a higher starting angle of thigh-calf contact were also likely to higher maximal flexion during both squatting and kneeling. Furthermore, most anthropometric parameters were, significant or not, negatively correlated to both starting angle of thigh-calf contact and the flexion angle at maximum total thigh-calf contact force in all activities. This finding means that as anthropometric parameters increased, both the starting angle of thigh-calf contact and the maximum flexion angle obtained tended to decrease.

5.6 Effect of Thigh-Calf Contact on Tibiofemoral Joint Contact Force

The net joint force calculated without the incorporation of maximum total thigh-calf contact force, for the single participant during heels up squatting (3.20 N/kg) lay within, albeit on the lower end, of the range of values reported in previous literature of 2 to 7 N/kg (Dahlkvist et al.,1982; Nagura et al.,2006; Smith et al., 2008). Force requirements used in the design and testing of TKRs are based on tibiofemoral joint contact force estimates calculated from knee joint models that have neglected to account for the contact between the thigh and calf during high-flexion, resulting in maximum tibiofemoral joint contact forces being estimated near full flexion (Hefzy et al., 1998; Nagura et al., 2002; Argenson et al., 2004). Based on a single muscle equivalent estimate, the compressive tibiofemoral joint contact force decreased by 221.78 N in the longitudinal direction and 84.96 N in the anterior-posterior direction. As such, current thigh-flexion TKRs may be subjected to significantly less load at full flexion than what was previously assumed and the need for reinforcement of high-flexion implants near the end range of flexion,

such as the metal pin in the tibial post of Sigma RP-F (Depuy, Warsaw, IN, USA) should be revisited.

Chapter 6: Summary, Conclusions, and Recommendations for Future Work

6.1 Summary

This Master's thesis project was motivated by a fundamental lack of understanding of thigh-calf contact during deep flexion activities. Very few investigations have attempted to characterize thigh-calf contact force, and even fewer knee joint contact force models have incorporated thigh-calf contact force into tibiofemoral joint contact force calculations during high-flexion. To the author's knowledge, the only previous publication that had attempted to model thigh-calf contact force and contact force location on the tibia was conducted by Zelle et al. (2009), using data from a single participant and neglecting to account for the possible effect of anthropometrics on thigh-calf contact force.

The purposes of this Master's thesis project was to compare thigh-calf contact forces between activities and sexes and to determine the correlation between anthropometric measures and thigh-calf contact parameters. This work was guided by four key hypotheses pertaining to thigh-calf contact characteristics.

The first hypothesis was that maximum total thigh-calf contact force would not be significantly different between the three activities. This hypothesis was incorrect. The average maximum total thigh-calf contact force during squatting (1.1 N/kg+/- 0.6) was significantly lower than those found during the dorsi-flexed (2.0 N/kg+/-0.7) and plantar- flexion kneeling (2.2 N/kg +/- 0.9). For all thigh-calf contact parameters, except flexion angle at maximum total thigh-calf contact force, there was a main effect of activity (maximum total thigh-calf contact force $p<0.0001$, center of pressure at maximum total thigh-calf contact force $p=0.01$, starting

angle of thigh-calf contact p=0.02). Tukey post-hoc analysis indicated that the squatting activity was significantly different from the kneeling activities (Appendix D).

The second hypothesis postulated that body weight, thigh and calf-circumference will be significantly, positively correlated to maximum total thigh-calf contact force. Maximum total thigh-calf contact force, normalized to participant mass, were only significantly positively related to anthropometric parameters during plantar-flexed kneeling.

The third hypothesis postulated that a participant's thigh and calf circumference would be significantly, negatively correlated to the starting angle of thigh-calf contact and that women would have an earlier starting angle of thigh-calf contact than men. The first part of this hypothesis was proven correct in that all lower limb circumference measures were significantly negatively correlated to the starting angle of thigh-calf contact for all activities. This finding means that, as anthropometric parameters increased, the starting angle of thigh-calf contact tended to decrease. For all activities, thigh-calf contact was initiated at a lower flexion angle, on average, in men than in women, contrary to the hypothesis (p=0.02).

The fourth hypothesis postulated that thigh and calf circumference would be significant predictors of the location of the centre of pressure at maximum total thigh-calf contact force. Given the lack of significant correlations between centre of pressure at maximum total thigh-calf contact force and any anthropometric measures, thigh and calf circumference measures were not significant predictors of COP at maximum total thigh-calf contact force. In general, the average COP at maximal thigh-calf contact force was more distal in men than in woman, however this difference was not significant (p=0.1).

This investigation generated important information on thigh-calf contact force and COP for the range of flexion after thigh-calf contact initiation and at maximum total thigh-calf contact force. To the author's knowledge, this is the first investigation to characterize the effect of kneeling type (dorsi-flexed versus plantar-flexed kneeling) and sex on thigh-calf contact parameters and to provide equations for the mean total thigh-calf contact force and mean COP for the full range of flexion after initial thigh-calf contact based on data from more than a single participant (30 participants in this study) during squatting and kneeling.

The major findings of the work in this Master's thesis project are summarized below.

1. The maximum total thigh-calf contact force were both significantly lower during the squatting activity than during the kneeling activities (Appendix D, Table D-7).
2. The starting angle of thigh-calf contact was significantly lower in squatting compared to kneeling (Appendix D, Table D-1).
3. The centre of pressure at maximum total thigh-calf contact force during full flexion was closer (but not significantly so) to the epicondylar axis during squatting than during the kneeling activities (Appendix D, Table D-3).
4. All measured anthropometric parameters, except height, were positively correlated with non-normalized maximum total thigh-calf contact force (in Newtons) for all activities. However, when thigh-calf contact force was normalized to participant body mass, the anthropometric parameters were only significantly positively related to maximum total thigh-calf contact force during plantar-flexed kneeling.
5. There was very little correlation between measured anthropometric parameters and the COP at maximum total thigh-calf contact force for both squatting and kneeling.

6. At maximal total thigh-calf contact force, the addition of thigh-calf contact force into the model changed the tibiofemoral contact force from 23.54 N/kg to 17.08 N/kg.

6.2 Study Limitations

The use of optoelectronic markers to track the motion of palpable landmarks may have introduced some uncertainty. Soft tissue artifact can affect the estimation of joint angles. Whenever possible, areas of severe soft tissue deformation were avoided when placing markers.

In general, interface pressure mapping systems (IPM), such as the Tekscan Conformat pressure mapping sensor (model #5315, Tekscan, Boston, MA, used in this investigation) are prone to artifacts such as temperature drift, creep, bending and hysteresis with respect to accuracy and repeatability. Resistive IPM systems have been found to introduce creep in the measurement of static forces by varying the static force measurements by -10% to +20% (Morin et al., 2000) although comparable average pressures are achieved during the first few seconds of an application of force (Stinson et al., 2002) as was the case in this investigation. Steps were taken to minimize and quantify these artifacts by calibrating the IPM system using conditions similar to what would be experienced during actual data collection (IScan User's Manual., 1999). The accuracy of the sensor in measuring a known applied load is calculated in *Appendix B.* The active sensing units on the Tekscan Conformat (model #5315, Tekscan, Boston, MA) are located 2.6cm away from the top of the sensor, leaving a non-sensing space between the popliteal crease and the first row of sensels. This distance was added to the calculation of centre of pressure of thigh-calf contact force, however the effect of the distribution of force within this sensing area was not included; and the lack of force measurements in this area decreased the total measured force, resulting in an underestimation of the overall thigh-calf contact force. A sensitivity

analysis was performed on the effect of the missing 2.6cm of thigh-calf contact on thigh-calf contact force and can be found in *Appendix B.*

Thigh-calf contact pressures create tissue deformation which may act to distribute the axial load in multiple directions. However the IPM system used to measure thigh-calf contact force in this investigation was only capable of measuring pressure normal to the IPM. Although the posterior thigh and calf are not flat when a person is standing upright, the contact force between the segments in high flexion causes the soft tissue on the segments to deform to a reasonably flat surface. It was assumed that the dominant component of the thigh-calf contact force was perpendicular to the long axis of the tibia, normal to the IPM system, and that other components of the thigh-calf contact force were negligible.

Heel-gluteal contact forces were not measured in this study; however, some participants did exhibit heel-gluteal contact near full flexion. This contact force would further affect the calculated tibiofemoral joint contact force, at and near full flexion.

There were no significant correlations between anthropometric measures and mass-normalized maximum total thigh-calf contact force in any activity except maximal thigh-circumference during plantar-flexed kneeling. There may be other body measures that would better explain the variance in thigh-calf contact force and centre of pressure. Another possibility is that the precise mechanics of deep knee flexion postures may be participant specific which in turn may cause thigh-calf contact characteristics to be too individualized to be able to develop predictive models for a wide population range.

6.3 Recommendations for Future Work

Recommendations for future work pertaining to characterizing and modeling thigh-calf contact parameters are listed below:

1. Use a measurement tool capable of measuring the entire contact area. The IPM system used in this investigation had a non-sensing area of 2.6cm surrounding the sensing matrix, so that contact forces between the popliteal crease and the edge of the sensing area could not be measured.
2. Investigate the change in thigh-calf contact force characteristics over prolonged deep flexion postures. Soft tissues may show viscoelastic behaviour like relaxation or creep (Holzapfel, G., 2000). It remains to be seen how the deformation of the soft tissues of the thigh and the calf would affect thigh-calf contact force characteristics over prolonged deep flexion postures.
3. Include the contact between the heel and the gluteal muscles evident for some participants during deep flexion activities.
4. Determine the effect of tissue composition on thigh-calf contact characteristics.

References:

1. Acker SM, Cockburn RA, Krevolin J, Li RM, Tarabichi S, Wyss UP. Knee kinematics of high-flexion activities of daily living performed by male muslims in the middle east. *J Arthroplasty*. 2011;26(2):319-327.

2. Ahn C, Tonidandel S, Overall JE. Issues in use of SAS PROC.MIXED to test the significance of treatment effects in controlled clinical trials. *J Biopharm Stat*. 2000;10(2):265-286.

3. Anderson AF, Dome DC, Gautam S, Awh MH, Rennirt GW. Correlation of anthropometric measurements, strength, anterior cruciate ligament size, and intercondylar notch characteristics to sex differences in anterior cruciate ligament tear rates. *Am J Sports Med*. 2001;29(1):58-66.

4. Andriacchi TP. Functional analysis of pre and post-knee surgery: Total knee arthroplasty and ACL reconstruction. *J Biomech Eng*. 1993;115(4 B):575-581.

5. Argenson J-A, Komistek RD, Mahfouz M, Walker S, Aubaniac J, Dennis D. A high flexion total knee arthroplasty design replicates healthy knee motion. *Clinical Orthopaedics & Related Research*. 2004;428:174-179.

6. Bal B, Greenberg D. Failure of a metail-reinforced tibial post in total knee arthroplasty. *Journal of Arthroplasty*. 2007;22(3):464-467.

7. Baliunas AJ, Hurwitz DE, Ryals AB, et al. Increased knee joint loads during walking are present in subjects with knee osteoarthritis. *Osteoarthritis and Cartilage*. 2002;10(7):573-579.

8. Banks, S., Bellemans, J., Nozaki, H., Whiteside, L.A., Harman, M., Hodge, W.A. Knee motions during maximum flexion in fixed and mobile-bearing arthroplasties. *Clinical Orthopaedics & Related Research*. 2003;410:131-139.

9. Bars DR, Schindler C. Mixed general linear model analysis of quantitative electroencephalographic (qEEG) data. *Journal of Neurotherapy*. 2004;8(4):63-75.

10. Bland JM, Altman DG. Agreement between methods of measurement with multiple observations per individual. *J Biopharm Stat*. 2007;17(4):571-582.

11. Booth Jr. RE. Sex and the total knee: Gender-sensitive designs. *Orthopedics*. 2006;29(9):836-838.

12. Burton P, Gurrin L, Sly P. Extending the simple linear regression model to account for correlated responses: An introduction to generalized estimating equations and multi-level mixed modelling. *Stat Med*. 1998;17(11):1261-1291.

13. Canoy D, Boekholdt SM, Wareham N, et al. Body fat distribution and risk of coronary heart disease in men and women in the european prospective investigation into cancer and nutrition in norfolk cohort: A population-based prospective study. *Circulation*. 2007;116(25):2933-2943.

14. Caruntu DI, Hefzy MS, Goel V, Goitz H. Modeling the knee joint in deep flexion: "thigh and calf" contact. . 2003.

15. Caruntu DI, Hefzy MS. 3-D anatomically based dynamic modeling of the human knee to include tibio-femoral and patello-femoral joints. *J Biomech Eng*. 2004;126(1):44-53.

16. Chin KR, Dalury DF, Zurakowski D, Scott RD. Intraoperative measurements of male and female distal femurs during primary total knee arthroplasty. *The journal of knee surgery*. 2002;15(4):213-217.

17. Crook GH, Bennett CA, Norwood WD, Mahaffey JA. Evaluation of skin-fold measurements and weight chart to measure body fat. *J Am Med Assoc*. 1966;198(1):157-162.

18. Dahlkvist NJ, Mayo P, Seedhom BB. Forces during squatting and rising from a deep squat. *Eng Med*. 1982;11(2):69-76.

19. Davis MA, Ettinger WH, Neuhaus JM. Obesity and osteoarthritis of the knee: Evidence from the national health and nutrition examination survey (NHANES I). *Semin Arthritis Rheum*. 1991;20(3 SUPPL. 1):34-41.

20. Dempster WT, Gaughran GL. **Properties of body segments based on size and weight**. *American Journal of Anatomy*. 1967;120(1):33-54.

21. D'Lima DD, Chen PC, Colwell Jr. CW. Polyethylene contact stresses, articular congruity, and knee alignment. *Clin Orthop*. 2001(392):232-238.

22. D'Lima DD, Steklov N, Patil S, Colwell Jr. CW. The mark coventry award: In vivo knee forces during recreation and exercise after knee arthroplasty. *Clin Orthop*. 2008;466(11):2605-2611.

23. Drikvandi R, Verbeke G, Khodadadi A, Partovi Nia V. Testing multiple variance components in linear mixed-effects models. *Biostatistics*. 2013;14(1):144-159.

24. Duncan R, Peat G, Thomas E, Hay EM, Croft P. Incidence, progression and sequence of development of radiographic knee osteoarthritis in a symptomatic population. *Ann Rheum Dis*. 2011;70(11):1944-1948.

25. Durnin JV, Rahaman MM. The assessment of the amount of fat in the human body from measurements of skinfold thickness. *Br J Nutr*. 1967;21(3):681-689.

26. Edwards LJ, Muller KE, Wolfinger RD, Qaqish BF, Schabenberger O. An R2 statistic for fixed effects in the linear mixed model. *Stat Med*. 2008;27(29):6137-6157.

27. Eston RG, Rowlands AV, Charlesworth S, Davies A, Hoppitt T. Prediction of DXA-determined whole body fat from skinfolds: Importance of including skinfolds from the thigh and calf in young, healthy men and women. *Eur J Clin Nutr*. 2005;59(5):695-702.

28. Felson DT. The epidemiology of knee osteoarthritis: Results from the framingham osteoarthritis study. *Semin Arthritis Rheum*. 1991;20(3 SUPPL. 1):42-50.

29. Felson DT, Anderson JJ, Naimark A, Walker AM, Meenan RF. Obesity and knee osteoarthritis. the framingham study. *Ann Intern Med*. 1988;109(1):18-24.

30. Felson DT, Zhang Y, Anthony JM, Naimark A, Anderson JJ. Weight loss reduces the risk for symptomatic knee osteoarthritis in women: The framingham study. *Ann Intern Med*. 1992;116(7):535-539.

31. Fergenbaum M, Hadcock L, Stevenson J, Morin E, Bryant T, Reed S. Presure measurement applications for humans. . 2003.

32. Fernandes L, Hagen KB, Bijlsma JWJ, et al. EULAR recommendations for the non-pharmacological core management of hip and knee osteoarthritis. *Ann Rheum Dis*. 2013;72(7):1125-1135.

33. Fieuws S, Verbeke G, Molenberghs G. Random-effects models for multivariate repeated measures. *Stat Methods Med Res*. 2007;16(5):387-397.

34. Fryar CD, Gu Q, Ogden CL, eds. *Anthropometric reference data for children and adults: United states, 2007-2010*. ; 2012Vital and Health Statistics, Series 11: Data from the National Health Survey, the National Health and Nutrition Examination Surveys, and the Hispanic Health and Nutrition Examination Survey; No. 11.

35. Fukubayashi T, Kurosawa H. The contact area and pressure distribution pattern of the knee. A study of normal and osteoarthrotic knee joints. *Acta Orthop Scand*. 1980;51(6):871-879.

36. Ghidey W, Lesaffre E, Verbeke G. A comparison of methods for estimating the random effects distribution of a linear mixed model. *Stat Methods Med Res*. 2010;19(6):575-600.

37. Grood ES, Suntay WJ. A joint coordinate system for the clinical description of three-dimensional motions: Application to the knee. *J Biomech Eng*. 1983;105(2):136-144.

38. Hefzy MS, Kelly BP, Cooke DV. Kinematics of the knee joint in deep flexion: A radiographicassessment. *Medical and Engineering Physics*. 1998;20:302-307.

39. Heinlein B, Kutzner I, Friedmar G, Bender A, Rohlmann A. Complete data of total knee replacement loading for level walking and stair climbing measured in vivo with a follow-up of 6–10 months. *Clinical Biomechanics*. 2009;24:315-326.

40. Heinlein B, Kutzner I, Graichen F, et al. ESB clinical biomechanics award 2008: Complete data of total knee replacement loading for level walking and stair climbing measured in vivo with a follow-up of 6-10 months. *Clin Biomech*. 2009;24(4):315-326.

41. Hemmerich A, Brown H, Smith S, Marthandam SSK, Wyss UP. Hip, knee, and ankle kinematics of high range of motion activities of daily living. *Journal of Orthopaedic Research*. 2006;24(4):770-781.

42. Herzog W, Read L. Lines of action and moment arms of the major force-carrying structures crossing the human knee joint. *Journal of Anatomy*. 1993;182(213):230.

43. Hickerson WL, Slugocki GM, Thaker RL, Duncan R, Bishop JF, Parks JK. Comparison of total body tissue interface pressure of specialized pressure-relieving mattresses. *J Long Term Eff Med*. 2004;14(2):81-93.

44. Hill PF, Vedi V, Williams A, Iwaki H, Pinskerova V, Freeman MAR. Tibiofemoral movement 2: The loaded and unloaded living knee studied by MRI. *Journal of Bone and Joint Surgery - Series B*. 2000;82(8):1196-1198.

45. Hirokawa S. Biomechanics of the knee joint: A critical review. *Crit Rev Biomed Eng*. 1993;21(2):79-135.

46. Hirokawa S, Fukunaga M. Knee joint forces when rising from kneeling positions. *Journal of Biomechanical Science and Engineering*. 2013;8(1):27-39.

47. Hitt K, Shurman II JR, Greene K, et al. Anthropometric measurements of the human knee: Correlation to the sizing of current knee arthroplasty systems. *Journal of Bone and Joint Surgery - Series A*. 2003;85(SUPPL. 4):115-122.

48. Iwaki H, Pinskerova V, Freeman MAR. Tibiofemoral movement 1: The shape and relative movements of the femur and tibia in the unloaded cadaver knee. *Journal of Bone and Joint Surgery - Series B*. 2000;82(8):1189-1195.

49. Jevsevar DS, Riley PO, Hodge WA, Krebs DE, Rodgers MM. Knee kinematics and kinetics during locomotor activities of daily living in subjects with knee arthroplasty and in healthy control subjects. *Phys Ther*. 1993;73(4):229-242.

50. Jones CD. Gender differences in patellofemoral joint biomechanics. *Clin Orthop*. 2004(419):317; author 317-318.

51. Jordan KM, Arden NK, Doherty M, et al. EULAR recommendations 2003: An evidence based approach to the management of knee osteoarthritis: Report of a task force of the standing committee for international clinical studies including therapeutic trials (ESCISIT). *Ann Rheum Dis*. 2003;62(12):1145-1155.

52. Kadaba MP, Ramakrishnan HK, Wootten ME. Measurement of lower extremity kinematics during level walking. *Journal of Orthopaedic Research*. 1990;8(3):383-392.

53. Kanekasu K, Banks SA, Honjo S, Nakata O, Kato H. Fluoroscopic analysis of knee arthroplasty kinematics during deep flexion kneeling. *J Arthroplasty*. 2004;19(8):998-1003.

54. Karrholm J, Brandsson S, Freeman MAR. Tibiofemoral movement 4: Changes of axial tibial rotation caused by forced rotation at the weight-bearing knee studied by RSA. *Journal of Bone and Joint Surgery - Series B*. 2000;82(8):1201-1203.

55. Kaufman KR, Kovacevic N, Irby SE, Colwell CW. Instrumented implant for measuring tibiofemoral forces. *J Biomech*. 1996;29(5):667-671.

56. Khaw F-, Kirk LMG, Gregg PJ. Survival analysis of cemented press-fit condylar total knee arthroplasty. *J Arthroplasty*. 2001;16(2):161-167.

57. Kirking B, Krevolin J, Townsend C, Colwell Jr. CW, D'Lima DD. A multiaxial force-sensing implantable tibial prosthesis. *J Biomech*. 2006;39(9):1744-1751.

58. Komistek RD, Kane TR, Mahfouz M, Ochoa JA, Dennis DA. Knee mechanics: A review of past and present techniques to determine in vivo loads. *J Biomech*. 2005;38(2):215-228.

59. Komistek RD, Stiehl JB, Dennis DA, Paxson RD, Soutas-Little RW. Mathematical model of the lower extremity joint reaction forces using kane's method of dynamics. *J Biomech*. 1997;31(2):185-189.

60. Kutzner I, Heinlein B, Grachen F, et al. Loading of the knee joint during activities of daily living measured in vivo in five subjects. *Journal of Biomechanics*. 2010;43:2164-2173.

61. Lean MEJ, Han TS, Deurenberg P. Predicting body composition by densitometry from simple anthropometric measurements. *Am J Clin Nutr*. 1996;63(1):4-14.

62. Li G, Zayontz S, DeFrate LE, Most E, Suggs JF, Rubash HE. Kinematics of the knee at high flexion angles: An in vitro investigation. *Journal of Orthopaedic Research*. 2004;22(1):90-95.

63. Liang KY, Zeger SL. Longitudinal data analysis using generalized linear models. *Biometrika*. 1986;73(1):13-22.

64. Linn S, Murtaugh B, Casey E. Role of sex hormones in the development of osteoarthritis. *PM and R*. 2012;4(5 SUPPL.):S169-S173.

65. Littell RC, Henry PR, Ammerman CB. Statistical analysis of repeated measures data using SAS procedures. *J Anim Sci*. 1998;76(4):1216-1231.

66. Littell RC, Pendergast J, Natarajan R. Modelling covariance structure in the analysis of repeated measures data. *Stat Med*. 2000;19(13):1793-1819.

67. Liu B, Balkwill A, Banks E, Cooper C, Green J, Beral V. Relationship of height, weight and body mass index to the risk of hip and knee replacements in middle-aged women. *Rheumatology*. 2007;46(5):861-867.

68. MacDonald SJ, Charron KD, Bourne RB, Naudie DD, McCalden RW, Rorabeck CH. The john insall award: Gender-specific total knee replacement: Prospectively collected clinical outcomes. *Clin Orthop*. 2008;466(11):2612-2616.

69. Maetzel A, Mäkelä M, Hawker G, Bombardier C. Osteoarthritis of the hip and knee and mechanical occupational exposure - A systematic overview of the evidence. *J Rheumatol*. 1997;24(8):1599-1607.

70. Manal K, McClay Davis I, Galinat B, Stanhope S. The accuracy of estimating proximal tibial translation during natural cadence walking: Bone vs. skin mounted targets. *Clin Biomech*. 2003;18(2):126-131.

71. Martinelli L, Hurschler C, Rosenbaum D. Comparison of capacitive versus resistive joint contact stress sensors. *Clin Orthop*. 2006(447):214-220.

72. Meneghini, R. M., Pierson, J. L., Bagsby, D., Ziemba-Davis, M., Berend, M. E., & Ritter, M. A. Is there a functional benefit to obtaining high flexion after total knee arthroplasty? *The Journal of arthroplasty*. 2007;22(6):43-46.

73. Messier SP, Gutekunst DJ, Davis C, DeVita P. Weight loss reduces knee-joint loads in overweight and obese older adults with knee osteoarthritis. *Arthritis Rheum*. 2005;52(7):2026-2032.

74. Miranda H, Viikari-Juntura E, Martikainen R, Riihimäki H. A prospective study on knee pain and its risk factors. *Osteoarthritis and Cartilage*. 2002;10(8):623-630.

75. Morrison J. Bioengineering analysis of force actions transmitted by the knee joint. *Biomedical Engineering*. 1968;3(4):164-170.

76. Nagura T, Dyrby CO, Allexander EJ, Andriacchi TP. Mechanical loads at the knee joint during deep flexion. *Journal of Orthopaedic Research*. 2002;20:881-886.

77. Nagura T, Matsumoto H, Kiriyama Y, Chaudhari A, Andriacchi TP. Tibiofemoral joint contact force in deep knee flexion and its consideration in knee osteoarthritis and joint replacement. *Journal of Applied Biomechanics*. 2006;22(4):305-313.

78. Neogi T, Zhang Y. Epidemiology of osteoarthritis. *Rheumatic Disease Clinics of North America*. 2013;39(1):1-19.

79. Nguyen U-DT, Zhang Y, Zhu Y, Niu J, Zhang B, Felson DT. Increasing prevalence of knee pain and symptomatic knee osteoarthritis: Survey and cohort data. *Ann Intern Med*. 2011;155(11):725-732.

80. Niu J, Zhang YQ, Torner J, et al. Is obesity a risk factor for progressive radiographic knee osteoarthritis? *Arthritis Care and Research*. 2009;61(3):329-335.

81. Owens S. Prediction of visceral adipose tissue from simple anthropometric measurements in youths with obesity. *Obes Res*. 1999;7(1):16-22.

82. Papaioannou G, Protopappas V, Panagiotis T, Mitrogiannis C, Nianios G, Tashman S. A new method for pressure sensor equilibration and conditioning. *Brazilian Journal of Biomotricity*. 2008;2(3):176-195.

83. Pavlovic, J. L., Takahashi, Y., Bechtold, J. E., Gustilo, R. B., & Kyle, R. F. Can the tekscan sensor accurately measure dynamic pressures in the knee joint. . . 1993:135-136.

84. Perissinotto E, Pisent C, Sergi G, Grigoletto F, Enzi G. Anthropometric measurements in the elderly: Age and gender differences. *Br J Nutr*. 2002;87(2):177-186.

85. Perry J, Antonelli D, Ford W. Analysis of knee joint forces during flexed knee stance. *Journal of Bone and Joint Surgery - Series A*. 1975;57(7):961-967.

86. Pollard JP, Porter WL, Redfern MS. Forces and moments on the knee during kneeling and squatting. *Journal of Applied Biomechanics*. 2011;27(3):233-241.

87. Rand JA. Role of arthroscopy in osteoarthritis of the knee. *Arthroscopy: The Journal of Arthroscopic and Related Surgery*. 1991;7(4):358-363.

88. Seidell JC, Deurenberg P, Hautvast JG. Obesity and fat distribution in relation to health--current insights and recommendations. *World Rev Nutr Diet*. 1987;50:57-91.

89. Seidell JC, Oosterlee A, Thijssen MAO, et al. Assessment of intra-abdominal and subcutaneous abdominal fat: Relation between anthropometry and computed tomography. *Am J Clin Nutr*. 1987;45(1):7-13.

90. Selya AS, Rose JS, Dierker LC, Hedeker D, Mermelstein RJ. A practical guide to calculating cohen's f 2, a measure of local effect size, from PROC MIXED. *Frontiers in Psychology*. 2012;3(APR).

91. Shimokata H, Tobin JD, Muller DC, Elahi D, Coon PJ, Andres R. Studies in the distribution of body fat: I. effects of age, sex, and obesity. *Journals of Gerontology*. 1989;44(2):M66-73.

92. Smith SM, Cockburn RA, Hemmerich A, Li RM, Wyss UP. Tibiofemoral joint contact forces and knee kinematics during squatting. *Gait and Posture*. 2008;27(3):376-386.

93. Stinson M, Porter A, Eakin P. Measuring interface pressure: A laboratory-based investigation into the effects of repositioning and sitting. *American Journal of Occupational Therapy*. 2002;56(2):185-190.

94. Stinson MD, Porter-Armstrong AP, Eakin PA. Pressure mapping systems: Reliability of pressure map interpretation. *Clin Rehabil*. 2003;17(5):504-511.

95. Stürmer T, Günther K-, Brenner H. Obesity, overweight and patterns of osteoarthritis: The ulm osteoarthritis study. *J Clin Epidemiol*. 2000;53(3):307-313.

96. Tarabichi S, Tarabichi Y, Hawari M. Achieving deep flexion after primary total knee arthroplasty. *J Arthroplasty*. 2010;25(2):219-224.

97. Thambyah A, Goh JCH, Das De S. Contact stresses in the knee joint in deep flexion. *Medical Engineering and Physics*. 2005;27(4):329-335.

98. Van der Borght K, Verbeke G, van Vlijmen H. Multi-model inference using mixed effects from a linear regression based genetic algorithm. *BMC Bioinformatics*. 2014;15(1).

99. Velotta, J., Weyer, J., Ramirez, A., Winstead, J., & Bahamonde, R. Relationship between leg dominance tests and type of task. *Methods*. 2011;11(2).

100. Verbeke G, Fieuws S, Molenberghs G, Davidian M. The analysis of multivariate longitudinal data: A review. *Stat Methods Med Res*. 2014;23(1):42-49.

101. Wang J, Thornton JC, Russell M, Burastero S, Heymsfield S, Pierson Jr. RN. Asians have lower body mass index (BMI) but higher percent body fat than do whites: Comparisons of anthropometric measurements. *Am J Clin Nutr*. 1994;60(1):23-28.

102. West B, Welch K, Galecki A. *Linear mixed models: A practical guide using statistical software.* 1st ed. Boca Raton, FL.: Taylor & Francis Group; 2007. 2007.

103. Wilson DR, Apreleva MV, Eichler MJ, Harrold FH. Accuracy and repeatability of a pressure measurement system in the patellofemoral joint. *Orthopedic Biomechanics Laboratory*. 2003;36(12):1909-1915.

104. Winter DA, Patla AE, Frank JS, Walt SE. Biomechanical walking pattern changes in the fit and healthy elderly. *Phys Ther*. 1990;70(6):340-347.

105. Yeadon MR. Simulation of aerial movement. I. the determination of orientation angles film data. *J Biomech*. 1990;23(1):59-66.

106. Yildirim G, Walker PS, Sussman-Fort J, Aggarwal G, White B, Klein GR. The contact locations in the knee during high flexion. *Knee*. 2007;14(5):379-384.

107. Zeger SL, Liang K-, Albert PS. Models for longitudinal data: A generalized estimating equation approach. *Biometrics*. 1988;44(4):1049-1060.

108. Zelle J, Barink M, De Waal Malefijt M, Verdonschot N.
Thigh–calf contact: Does it affect the loading of the knee in the high-flexion range? *Journal of Biomechanics*. 2009;42:587-593.

109. Zelle J, Barink M, Loeffen R, De Waal Malefijt M, Verdonschot N. Thigh-calf contact force measurements in deep knee flexion. *Clinical Biomechanics*. 2007;22:821-826.

110. Zelle J, Janssen D, Van Eijden J, De Waal Malefijt M, Verdonschot N. Does high-flexion total knee arthroplasty promote early loosening of the femoral component? *Journal of Orthopaedic Research*. 2011;29(7):976-983.

Appendix

Appendix A: Tekscan pressure mat calibration.

Conditioning, equilibration and calibration were carried out using a gas-powered air compressor connected to a calibration jig (PB100B Tekscan, Tekscan Inc.), consisting of a control panel connected to an air bladder sandwiched between a wooden scaffold (Figure A-1). The pressure mat was placed in the wooden scaffold under the air bladder to ensure an equal distribution of pressure. The control panel toggle controls the inflow of air to and from the air bladders and the analog gauge on the wooden scaffold tells how much pressure is currently in the air bladder.

Figure A-1: Calibration and equilibration equipment showing the air compressor, control panel and pressure mat in the wooden scaffold.

First, the device was conditioned by loading and unloading the pressure mat. Conditioning has been shown to lessen the effects of drift and hysteresis (IScan User's Manual., 1999). Conditioning was accomplished by cycling pressure from 0 to 15 psi (103.4 kPa), using the air bladder, over the entire sensor ten times.

Equilibration and calibration were carried out in accordance with the manufacturer's recommendations (Tekscan IScan User's Manual, 1999) Equilibration is a process which attempts to minimize the variation between individual sensor elements (sensels) when a uniform pressure is applied. This process was accomplished by applying a uniform pressure at 7.5 psi (51.7 kPa), via the air bladder in the calibration jig, across the entire sensing area of the pressure mat for 15 seconds. Ideally, each element within the sensor should have produced a uniform output. When this was not the case, the software determined a unique scaling factor for that sensel to compensate for the slight variation and this scaling factor was then applied for subsequent trials.

The application of a normal force to an active sensor results in changes in the resistance of each sensing element in inverse proportion to the force applied. Calibration is the method by which the digital output from the application of a normal force to an active sensor element is converted to force. In order to minimize the effect of drift on the IPM system's output, the sensor calibration was performed in a time frame similar to that which will be used in the application of the system (Tekscan IScan User's Manual, 1999). Therefore the loading rate (2.5 psi/sec) and duration over which the full load was applied (3 seconds) to the pressure mat were similar to those expected in the actual experiment. Two different loads, 7.5 psi (51.7 kPa) and 15 psi (103.4 kPa), were applied to the pressure mat using the calibration jig and analog gauge, each for 15 seconds.

A 2-point power law interpolation was then performed by the IScan software (Tekscan, Boston, MA) based on the two known calibration loads, using the equation: $y = ax^b$ where a and b are the calibration coefficients, x is the raw output of pressure mat (equilibrated raw output), and y is the pressure in units of PSI.

Appendix B: Tekscan Validation

In order to assess the validity of the Tekscan Conformat System several tests were performed in order to determine the accuracy of the system in measuring an applied force, the synchronicity of the system with signals collected in First Principles, the presence of a non-sensing area within the thigh-calf contact area and hysteresis.

B.1 Accuracy

Pilot testing aimed to quantify the accuracy of the system in measuring an applied force, taking into account a delay in the IPM system.. Ten trials each of loading and unloading between 0 and 300 N and 0 and 400 N were carried out. Force was applied to the Tekscan Conformat pressure mapping system (Tekscan Inc., Boston, MA) using a force transducer via a curved platen (Chatillion CDS 200 Dynamometer, AMTEK Test & Calibration Instruments, Largo, Florida, U.S.A.). The analog output from the force transducer was sampled at a frequency of 60 Hz through the Optotrak Data Acquisition Unit (ODAU) using First Principles software (Northern Digital Inc., Waterloo, ON). The pressure mat output was sampled at 60Hz, using ISCAN software (ISCAN v3 820, Tekscan Inc., Boston, MA). Data collection was synchronously started using an external trigger that sent a low-to-high signal (5 v) to the ISCAN software (ISCAN v3 820, Tekscan Inc., Boston, MA) and a high-to-low signal to First Principles software (Northern Digital Inc., Waterloo, ON). During force application, the pressure mat lay on a participant's thigh in order to attempt to mimic thigh-calf contact (Figure B-1).

Figure B-1: Experimental set-up involving the application of a force transducer to the IPM while it rests over a participant's thigh.

The loading rates (2.5-5 psi/sec), maximum loads (300N or 400N), were all similar to those expected in the actual experiment, based on previous pilot testing. The applied force (blue curves) and the IPM output (orange curves) from each of the 20 trials are shown in Figure B-2. In order to determine the accuracy of the IPM in measuring the known applied load, the delay between the two systems was first quantified and corrected for, and then a limits of agreement analysis (Bland & Altman, 2007). was carried out to determine the agreement between the known load and the delay-removed IPM data.

For each trial, the delay between the output from the force transducer and the IPM was determined by cross correlating the force transducer output and the IPM output (MATLAB R2014b, The MATHWORKS Inc., Natick, MA). This analysis showed that the time delay was

not uniform and varied between trials from 28 frames to 31 frames (indicated in the bottom right corner of the graph for each trial in Figure B-2). The delay value was used to determine how many frames to shift the IPM output in order to match up with the force transducer output, and by proxy the kinematic data.

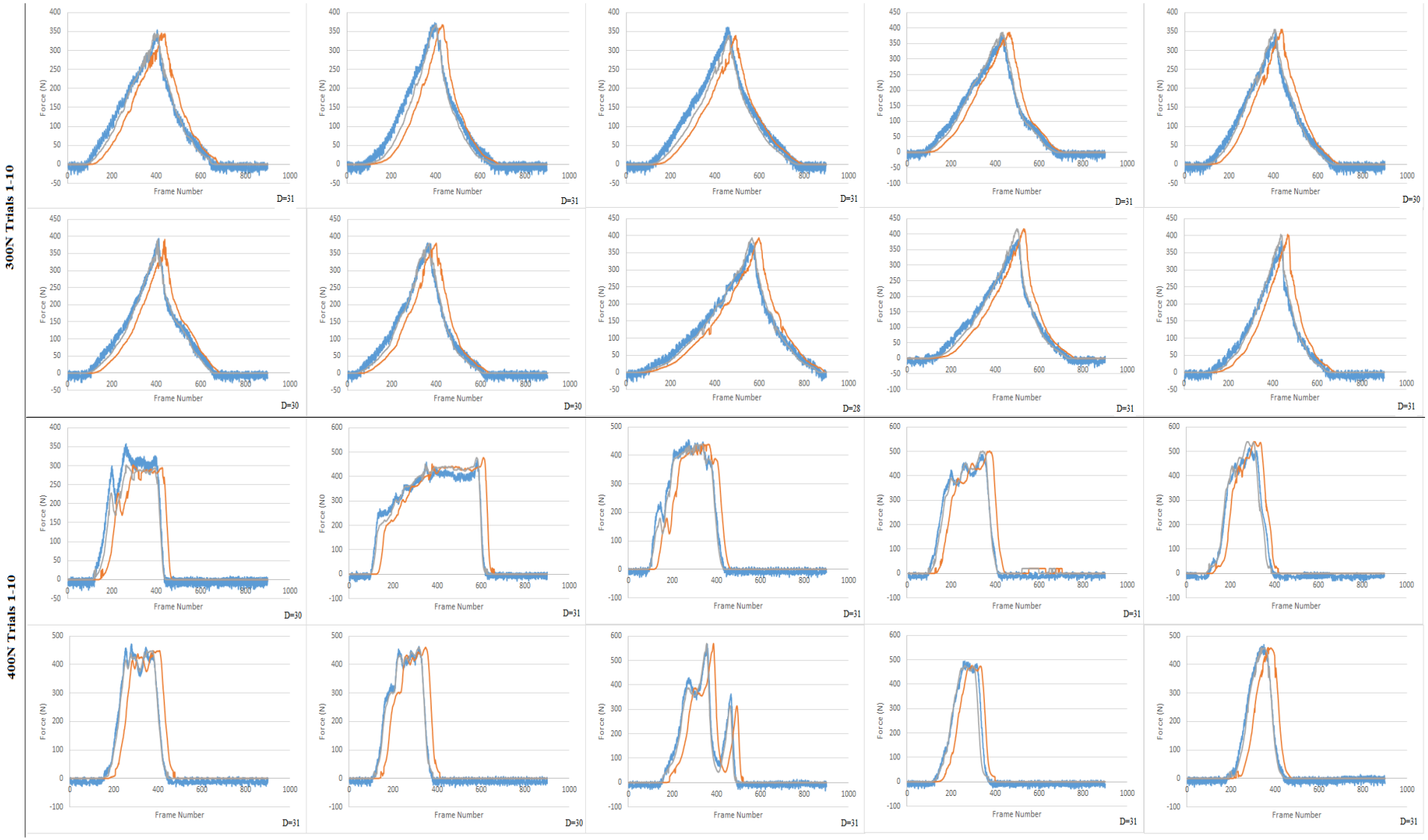

Figure B-2: Plots showing the difference between the force transducer output (blue) and the pressure mat data (orange). The shifted pressure mat data, after delay calculation (grey), are also displayed.

In order to determine the agreement between the magnitudes of the force output from the force transducer and the delay-removed force output from the pressure mapping sensor, a limits of agreement analysis was used (Altman and Bland, 1983; Bland and Altman, 1986). Limits of Agreement (LoA) define the agreement between different methods measuring the same quantity (Bland and Altman, 1992 and Woodall, 2005). The LoA provide an upper and lower limit within which 95% of the differences between the force outputs from the IPM system and the force transducer can be expected to fall.

The LoA method applied was appropriate for situations when there is repeated data, either as repeated pairs of measurements on the same participant and the true value of the measured quantity may be changing (Bland & Altman, 2007). In the case of this investigation, all pairs of data points for all the trials for the force transducer and pressure mapping system were taken into account. Since a single factor ANOVA showed a trial effect, each trial was treated separately and a pooled variance was used (Bland & Altman, 2007). Figure B-3 shows a Bland-Altman plot of differences between the force transducer and IPM system against the average of the two measurements. The 95% limits of agreement for the difference between the force transducer and the IPM system were estimated to be -39.4 to 40.3 N. As can be seen in Figure B-3, some trials were found to be significantly above the LoA. Those trials in particular were trials 2, 11 and 19 from Figure B-2. As can be seen in Figure B-2, in those trials the shifted pressure mat data was still slightly delayed in some locations in comparison to the force transducer output. This would cause huge differences between the measured values and shifted pressure mat values during periods of force loading or unloading.

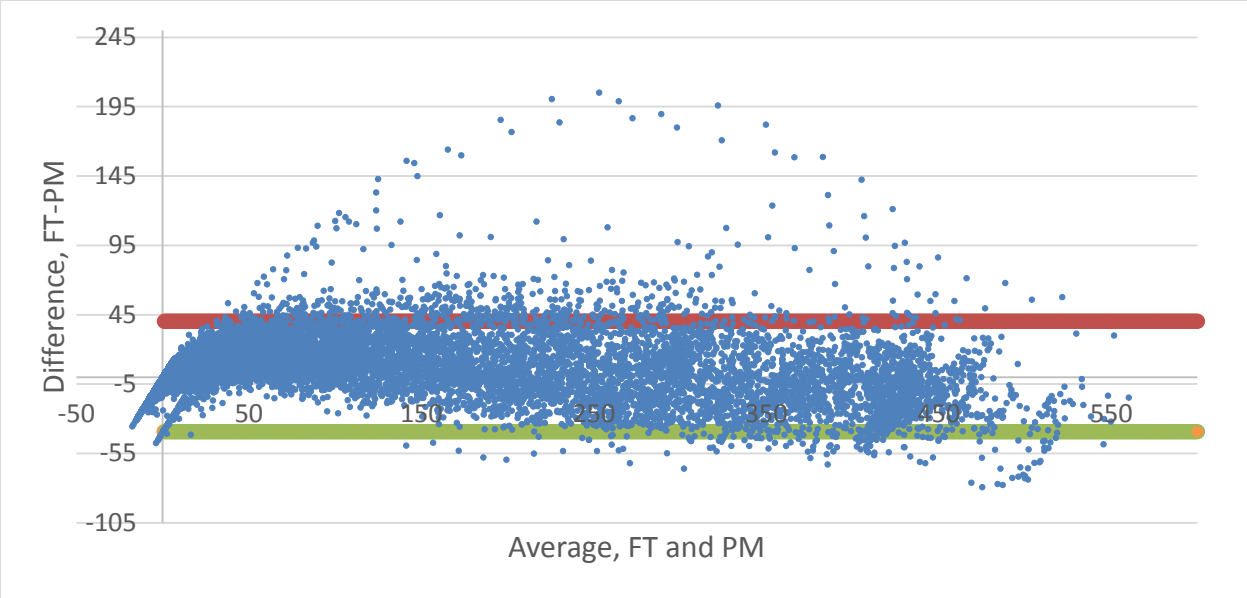

Figure B-3: Scatter Bland-Altman plot of difference between methods against the average of the two measurements. The red and green lines represent the calculated upper and lower 95% limits of agreement.

B.2 Effect of Non-Sensing Area

The length of the thigh-calf contact are along the y-axis of the IPM at maximal flexion is approximately 20cm. Given that there was a non-sensing area of 2.6cm, equivalent to approximately two columns of sensels, the IPM measurement could be potentially be missing 10% of thigh-calf contact area, or even more, given that the thigh-calf contact area becomes more narrow (less rows per column) as the measurements become more distal on the calf. A sensitivity analysis was performed to determine the difference in force, normalized to participant mass, between the IPM output and a hypothetical full sensing matrix without a non-sensing area. The force at the starting angle of thigh-calf contact and the maximum total force were taken from all activity trials from four different participants, chosen at random from the study population. In the hypothetical case, it was assumed that instead of a non-sensing area, there were two columns of sensels with the same dimensions of the sensels on the rest of the pressure mat. The force distribution on each column of these sensels was assumed to be identical to the last column before the non-sensing area (closest to the popliteal crease). The resulting force including the

measured sensels and the two columns of hypothetical sensels was calculated and then normalized to participant mass. For the four participants, the average difference in force at the starting angle of thigh-calf contact was 0.0006 N/kg (S.D. 0.006) and the average difference in force for maximum total force was 0.39 N/kg (S.D. 0.07).

B.3 Effect of Hysteresis

In order to determine the effect of hysteresis, the IPM system was placed inside a custom calibration jig with an air bladder. With the assistance of an air compressor, pressure was applied to the IPM system, increasing in1 psi (6.9 kPa) increments increasing pressure from 1psi to 10psi (68.9 kPa) and then decreasing in 1 psi increments pressure from 10psi to 1psi. The results from the hysteresis analysis can be found in Figure B-4 and were converted to force by multiplying the pressure by the total area of all the sensels on the pressure mat.

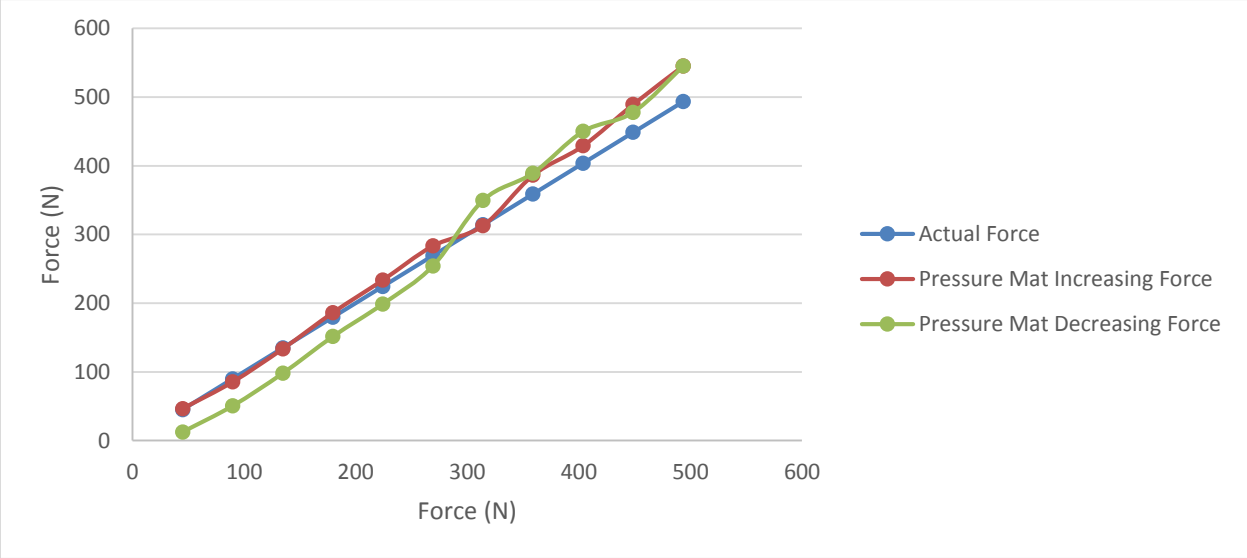

Figure B-4: Hysteresis analysis showing the difference between the actual applied force (blue), to the measured force during a linearly increasing force condition (orange), and a linearly decreasing force condition (green).

The hysteresis analysis shows general agreement between the applied load and the load measured by the IPM system in the increasing pressure condition, especially at forces below 350

N. The Tekscan Conformat system (Tekscan, Boston, MA), as with most IPM systems, are known for experiencing hysteresis in the decreasing pressure conditions (Pavlovic et al., 1993). The results of the hysteresis analysis show better agreement between the actual applied force and the force measured by the IPM system during the increasing pressure condition than during the decreasing condition below 350 N. Given that all force values measured from participants in this investigation were below 400 N, only the data from the portion of the deep flexion movement where the participant was descending into maximal flexion (increasing thigh-calf contact force) were used.

A paired t-test determined that the differences between the actual applied force and increasing force values from the pressure mat were not statistically significant ($p= 0.2$) with a 95% confidence interval from -9.7 N to 2.74 N. In terms of the thigh-calf contact measurements taken during this investigation, the calculated confidence interval would encompass the true population parameter 95% of the time. Meaning that the measured force from the IPM system will lie within -9.7 N to 2.74 N from the true applied force 95% of the time. When comparing the actual applied force to the pressure mat output from the descending force condition, the paired t-test determined that the differences were also not statistically significant ($P=0.08$) with a 95% confidence interval of this difference from -3.7 N to 44.2 N. When comparing the differences between the increasing and decreasing force conditions from the pressure mat the paired t-test determined that the differences were statistically significant ($P=0.02$) with a confidence interval of 2.9 N to 27.9 N.

Appendix C: Mass-Normalized Thigh-Calf Contact Force and COP with Respect to Absolute Flexion Angle

The thigh-calf contact force, normalized to body mass, was presented in Figure 4-1, earlier in this document. The flexion angles that corresponded to thigh-calf contact forces in that figure were normalized to percent flexion range after contact. In order to show the variation in absolute flexion angles that were measured in this study, Figure C-1 shows thigh-calf contact force for squatting, dorsi-flexed and plantar-flexed kneeling with knee flexion expressed in degrees.

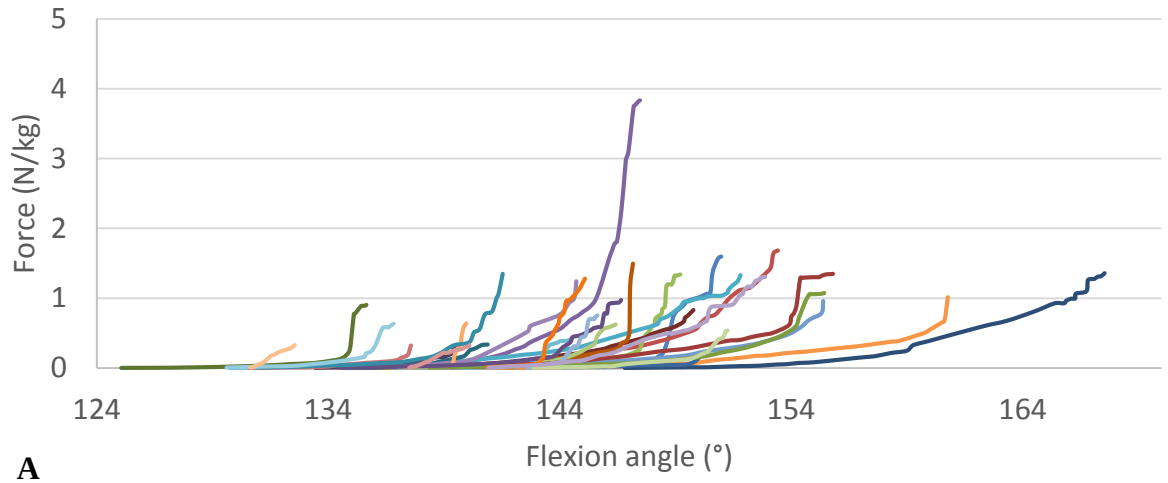

A

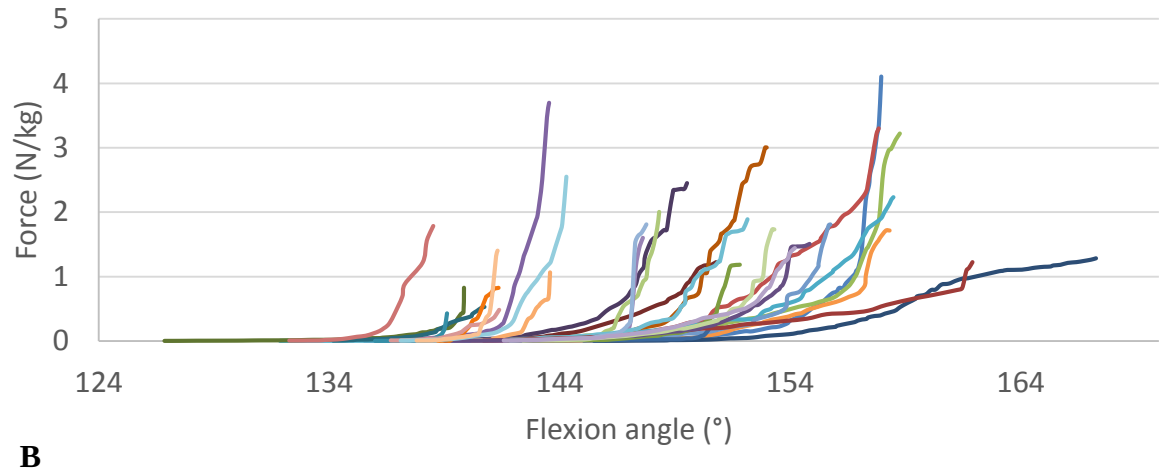

B

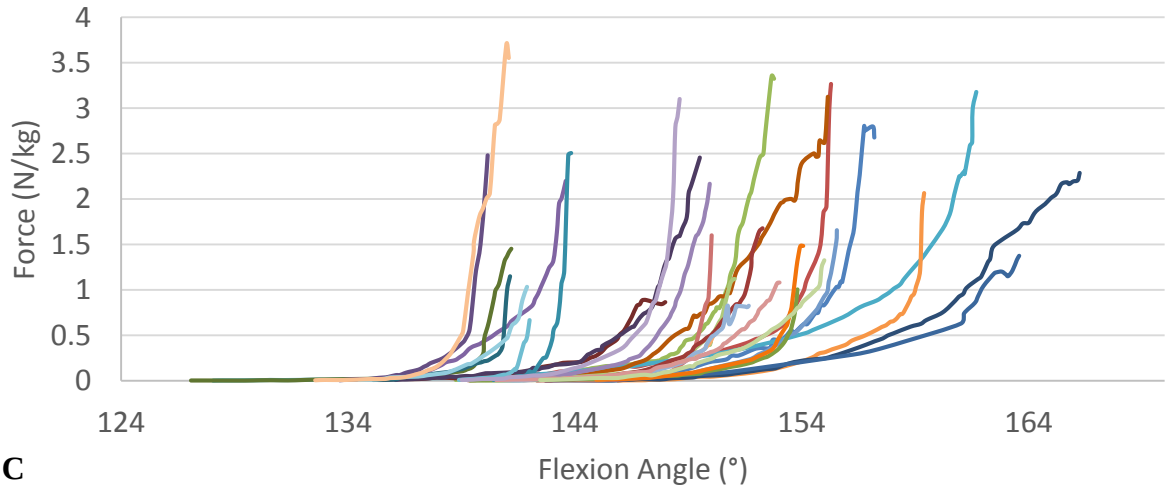

C

Figure C-1: Thigh-calf contact force for (A) squatting (B) dorsi-flexed and (C) plantar-flexed kneeling for the full range of flexion in degrees. Individual colours represent the average thigh-calf contact force curve for individual participants.

The center of pressure, normalized to body mass, was presented in Figure 4-2, earlier in this document. The flexion angles that corresponded to center of pressure in that figure were normalized to percent flexion range after contact. In order to show the variation in absolute flexion angles that were measured in this study, Figure C-2 shows the center of pressure of thigh-calf contact for squatting, dorsi-flexed and plantar-flexed kneeling with knee flexion expressed in degrees.

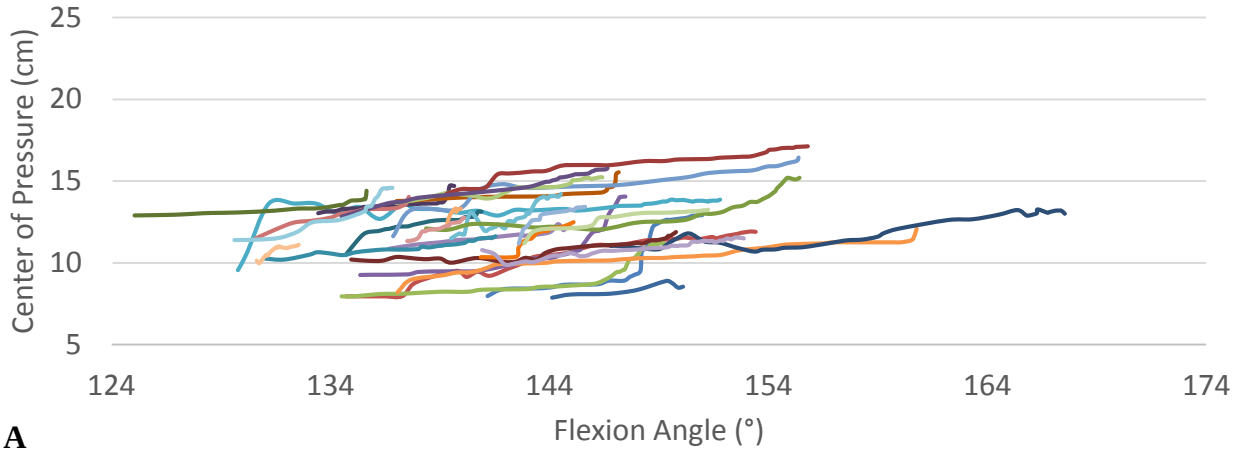

A

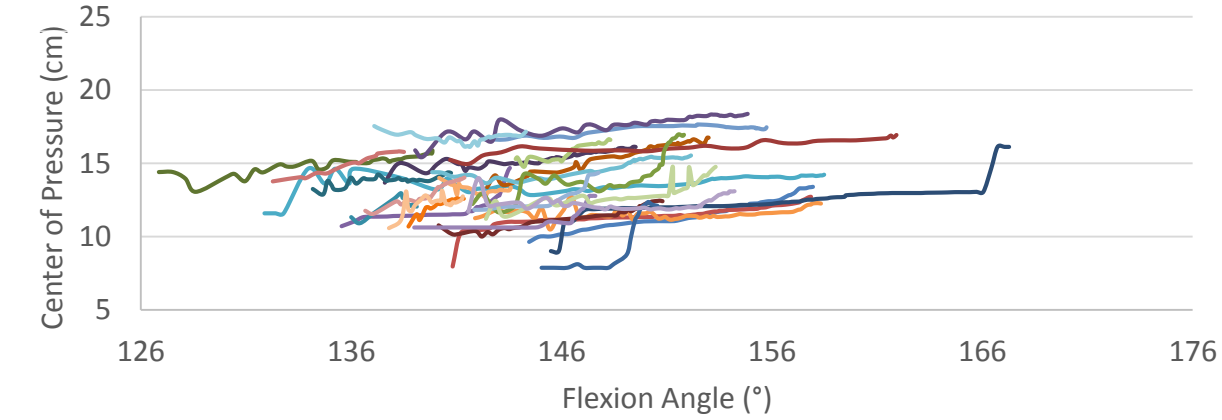

B

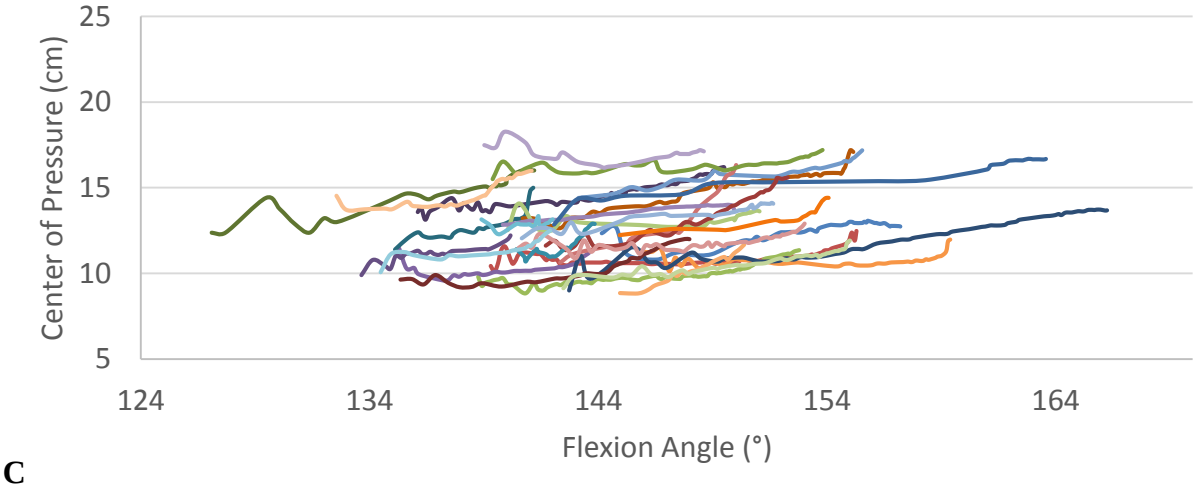

C

Figure C-2: Center of pressure for (A) squatting (B) dorsi-flexed and (C) plantar-flexed kneeling for the full range of flexion in degrees. Individual colours represent the average thigh-calf contact force curve for individual participants.

Appendix D: ANOVA Outputs

The following tables show the analysis of variance output and post hoc tests for total maximal thigh-calf contact force, centre of pressure at maximum total force, flexion angle at maximum total force and the starting angle of thigh-calf contact respectively where significant P values are denoted with an (*). Note that the sum of squares values for activity, sex and activity*sex are Type 1 sum of squares. For the post hoc tables trial 1 represents the squatting activity whereas trials 2 and 3 represent dorsi-flexed and plantar-flexed kneeling.

Table D-1: ANOVA table values for the starting angle of thigh-calf contact where significant values are denoted with an asterisk (*). These results were described in Section 4.3 and discussed in Section 5.3.

Source	**Degrees of Freedom**	**Sum of Squares**	**Mean Square**	**F Value**	**Pr > F**
Model	5	299.70	59.94	3.32	0.03*
Error	84	1518.29	18.07	-	-
Corrected Total	89	1817.99	-	-	-
Activity	2	145.31	72.65	4.02	0.01*
Sex	1	151.66	151.66	8.39	0.016*
Activity*Sex	2	2.74	1.37	0.08	0.93

Table D-2: Post Hoc Tukey test showing least squares means for starting angle of thigh-calf contact for effect of trial.

Trial	**Tukey Letter: Differences for Alpha = 0.05**
Squatting	A
Dorsi-Flexed Kneeling	B
Plantar-Flexed Kneeling	B

Table D-3: ANOVA table values for the centre of pressure at maximum total force where significant values are denoted with an (*)

Source	Degrees of Freedom	Sum of Squares	Mean Square	F Value	Pr > F
Model	5	36.40	7.28	2.32	0.2
Error	84	263.93	3.14	-	-
Corrected Total	89	300.33	-	-	-
Activity	2	26.99	13.50	4.30	0.04*
Sex	1	8.48	8.48	2.70	0.41
Activity*Sex	2	0.93	0.46	0.15	0.86

Table D-4: Post Hoc Tukey test showing least squares means for the centre of pressure at maximum total force for effect of trial.

Trial	Tukey Letter: Differences for Alpha = 0.05
Squatting	A
Dorsi-Flexed Kneeling	B
Plantar-Flexed Kneeling	B

Table D-5: ANOVA table values for the flexion angle at maximum total force where significant values are denoted with an (*)

Source	Degrees of Freedom	Sum of Squares	Mean Square	F Value	Pr > F
Model	5	236.29	47.26	0.76	0.58
Error	84	5189.45	61.78	-	-
Corrected Total	89	5425.74	-	-	-
Activity	2	224.62	112.31	1.82	0.17
Sex	1	10.76	10.76	0.17	0.68
Activity*Sex	2	0.91	0.45	0.01	0.99

Table D-6: Post Hoc Tukey test showing least squares means for the flexion angle at maximum total force for effect of trial.

Trial	Tukey Letter: Differences for Alpha = 0.05
Squatting	A
Dorsi-Flexed Kneeling	A
Plantar-Flexed Kneeling	A

Table D-7: ANOVA table values for the maximum total thigh-calf contact force where significant values are denoted with an (*)

Source	Degrees of Freedom	Sum of Squares	Mean Square	F Value	Pr > F
Model	5	23.12	4.62	7.94	<0.0001*
Error	84	48.91	0.58	-	-
Corrected Total	89	72.03	-	-	-
Activity	2	22.41	11.20	19.24	<0.0001*
Sex	1	0.39	0.39	0.67	0.41
Activity*Sex	2	0.32	0.16	0.27	0.76

Table D-8: Post Hoc Tukey test showing least squares means for maximum total force for effect of trial.

Trial	Tukey Letter: Differences for Alpha = 0.05
Squatting	A
Dorsi-Flexed Kneeling	B
Plantar-Flexed Kneeling	B

Table D-9: Summary of the forward selection regression for the starting angle of thigh-calf contact during squatting

Summary of Forward Selection							
Step	Variable Entered	Number Vars In	Partial R-Square	Model R-Square	C(p)	F Value	Pr > F
1	mtc	1	0.5027	0.5027	7.8685	18.20	0.0005
2	sx	2	0.1139	0.6166	4.4021	5.05	0.0382
3	pcc	3	0.0740	0.6906	2.8498	3.83	0.0681
4	ht	4	0.0171	0.7077	4.0283	0.88	0.3635

Table D-10: Summary of the forward selection regression for the starting angle of thigh-calf contact during dorsi-flexed kneeling

Summary of Forward Selection							
Step	Variable Entered	Number Vars In	Partial R-Square	Model R-Square	C(p)	F Value	Pr > F
1	pcc	1	0.3885	0.3885	5.7988	11.44	0.0033
2	sx	2	0.1850	0.5736	1.2027	7.38	0.0147
3	mtc	3	0.0289	0.6024	2.1740	1.16	0.2972

Appendix E: Free Body Diagrams

The following FBD and equations show how sagittal-plane knee joint reaction forces and net joint moments were determined with respect to the shank anatomical coordinate system. These forces and moment were calculated both with and without the incorporation of the average maximum total thigh-calf contact force (Figure 4-1).

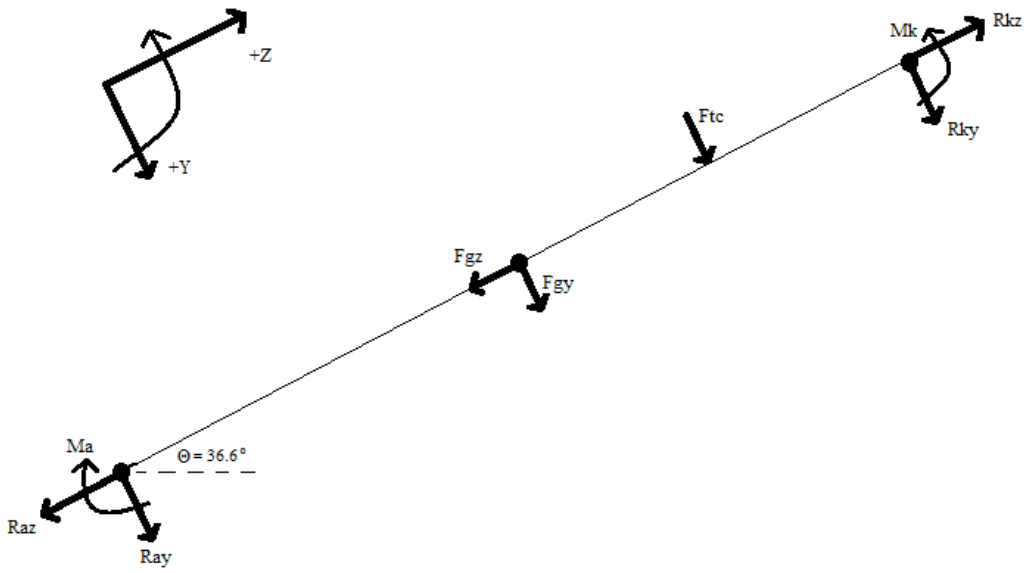

Figure E-1: Free body diagram of the shank for the external forces and moments during squatting at full flexion with respect to the anatomical coordinate system of the shank. For the purposes of this diagram forces and moments were assumed to act in a positive direction.

The foot segment analysis did not change between the two scenarios. The calculation of the segment masses (foot and shank) and the solving of the static equilibrium equations for the foot were completed in Visual 3D V 4.85.0 (C-Motion Inc., Germantown, Maryland, USA). The values calculated are listed below as "Known".

Ray = Reaction force at the ankle along the y-axis in the shank coordinate system
Raz = Reaction force at the ankle along the z-axis in the shank coordinate system
Rky = Reaction force at the knee along the y-axis in the shank coordinate system
Rkz = Reaction force at the knee along the z-axis in the shank coordinate system
M= Mass of subject
Ma = Net ankle joint moment about the x-axis in the shank coordinate system
Mk = Net knee joint moment about the x-axis in the shank coordinate system
ms = Mass of the shank
FTC = Thigh-calf contact force (acts parallel to the y-axis of the shank)
COPTC = Distance between the thigh-calf contact center of pressure and the knee joint along the z axis of the shank.
$Fg_{y,z}$: Force of gravity in the y and z directions
Ankle = Ankle coordinates in the x, y and z direction in the global coordinate system. Where +z is proximal, +y points anteriorly and +z points laterally.
Knee = Knee coordinates in the x, y and z direction
CM = Centre of mass in the x, y and z coordinates
FQ= Estimate of the quadriceps force
FQy,z= Estimate of the quadriceps force in the y and z direction
MA_{PT} = Moment arm of patella tendon calculated from Herzog, W. & Read, L. (1993)
Θ = Angle of shank
FA= Knee joint flexion angle
Φ = Line of action of patella tendon relative to x axis of tibia; calculated from Herzog, W. & Read, L. (1993) based on knee joint flexion of 149.63°
FTFy,z = Tibiofemoral joint contact force in the y and z direction
$a_{y,z}$ = Acceleration in the y and z directions (zero)

Known

M = 99.5 kg

Coordinates expressed in global coordinate system:
Ankle = (0.88, 0.938, 0.12)
Knee = (0.60, 1.046, 0.36)
CM = (0.73, 0.99, 0.25)

Forces and moments expressed in shank coordinate system:
Ray = -355.85 N
Raz = 258.66 N
Ma = 43.41 Nm

ms = 4.62 kg (Dempster, W.T. & Gaughran, G.R., 1967)
FTC = 101.09 N
COPTC = 0.13 m
Θ = 36.6°

Using the values above, the reaction forces in the y and z directions at the knee were calculated in the shank coordinate system both with and without the incorporation of thigh-calf contact force. Moment arm estimations were calculated from Herzog, W. & Read, L. (1993)

Y-Direction	**Z-Direction**
$\Sigma Fy = m_s a_y = 0$	$\Sigma F_Z = m_s a_z = 0$
$- R_{ay} + F_{gy} + R_{ky} + F_{TC} = 0$	$+ R_{aZ} - Fg_Z + Rk_Z = 0$
$Rk_y = + R_{ay} - F_{gy} - F_{TC}$	$Rk_Z = - R_{aZ} + F_{gz}$

Without F_{TC}

$R_{ky} = (355.85) - (45.32\cos 36.6°) - 0$ $\quad$ $R_{kz} = - 258.66 + (45.32\sin 36.6°)$

$R_{ky} = 319.47$ N = 3.21 N/kg $\quad$ $R_{kz} = -231.64$ N = 2.33 N/kg

With F_{TC}

$R_{ky} = (355.85) - (45.32\cos 36.6) - 101.09$ $\quad$ $R_{kz} = -258.66 + (45.32\sin 36.6°)$

$R_{ky} = 218.38$ N = 2.19 N/kg $\quad$ $R_{kz} = -231.64$ N = 2.33 N/kg

Moment Arm Calculations

$d_{Ray} = \|Ankle_z - CM_z\| = \|(0.88, 0.938, 0.12) - (0.73, 0.99, 0.25)\| = 0.205$ m

$d_{Rky} = \|Knee_z - CM_z\| = \|(0.60, 1.046, 0.36) - (0.73, 0.99, 0.25)\| = 0.179$ m

$d_{FTC} = \|d_{Rky} - COP_{FTC}\| = \|0.17 - 0.13\| = 0.049$ m

$\Sigma M_{COM} = I_{COM}\, a$

$+M_a - M_{Ray} - M_{FTC} + M_k - M_{Rky} = 0$

$M_k = - M_a + M_{Ray} + M_{FTC} + M_{Rky}$

Without F_{TC}

$M_k = -43.41 + (0.205*355.85N) + 0 + (0.179*319.47N) = 86.88$ Nm

With F_{TC}

$M_k = -43.41 + (0.205*355.85N) + (0.049*101.09) + (0.179*218.38N) = 73.75$Nm

Estimation of Quadriceps and Tibiofemoral Joint Contact Force

$F_Q = M_k / MA_{PT}$

$F_{Qz} = F_Q \sin\Phi$

$F_{Qy} = F_Q \cos\Phi$

$F_{TF} = R_k - F_Q$

$F_{TFy} = R_{ky} - F_{Qy}$

$F_{TFz} = R_{kz} - F_{Qz}$

$MA_{PT} = B0 + B1(FA) + B2(FQ)^2 + B3(FA)^3$ (Herzog, W. & Read, L., 1993)

$MA_{PT} = (0.471*10^{1)} + ((0.42*10^{-1})*149.63) - ((0.896*10^{-3})149.63^2) + ((0.447*10^{-5})*(149.63^3)$

$MA_{PT} = 0.0591$ m

$\Phi = A0 + A1(FA) + A2(FQ)^2 + A3(FA)^3$

$\Phi = (-0.744*10^2) - ((0.575*10^{-1})*149.63) - ((0.475*10^{-2})149.63^2) + ((0.309*10^{-4})*(149.63^3)$

$\Phi = 85.84°$

<u>Without F_{TC}</u>

$F_Q = 86.88$ Nm / 0.0591m = 1469.99 N

$F_{Qz} = 1469.99 \sin 85.84° = 1466.13$ N

$F_{Qy} = 1469.99 \cos 85.84° = 106.64$ N

$F_{TFy} = 319.47$ N – 106.64 N = 212.83N = 2.14 N/kg

$F_{TFz} = -231.647$ N – -1466.13 N = -1697.77 N = -17.06 N/kg

<u>With F_{TC}</u>

$F_Q = 73.75$ Nm / 0.0591 m = 1247.64 N

$F_{Qz} = 1247.64$ N $\sin 85.84° = 1244.35$ N

$F_{Qy} = 1247.64$ N $\cos 85.84° = 90.51$ N

$F_{TFy} = 218.38$ N -90.51 N = 127.87 N = 1.28 N/kg

$F_{TFz} = -231.64$ N – 1163.21 N = -1475.99 N = -14.83 N/kg